December 2018

Graphene-Based Materials Coated on Zeolite for the Removal of Persistent Organic Pollutants from Water

Yan Zhang
University of Wisconsin-Milwaukee

GRAPHENE-BASED MATERIALS COATED ON ZEOLITE FOR THE REMOVAL OF PERSISTENT ORGANIC POLLUTANTS FROM WATER

by

Yan Zhang

A Dissertation Submitted in

Partial Fulfillment of the

Requirements for the Degree of

Doctoral of Philosophy

in Engineering

at

The University of Wisconsin-Milwaukee

December 2018

ABSTRACT

GRAPHENE-BASED MATERIALS COATED ON ZEOLITE FOR THE REMOVAL OF PERSISTENT ORGANIC POLLUTANTS FROM WATER

by

Yan Zhang

The University of Wisconsin-Milwaukee, 2018

Under the Supervision of Dr. Nidal H Abu-Zahra and Dr. Marcia Silva

Adsorption is a fast, low-cost and the most commonly implemented water treatment technology for the removal of multiple contaminations from ground water, drinking water or wastewater. Difficulties in removing persistent organic pollutants (POPs) to improve quality and safety of treated water sources require the exploration of novel and multifunctional materials. Graphene-based materials having unique structures, high specific surface areas and tailorable functional groups are promising candidates as adsorbents.

The main goal of this work is to fabricate a novel adsorbent made of GO/rGO attached on natural zeolite substrates for the removal of variably charged organic model compounds and POPs in aqueous solutions. The thin-layered GO/rGO sheets coated on zeolites surface is expected to have a higher removal efficiency for POPs, wider selectivity, lower cost and better recyclability than most of the commercially available adsorbents, such as granular activated carbon (GAC).

Initially, *ex-situ* hybridization of GO and natural zeolite are developed and studied. Three different coating methods were evaluated: spin coating, vacuum coating, and dry coating. Surface

morphology, elementary, structural and physical properties of the coated zeolites were assessed. Chemical and structural analysis shows that the presence of GO on the surface of natural zeolite for these samples. Results from desorption experiments indicated that the dry-coated samples exhibit strongest bonding between GO and zeolites. The adsorption capability of GO coated zeolites for organic model compounds are strongly dependent on the loading of GO. The removal efficiencies of POPs by DCGZ showed comparable results with granular activated carbon (GAC). It reveals that the dry coating method to attach the GO sheets on the surface of zeolites is an effective and straightforward approach with a higher loading of GO and a better physical stability. In addition, optimization of column test operating conditions was carried out at different pH, temperature, and concentrations of organic model compounds.

In the second phase, variable-charge surfactants including cationic hexadecyl trimethyl ammonium bromide (CATB), nonionic polyethylene glycol p-(1,1,3,3-tetramethylbutyl)-phenyl ether (Triton-X 100) and anionic sodium dodecyl sulfate (SDS), are used in conjunction with the GO sheets and zeolites to enhance interaction of GO on zeolites surface. Besides the elemental and morphological characterization, electrochemical analysis is employed to understand the mechanism of interactions between GO, surfactants and zeolites. The electrochemical analysis and desorption experiment studies show that the enhancement of electrostatic interaction and hydrophilicity of GO and natural zeolite can lead to a strong bonding of GO on zeolites surface. The batch adsorption experiment displays that the charged surfactants added DCGZ have strong adsorption capacities for oppositely charged organic model compounds, while they showed the weak adsorption to the same charged ones. Nonionic Triton X-100 is found to effectively enhance the hydrophilicity and stability of the adsorbent, and consequently improve the adsorption performance for a wide variety of organic model compounds.

In the third phase, higher loading of GO and *in-situ* reduction of GO attached on the modified zeolites surface are prepared and studied. To understand and control the properties of the adsorbents, a wide range of characterization were used to evaluate the physical, chemical and morphological properties of GO/rGO and zeolites surface. On one side, the experimental results show that zeolites surface modification by APTES enhances the bonding between the GO sheets and zeolites. A step-wise GO coating process increases the loading of GO on modified zeolites due to the positive surface modification. The effect of loading of GO on adsorption capacity for variable-charged organic model compounds was examined by the column test. A better physical stability of four-time graphene-based materials coated on modified zeolites was confirmed by the desorption experiment. On the other side, two methods by microwave and vitamin C for *in-situ* reduction of GO on the natural zeolite was studied and evaluated. The extent of GO reduction are characterized and well controlled by the factors including reaction time, concentration and adding methods. The thin-layered GO/rGO on modified zeolites substrate has shown a high affinity for organic model compounds exceeding the performance of a reference GAC. Column adsorption studies of a four-time coated rGO on modified zeolites for polychlorinated biphenyl (PCB), perfluorooctanoic acid (PFOA), and bisphenol-A (BPA) show that over 81% adsorbate removal rate is maintained after 24 hours. The thermal stability and recyclability of a four-time coated rGO on modified zeolites were also investigated. The experimental results show that it has a good thermal which maintains over 91% after five cycles after thermal treatment at 500^{o}C for 1 hour.

Finally, the modeling of adsorption mechanisms of the four-time coated rGO on modified zeolites for organic model compound was studied. The pseudo-second-order kinetics model and Langmuir isothermal model were fitted to the batch experiment results.

TABLE OF CONTENTS

LIST OF FIGURES

LIST OF TABLES

LIST OF ABBREVIATIONS

AC	Activated carbon
AMZ	APTES modified zeolites
APTES	(3-Aminopropyl) triethoxysilane
BET	Brunauer, Emmett and Teller
BPA	bisphenol A
CZ	Clean zeolite
CEC	cation-exchange capacity
DB	disperse blue 26
DCGZ	drying method graphene oxide coated zeolites
EDCs	endocrine disrupting compounds
EDS	X-ray spectroscopy
FT-IR	Fourier-transform infrared spectroscopy
FRGAMZ	4 times recoated GO coated APTES modified zeolites
FRrGAMZ	4 times recoated reduced GO coated APTES modified zeolites
GAC	granular activated carbon
GAMZ	GO coated APTES modified zeolites
GBMZS	Graphene based material coated on modified zeolites substrate
GO	graphene oxide
LC-MS	liquid chromatography coupled with tandem mass spectrometry
MB	methylene blue
Mt	million ton
PFCs	perfluorinated compounds

PFOA	perfluorooctanesulfonic acid
POPs	persistent organic pollutants
RB	reactive black 5
rGO	reduced graphene oxide
SEM	scanning electron microscope
SF	sodium fluorescein
UV	visible spectrophotometer
WTPs	water treatment processes
XPS	X-ray photoelectron spectroscopy

ACKNOWLEDGMENTS

First, I would like to thank my supervisors, Associate Prof. Nidal Abu-Zahra and Associate Scientist Dr. Marcia Silva, for their guidance during my Ph.D. study. Thank my undergraduate student Yuting Lin for assisting the experiment and paperwork. Also, I appreciate Dr. Heather. A. Owen for technical support with SEM analyses at the UWM Electron Microscope Laboratory, and Dr. Steven E. Hardcastle for technical assistance with BET and XPS analyses. I also thank all the members in my lab, my family who gave me support during my Ph.D. program.

Financially, this work was supported by the National Science Foundation Industry/University Cooperative Research Center on Water Equipment & Policy located at University of Wisconsin-Milwaukee (IIP-1540032) and Marquette University (IIP-1540010). The SEM imaging and EDS were conducted at the Electron Microscope Laboratory of University of Wisconsin-Milwaukee (UWM). I also thank all the members in my lab, my family who gave me support during my Ph.D. program.

Chapter 1 Introduction

1.1 Introduction of persistent organic pollutants

Persistent organic pollutants (POPs) are carbon-based organic compounds that are resistant to environmental degradation through chemical, biological, and photolytic processes. [1] Thousands of synthetic POPs were generated and widely used in industrial production after 1950's. They have been used in the past and are used today in pesticides, solvents, pharmaceuticals, and industrial chemicals, which have adverse effects on human health and environment. Once released to the atmosphere, they can be persistent for an extended period, widely distribute through natural processes, and accumulate in the fatty tissue of humans and wildlife, which can result in cancer, allergies, hypersensitivity, damage of nervous systems and disruption of the immune system. [2] When POPs accumulate in the fatty tissue of fish, predatory birds, mammals, humans, and the uppers in the food chain, their concentrations can become magnified by up to 700,000 times higher than background levels. [3] Most POPs are human-made, some are carcinogens, and they may cause developmental defects, chronic illnesses, and death. Because of their persistence and toxicity, POPs pose an issue due to their ability to bioaccumulate with potentially significant impacts on human health and remain in the environment for a long time.

POPs have been found on every continent in the world. They can be transported through various methods such as winds, ocean currents, soil and food chains. [4] Usually, POPs once used and released in one area can affect the environment and food chains far away from the contaminated region. POPs, especially in the surface water and local groundwater, have low removal by wastewater treatment plants and have been found in drinking water. [5] Some of these compounds

are well known, such as bisphenol A (BPA) and dichlorodiphenyltrichloroethane (DDT). Besides that, new POPs including organochlorine pesticides (OCPs), polychlorinated naphthalenes (PCNs), hexabromocyclododecanes (HBCDs), Dechlorane Plus (DPs), and related compounds (Dechloranes) have been found, analyzed and monitored. [5] The influence of new POPs requires more research on the risks to human health and the environment. The adverse effects caused by these toxic compounds in water, wastewater, human health, and ecosystems demand the development of useful treatment technologies that can remove high toxic organic contaminants at a low cost. Simultaneously, a one-step removal process for different kinds of POPs is considered as a convenient approach and preferred in the water treatment industry. In this thesis, variably charged POPs, nonionic BPA, anionic perfluorooctanoic acid (PFOA), and cationic polychlorinated biphenyls (PCBs), are introduced.

1.1.1 Bisphenol A

BPA, $C_{15}H_{16}O_2$, is used for synthesizing polycarbonate, epoxy resin, and flame retardants in a sector and manufactured from phenol and acetone. Figure 1.1 shows the molecular structure of BPA. It is a high -production-volume chemical used in plastics (CDs, cell phones, and bicycle helmets, etc.) and beverage containers (lacquers in linings of aluminum food and beverage cans). [6] It was reported that it migrates from the plastic, composites and other storage containers to outside environment when heated or exposed to acidic or alkali solutions due to the degradation of BPA. Usually, most humans are exposed to BPA through ingestion. Infants are especially at risk. They can be exposed by using baby bottles, and toys. [7] Numerous animal studies have demonstrated a correlation between BPA with obesity, thyroid and nervous system cancer. A review in 2008 concluded that BPA affects various dopaminergic processes resulting in hyperactivity, attention deficits, and a heightened sensitivity to drugs of abuse. [8] A report from

U.S. Environmental Protection Agency (EPA) from 2010 shows that over one million pounds of BPA are released into the environment annually. [9] In 2017, the European Chemicals Agency reported that "BPA should be listed as a substance of very high concern due to its properties as an endocrine disruptor." [10] Many research studies show that BPA was found in the blood and liver of animals and humans. [11,12] Currently, the human exposure limit set by the United States EPA is 50 μg kg^{-1} day^{-1} of BPA intake for drinking water [13]

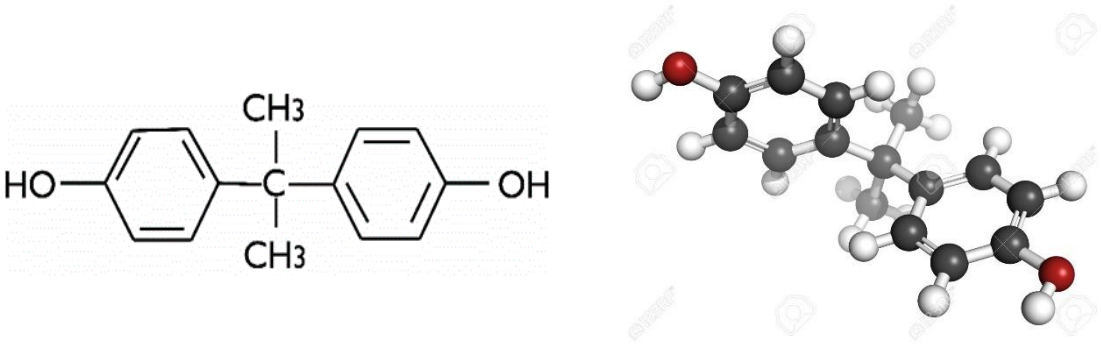

Figure 1.1 The molecular structure of BPA.

1.1.2 Perfluorooctanoic acid

PFOA, $C_8HF_{15}O_2$, also known as C_8, is used as a surfactant in the emulsion polymerization of fluoropolymers in industry. Figure 1.2 shows the molecular structure of PFOA. It persists indefinitely in the natural environment due to resistance to environmental degradation (metabolism, hydrolysis, photolysis or biodegradation), and is toxic to animals and humans. It can be absorbed through the skin or oral ingestion. [14] Recent studies are focusing on monitoring the global distribution and determination of the toxicology and mode of action of PFOA. [15] Animal studies showed that it could cause reduced birth size, physical, developmental delays, endocrine disruption, and neonatal mortality in mammals. [16] In 2007, research studies at the U.S. Food and Drug Administration (USFDA) investigated food contact papers as a potential source of PFOA to

humans and is ongoing. [17] In 2005, a USFDA study reported it had been detected in industrial waste, water, food, and polytetrafluoroethylene products, especially in the drinking water system and food packaging. [18] In 2007, the New Jersey Department of Environmental Protection issued a health-based guidance level of 0.04 μg L^{-1} in drinking water. [19] The Minnesota Department of Health recommends 0.014 μg L^{-1} day^{-1} for PFOA for adults. [20] The United States EPA reported health advisory level of PFOA for the drinking water is to 0.07 μg $L^{-1}day^{-1}$ in 2016. [21]

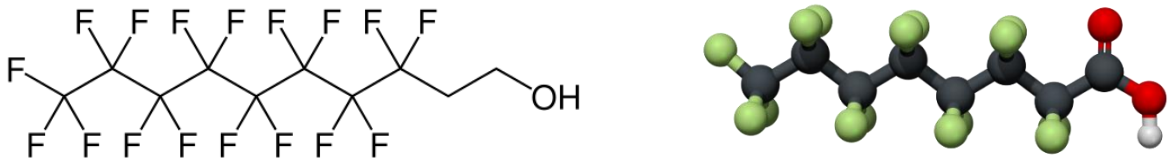

Figure 1.2 The molecular structure of PFOA.

1.1.3 Polychlorinated biphenyls

PCBs, $C_{12}H_{10-x}Cl_x$, were deployed as dielectric and coolant fluids in electrical systems, carbonless copy paper, and heat transfer fluids before the 1960s.[22,23] Figure 1.3 shows the series of molecule structures. Because of their longevity and toxicity to human beings, PCBs were classified as POPs and banned by the US Congress in 1979. [24,25,26] The United States EPA reported them as a likely cause of cancer, endocrine disruption, and neurotoxicity. They can be transported in the air and water due to their low vapor pressures. [27] In the ocean, PCBs become denser than water and concentrate on the increasing depth. People are usually exposed to food, breathing contaminated air and skin contact. [28] They can also cause skin conditions such as chloracne and rashes. Severe exposure accidents happened in Belgium, Italy, Japan, and the USA since the 1960s. In Japan, it was known as Yushō disease because over 1800 people were poisoned by 280 kg of PCB-

contaminated rice bran oil used as chicken feed in 1968. [29] In 2001, the United States EPA set the goal for drinking water's maximum contaminant level of PCBs is zero. [30]

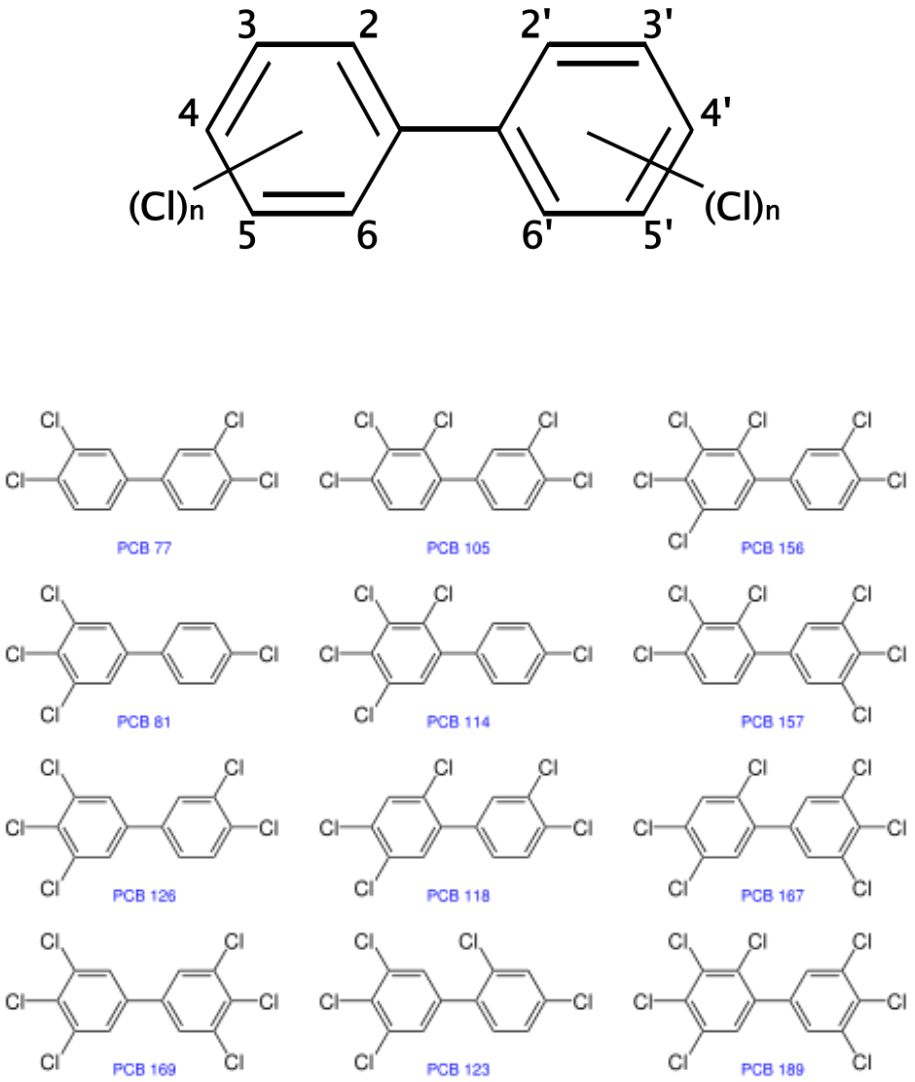

Figure 1.3 A series molecular structures of PCBs.

1.2 Introduction to adsorption technology for POPs removal

Nowadays, the world is facing water crisis due to lacking clean drinking water. With the fast development of various industries, a vast quantity of wastewater comes from industrial processes and is discharged into soils and water systems. [30] Surface water, groundwater, and industrial or household wastewater contain many different types of pollutants. [41] These pollutants include inorganic and organic compounds which can be more or less hazardous to humans, animals and plants. These pollutants usually contain cations, anions, oil, and organics which have toxic effects on organisms. Removal of these contaminants requires cost-effective technologies. Therefore, a variety of techniques have been developed in the past decades in dealing with wastewater treatment. [31]

There are two primary factors drive the development and implementation of water treatment technologies. (1) The discovery of new or rarer pollutants and the promulgation of new water quality standards. With a better understanding of the effect of chemicals on climate, wildlife and humans, people are more aware of new generation pollutants. For example, the United States EPA revises the national air and water quality standards and guide states and tribes almost every year. [32] It demands a higher efficiency and a wide range adsorption or filtration technology than traditional treatment process. (2) The cost of the industry approach to water treatment. Currently, it includes physical, biological, chemical and electromagnetic processes. Among these methods, adsorption technology has been well known for over centuries. Charcoal was considered as the first adsorbent for water purification. [33] The understanding of adsorption mechanism was studied by Brunauer, Emmett and Teller, McBain and Bakr, Langmuir, and later by Barrer, all in the early twentieth century. [34] They revealed that the adsorption is the accumulation of concentration of adsorbates at a surface and its driving force are the concentration gradient. After that, the

development and improvement of adsorption technology were best achieved by increasing the porous structure and interactive forces of physical attraction between the adsorbents and sorbates.

Currently, adsorption technology is believed to be a simple (one step), low-cost and effective (broad adsorption range) technique for wastewater treatment, and the success of the technique largely depends on the development of an efficient adsorbent. It has been found to be superior to other techniques for water re-use regarding initial cost, the simplicity of design, ease of operation and insensitivity to toxic substances. To achieve the anticipated function, adsorbents can be designed and modified in their compositions, structures, surfaces, and preparation methods. [35] These kinds of adsorbents can possess their special physical, chemical, and biological properties and exhibit some peculiar behaviors in the reactions, transformation, and removal of contaminants in water. In fact, the ability and efficiency of the adsorption technologies in water treatment also depends on the characteristics and functions of adsorbents. [36] Therefore, to transfer the species of pollutants for promoting the adsorption rate, we can design and prepare special composite adsorbents with multi-adsorptive functions which can remove different kinds of contaminations simultaneously. To eliminate some trace concentration of organic substances in water, we can synthesize some environmental-friendly sorbents and develop the similar technologies for water purification. [37] Also, modification of applied adsorbents, such as activated carbon (AC), clay, and polymers, undoubtedly is a more effective way to enhance the efficiency of water treatment process. [38,39]

1.2.1 Introduction to activated carbon

Due to its high surface area, porous structure, and specific surface reactivity, AC has been the most successful commercialized and widely used adsorbent in water purification all over the world. [40] The benchmark technology for contaminant removal from water/wastewater is AC-based

adsorbents. This adsorbent is highly inert and thermally stable under 200°C, and it can be used over a broad pH range. Although it has a high capacity of adsorbing various organic compounds and can be easily modified by chemical treatment to increase its adsorption capacity, AC has several disadvantages. It is expensive, and the powdered form is difficult to be separated from the aquatic system when it becomes exhausted, and the effluent reaches the maximum allowable discharge level. [40] Furthermore, the adsorption process transfers pollutants from one phase to another rather than eliminating them from the environment. So, the adsorbent should be regenerated or eliminated. The regeneration of exhausted AC by the chemical and thermal procedures are also expensive and result in the weight loss of the adsorbent. [41] Usually, the boiling point of various pollutants are higher than 200 °C, such as BPA (220 °C) and DDT (416.2 °C). This requires a better thermal stability for adsorbent. Another study showed that AC was ineffective to remove polar molecules. It binds to most substances through London dispersion forces. It means that it adsorbs larger molecules and non-polar molecules preferentially since they would have larger dispersion forces. Also, the oxygen associated with the surface of AC makes it more hydrophilic. So, it has a weak affinity for hydrophobic molecules which usually are polar molecules. For example, it has been reported that AC as a weak adsorption capacity for anionic metformin during drinking water treatment, which is one of the pharmaceuticals found in Lake Michigan waters. [42] Removal processes capable of eliminating these types of compounds are required. Table 1.1 shows that the advantages and disadvantages of AC.

Table 1.1 The advantage and disadvantage of commercial AC

	Advantage	Disadvantage
AC	Higher adsorption capacity for non-polar molecular, good thermal stability under 200°C, low price	(1) Poor recycle ability and thermal stability over 400°C. (2) Poor performance for polar molecules removal. (3) It must be regularly generated at a high temperature for recycle. If this is not economically viable, the activated carbon must be destroyed in an incinerator.

1.2.2 Introduction to natural zeolite

Since the original discovery of zeolitic minerals in the volcanogenic sedimentary rock, zeolitic tuffs have been found in many areas of the world. [43] In the past decades, natural zeolite has seen a variety of applications in adsorption, catalysis, building industry, agriculture, soil remediation, and energy. It has been estimated that the world natural zeolite consumption was 3.98 Mt in 2005 and reached 8.0 Mt in 2016. [44,45] Natural zeolite is hydrated aluminosilicate minerals with a porous structure and valuable physicochemical properties such as cation exchange, molecular sieving, catalysis, and adsorption. Figure 1.4 shows a typical natural zeolite (clinoptilolite). The application of natural zeolite with their properties and significant worldwide occurrence gains new research interests in environmental applications. [41] The use of natural zeolite for water and wastewater treatment has been realized and is still a promising technique in environmental cleaning processes. In the past decades, some review papers have indicated that the utilization of natural zeolite has been focused on ammonium and heavy metal removal due to the ion exchange property. [42] In recent years, natural zeolite and its modified forms have also been reported for removal of cationic organic pollutants from water systems.

Figure 1.4 The images of natural zeolite (clinoptilolite).

Some investigations using natural zeolite for cationic dyes adsorption have been reported, and Table 1.2 presents chemical composition and cation-exchange capacity of natural zeolite in the world.

Table 1.2 Chemical composition and cation-exchange capacity (CEC) of natural zeolite in the world. [42]

Zeolite	Chemical composition (%)								CEC (meq g^{-1})	Reference
	SiO_2	Al_2O_3	Fe_2O_3	CaO	MgO	Na_2O	K_2O	TiO_2		
Turkey clinoptilolite	70.9	12.4	1.21	2.54	0.83	0.28	4.46	0.089	1.6–1.8	[43]
Iranian clinoptilolite	70	10.46	0.46	0.2	–	2.86	4.92	0.02	–	[44]
Cuba clinoptilolite	62.36	13.14	1.63	2.72	1.22	3.99	1.2	–	–	[45]
Brazil mordenite	67.82	14.96	0.42	1.87	0.18	0.32	4.47	0.07	2.29	[46]
Italy phillipsite + chabazite	56.42	15.8	4.08	2.42	0.86	2.35	8.14	0.004	2.12	[47]

Turkey clinoptilolite	69.72	11.74	1.21	2.3	0.31	0.76	4.14	–	1.84	[48]
Chinese clinoptilolite	65.52	9.89	1.04	3.17	0.61	2.31	0.88	0.21	1.03	[49]
Chilean clinoptilolite +mordenite	67	13	2	3.2	0.69	2.6	0.45	0.2	2.05	[50]
Turkey clinoptilolite	69.31	13.11	1.31	2.07	1.13	0.52	2.83	–	–	[51]
Croatia clinoptilolite	64.93	13.39	2.07	2	1.08	2.4	1.3	–	1.45	[52]
Iranian clinoptilolite +mordenite	66.5	11.81	1.3	3.11	0.72	2.01	3.12	0.21	1.2	[53]
Turkey clinoptilolite	64.99	9.99	3.99	3.51	1.01	0.18	1.95	–		[54]
Chinese clinoptilolite	68.27	7.48	1.95	2.61	1.87	0.68	1.69	–	–	[55]
Turkey clinoptilolite	70	14	0.75	2.5	1.15	0.2	2.3	0.05		[56]
Chinese clinoptilolite	69.5	11.05	0.08	2.95	0.13	2.95	1.13	0.14	–	[57]
Ukrainian clinoptilolite	67.29	12.32	1.26	3.01	0.29	0.66	2.76	0.26	–	[58]
Ukrainian mordenite	64.56	12.02	0.95	3.58	0.68	0.94	2.03	0.23	–	[59]
Slovakian clinoptilolite	67.16	12.3	2.3	2.91	1.1	0.66	2.28	0.17	–	[60]
Croatian clinoptilolite	55.8	13.32	1.3	5.75	0.7	3.9	2.35	–		[61]
Ukraine clinoptilolite	66.7	12.3	1.05	2.1	1.07	2.06	2.96	–	0.64	[62]
Australian clinoptilolite	68.26	12.99	1.37	2.09	0.83	0.64	4.11	0.23	1.2	[63]

Apart from the presence of cations in water, anions and organic compounds are widely present in wastewater. [42] However, very few studies have been reported the removal of anions and organic compounds using natural zeolite. Benkli et al. investigated hexadecyltrimethylammonium bromide-modified clinoptilolite for removal of anionic dyes, reactive black 5, red 239 and yellow 176, in a fixed bed. The hexadecyltrimethylammonium bromide surfactant coverage on zeolites surface indicated that a layer formation is the most viable packing that enables maximum removal of the anionic dyes. [64] It also revealed the positively charged modification of natural zeolite have a significate impact on anionic dyes removal. ReyesSierra-Alvarez et al. investigated the removal of POPs with various zeolites. [65] It showed that the multiple sorbents for anionic heptadecafluorooctanesulfonic acid (PFOS) solution decreased as follows: hydrophobic zeolite > anaerobic granular sludge > activated sludge. However, the adsorption capacity of hydrophobic zeolite for anionic POPs is far below expectation.

1.2.3 Introduction to graphene-based materials

Graphene-based materials have been used in a variety of applications because of their useful properties, which can be listed as (1) possible to have various pores, (2) high thermal conductivity, (3) high chemical stability, (4) low thermal expansion coefficient, (5) high lubricity, (6) light weight, (7) high electrical conductivity, (8) nontoxic, (9) radiation resistant, (10) low absorption and high moderating for neutron, (11) high biocompatibility without the formation of blood clot, etc. By using graphene-based materials as one of the components, composites with various materials, plastics, ceramics, metals, as well as carbons, have been developed and used in multiple fields of industry such as electrochemistry, water purification, drug delivery and the photocatalyst. The successful applications of carbon fiber-reinforced plastics are well known to accelerate the development of modern engineering and technology. [67]

Graphene, the name is given to a two-dimensional sheet of sp^2-hybridized carbon [68], is a material made of carbon atoms which are bonded together in a repeating pattern of hexagons. Graphene's flat honeycomb pattern which results from long-range π-conjugation gives it many extraordinary characteristics. It has a large theoretical specific surface area (2630 $m^2 g^{-1}$), high intrinsic mobility (200 000 $cm^2 v^{-1}s^{-1}$), [69.70,71] high Young's modulus (~1.0 TPa) [72] thermal conductivity (~5000 $Wm K^{-1}$), [73] its optical transmittance (< 97.7%) and good electrical conductivity attracting the attention for applications such as for transparent conductive electrodes. [74] Graphene, experimentally studied over 40 years, has endless potential applications in almost every industry (like electronics, medicine, aviation and much more). Due to the relatively hard synthesis method and the high price of graphene, great efforts are taken to find effective yet inexpensive ways to produce and use graphene derivatives or related materials. [75]

Graphene oxide (GO) is a single-atomic-layered material, made by the powerful oxidation of graphite, which is cheap and abundant. It is an oxidized form of graphene, laced with oxygen-containing groups. The polar oxygen functional groups of GO render it hydrophilic so that it can be dispersible in water (and other solvents), and it can even be used to produce graphene. GO is synthesized by either the Brodie, [76] Staudenmaier, [77] or Hummers method, [78] or some variation of these methods. It is commonly sold in powder form, dispersed, or as a coating material on substrates. [79] It has been widely applied in field-effect transistors, sensors, transparent conductive films, clean energy devices, biomedical applications and the synthesis of the graphene-polymer nanocomposites. [80]

Reduced graphene oxide (rGO), with π-π stacking on the surface, has an excellent property as an adsorbent. Even though it has defects on the surface, rGO is the most low-cost solution to achieve the similar quality as graphene sheets. Usually, the reduction of GO is one of the critical reaction

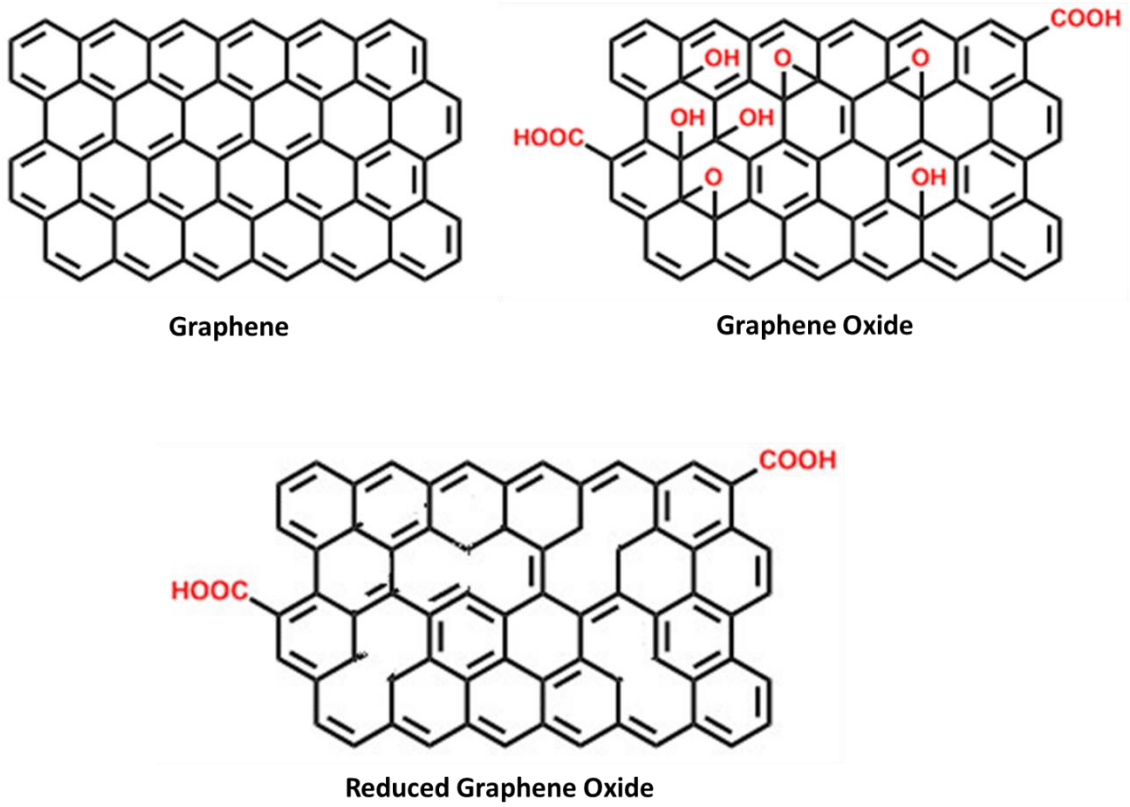

Figure 1.5 The molecule structure of graphene, GO and rGO.

for reduction of the oxygen-containing groups. Christopher W. Bielawski et al. summarized the reduction methods as follows: (1) chemical reduction by hydrazine monohydrate, hydrazine, sodium borohydride; (2) thermally-mediated reduction; (3) electrochemical reduction. [81] The technology platform of the proposed innovative material also allows targeting a single compound or a broad range of compounds depending on the application and modification on the functionalization of the particle. Figure 1.5 shows the molecular structure of graphene, GO and rGO.

Graphene based materials have been investigated during the last twenty years. Their composites have been applied to remove various organic pollutants, such as dyes, aromatic compounds, [82] naphthalene and 1-naphthol, bisphenol A, phenol, reactive black 5, tetracycline antibiotics, [83] and

oil. [84] Also, GO and rGO have a better thermal stability than AC, where morphological changes of GO/rGO exhibited a well-defined thermal stability up to 420 °C. [85] Different mechanisms may have simultaneous interactions between organic pollutants and graphene-based composites, including van der Waals type interactions, π–π bonds (cation–π bond), electrostatic interactions, hydrogen bonds and anion-cation interaction. [86] But the predominant adsorption mechanism is diverse for different organic chemicals (such as polar and nonpolar). For example, Ramesha et al. indicated that graphene and GO could be active adsorbents toward anionic and cationic dyes because of the high surface area and the negative surface charge. [87] The interactions between the charged dyes and adsorbents are electrostatic and van der Waals type interactions depending on the system. The mechanism is schematically represented in Figure. 1.6. [88]

Even though the graphene-based materials have a broad adsorption property for cationic, anionic and nonionic molecules, they are still hard to meet the requirement in the water treatment process. The crucial advantage of adsorption process is low-cost and broad adsorption property of primary source. The high price and toxicity of graphene-based materials should be considered. In the synthesis and adsorption process, some difficulties should be overcome, such as separation, recycle-ability, aggregation, distribution in the water solution, and easily irreversible agglomerates of graphene sheets.

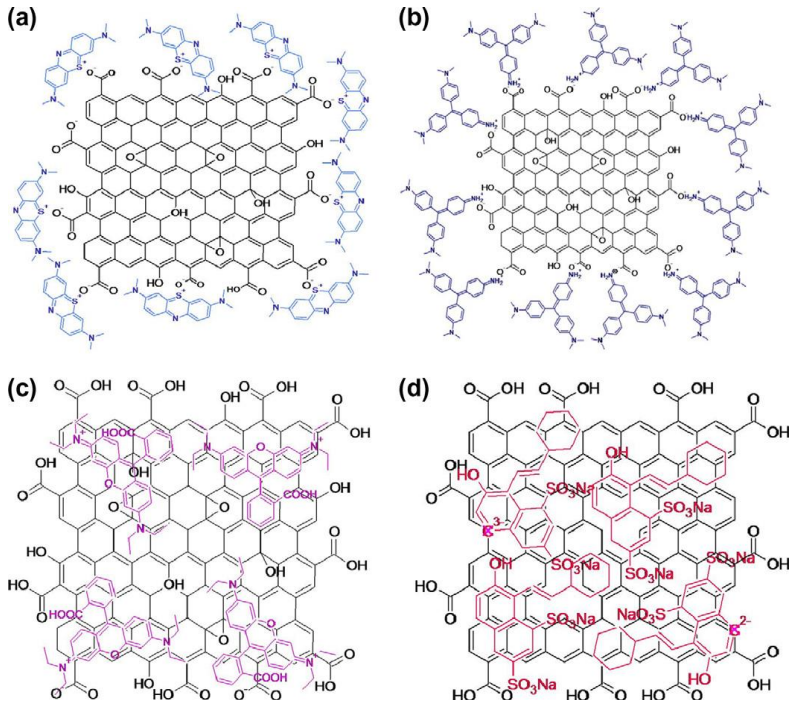

Figure 1.6 Schematics interaction interactions (a) EGO/MB, (b) EGO/MV, (c) EGO/RB, and (d) rGO/OG. [88]

Apart from that, single-layered GO suspensions demonstrate high adsorption capacity due to its homogeneity and large surface area. [89] However, its use as either suspended GO solution or dispersed nano-sized graphene-based materials is not practical for large-scale operation due to the issues with their removal and the resultant residues. The hydrophilicity of GO provided by a variety of oxygen functional groups on the surface, carboxyl, hydroxyl, and epoxy group, leads to high solubility in aqueous and organic solutions. [90] Previously, scientists were focusing on synthesis method or configuration of the graphene-based materials such as microspheres, hydrogels, membranes, magnetic nanoparticle composites to avoid their removal and the resultant residues in water purification. [92,93] However, the use of a graphene-based membrane or graphene composites, hydrogels are limited by multiple layered structures which can reduce the active sites, specific area and pores structure when compared with the single-layered structure.

1.2.4 Toxicity of graphene-based products

The toxicity of graphene-based products, especially graphene-based nanocomposites, has been studied with the application in the industry in recent years. It should be studied to ensure its safety to humans and wildlife. The discovery of graphene toxicity was evaluated with its safety profile and impact on human health by Ken Donaldson and his colleagues. They demonstrated that the graphene nanoplatelets "trigger the inflammatory response in lung cells and those found in the pleural space." [94] Moreover, GO, with higher solubility and dispensability, is widely used with nanomaterials for water purification. Recently, S. Zou et al. reported a systematic toxicity investigation of GO and revealed that it has a more significant impact on semi-adherent cell line and suspension cells. [95] Amedea B. Seabra et al. also summarized that GO is activated in the human organs and can agglomerate in the human respiratory system because of the screening of electrostatic charges and binding of the protein. [96] They revealed that the generation of reactive oxygen species in target cells is the most critical cytotoxicity mechanism of graphene. In summary, understanding the toxicity of graphene-based nanomaterials is vital for the sustainable development of water treatment process, and more studies on this topic are required. In general, the less graphene-based materials residues released during the water treatment process, the safer the water.

1.3 Literature review of graphene-based materials for POPs removal

The application of graphene-based materials as adsorbents for organic and inorganic removal have shown excellent results. M Paixão et al. summarized the adsorption of organic compounds by graphene, GO, and rGO shown in Table 1.3. [100]

Table 1.3 Adsorption of organic compounds by graphene, GO and rGO in water treatment process.

Adsorbent	Adsorbate	References
Graphene	naphthalene, 2-naphthol, 1-naphthylamine, phenol, p-toluenesulfonic acid, 1-naphthalenesulfonic acid, bisphenol A	[101,102]
GO	1,2,4-trichlorobenzene (TCB), 2,4,6-trichlorophenol (TCP), 2-naphthol, naphthalene, naphthalene, 1-naphthol	[103,104,105,106]
rGO	Phenanthrene, naphthalene, anthracene, pyrene, phenanthrene, biphenyl	[107,108,109,110]

1.3.1 Graphene-based nanocomposites for POPs removal

Recently numerous approaches have been investigated for the development of cheaper and more effective novel composite adsorbents. These composite materials deserve attention because they combine the properties and advantages of each of their components. They represent an exciting and attractive alternative as adsorbents and catalysts due to their high reactivity and excellent selectivity towards specific pollutant compounds. [36]

Several researchers have focused on the graphene-based nanocomposites by modification of graphene or GO and aim to increase the adsorption efficiency, capacity and widespread species of the contaminants in aqueous media. Two main topics have been researched. (1) Metal oxide nanocomposites. Usually, nanosized FeO, MgO, CuO_2, magnetic Fe_2O_3 and Fe_3O_4, and TiO_2 were chosen and synthesized with graphene-based materials as nanocomposites. Especially, the addition of magnetic Fe_3O_4 can achieve an easy manipulation in magnetic field for desired separation. Lu et al. and Wang et al. described a magnetic (Fe_3O_4)/rGO nanocomposite by one-step solvothermal synthesis or chemical deposition for dyes removal. [111,112] Srikanth et al. reported that the MgO decked multi-layered graphene (MDMLG) is synthesized and used as an adsorbent to remove Safranin O (SO) dye from water. [113] Yang et al. added FeO and Fe_2O_3 to GO and studied the

performance in the removal of 1-naphthylamine, 1-naphthol and naphthalene. [114] Moreover, photocatalyst by TiO_2 for POPs removal have been studied for years. Graphene-based materials have been impregnated into TiO_2 as nanocomposites and shown the adsorption and photocatalytic ability than pure TiO_2 nanoparticles. [115] (2) Monomers or polymers. Monomers can modify the graphene base materials surface, which increase the adsorption capacity of target pollutants. Zhao et al. reported that sulfonated graphene has been described as one of the most effective adsorbents for naphthalene and1-naphthol. [116] They also can be polymerized to modify and adjunct the layers of graphene-based materials. Dopamine, β-cyclodextrin, acrylic acid, vinyl alcohol, methyl methacrylate has also co-operated with graphene-based materials as adsorbents for organic pollutants removal. [117,118,119,120,121,122] Polymers, can be used as a crosslinked agent for surface modification of graphene-based materials. Graphene based materials can be formed as hydrogel, sponge, membrane, and bulk by polymerization. For example, chitosan, with primary and secondary hydroxyl groups, and highly reactive amino groups, is a multifunctional polymer. It was used as a cross-linking agent for graphene-based materials to fabricate graphene-based hydrogel or membrane. Yang et al. reported that combination of chitosan and GO has high efficiency in removal of various dyes and metal ions from aqueous solution. [117]

1.3.2 Graphene-based sponge, foam or hydrogel for POPs removal

The aim of fabrication of graphene-based film, sponge or hydrogel is to make porous and shape-plastic materials with a high specific surface area for versatility and recyclability during the water treatment process. Sun and Ruoff et al. studied hydrophobic spongy GO and rGO for removal of petroleum products, toxic solvents (toluene and chloroform). [124] Others have studied the hybrid foam with a combination of micro-AC or nanotube for removal of organic solvents. [125] With the addition of nanotube or micro-AC, the hybrid graphene-based foam has more porous volume and

active sites than bulks, which leads to an excellent adsorption performance than commercial AC. For example, Kim et al. presented carbon nanotube-bonded graphene hybrid aerogels that were prepared by growing carbon nanotubes on a graphene aerogel surface with nickel catalysts. It could remove both anionic and cationic dyes effectively from water. [126] Besides that, Huang et al. investigated self-assembly of the graphene-based hydrogel using a biocompatible polysaccharide as both a stabilizer and a physical cross-linking agent, which showed excellent dye adsorption and antibacterial capability. [127]

1.3.3 Graphene-based materials with sand composite

Another development, graphene–sand composites have been studied and applied as an adsorbent for organic containments. Sreeprasad et al. observed adsorption capacity of GO coated sand for the removal of rhodamine was 75.4 mg g^{-1}. It was also revealed that the particle size and the loading of GO had a substantial effect on the adsorption study. [128] Thalappil Pradeep et al. suggested that acetone could be used to regenerate for graphene–sand composite and presented an *in-situ* strategy for the preparation of graphene immobilized on sand using asphalt for water purification. They took Rhodamine-6G, a pesticide, as the model compound and showed that the adsorption capacity of graphene–sand composite is 75.4 mg g^{-1} while it is 44.7 mg g^{-1} for commercial AC. [129]

In conclusion, graphene-based composites are promising adsorbents as advanced materials for organic pollutants. The literature survey shows that they are alternatives to commercial AC. For economic aspect, simple, flexible and facile fabrication methods are attractive and preferred. However, A few many challenges should be overcome before practical application: (1) Adsorption test study. Most of the adsorption characteristics of graphene-based materials are restricted to batch experiment. Few reports about graphene-based materials are based on the column or fixed-bed dynamic adsorption. However, in practice, the results from fixed-bed column test for adsorbents

are critical in water purification. (2) The toxicity and biocompatibility of graphene-based materials and the chemicals used in the synthesis processes are rarely reported in the literature. The desorption of graphene-based materials during the adsorption process should be considered as a significant research topic, which can affect wildlife and humans. Moreover, fabrication methods may result in hazardous waste and poisonous gases. Green, environmental-friendly approaches should be designed. (3) Few studies focus on the regeneration and recyclability. The adsorbents should be performed to determine the reusability of an adsorbent which can contribute in evaluating of economic feasibility and effectiveness in practice. (4) Cost is of overriding importance in determining the application of graphene-based materials for large-scale industrial applications. The comparison between commercial AC should be included in cost-benefit analysis. (5) Moreover, very few adsorbents are available on multiple solutes system. The selectivity of graphene-based composites for different organic chemicals in different solvents should be pursued to provide insights into target species. A schematic diagram summarizing the challenges of graphene-based materials for POPs removal in water treatment are shown in Figure 1.7.

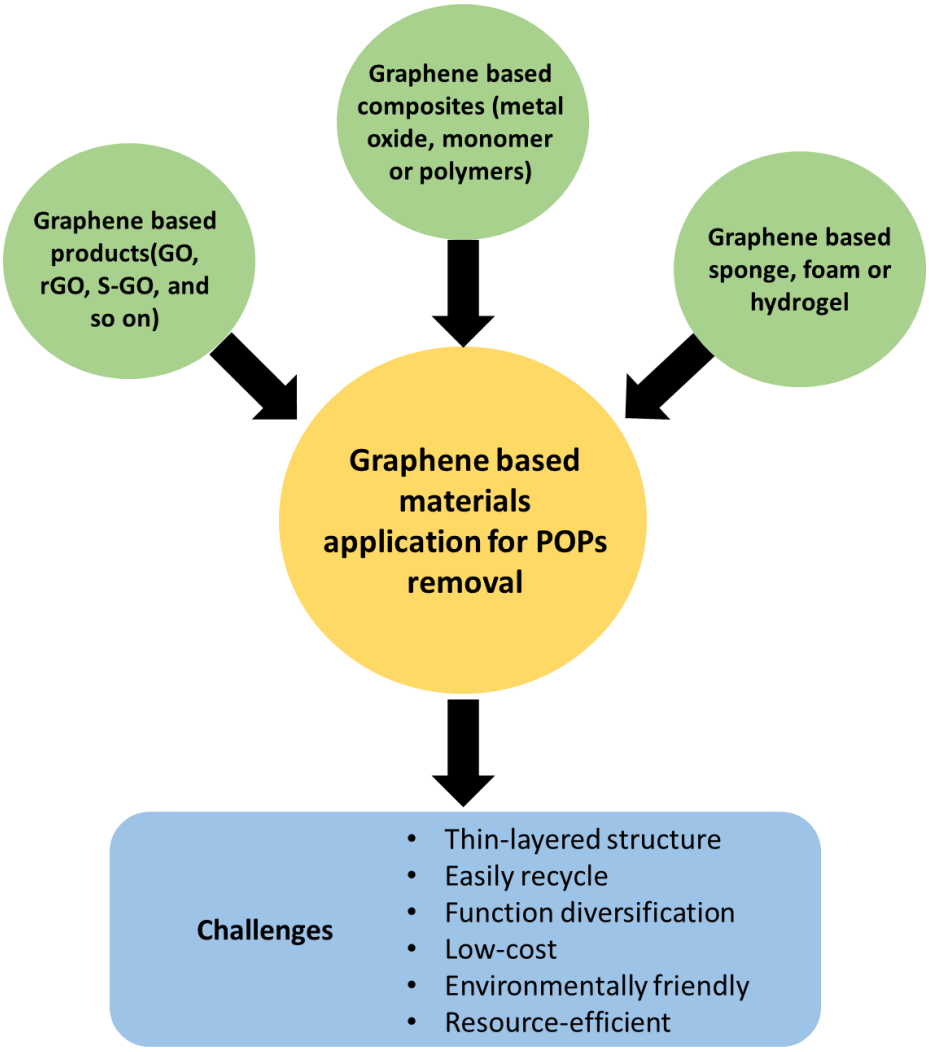

Figure 1.7 A schematic diagram summarizing the challenges of graphene-based materials for POPs removal in water treatment.

Chapter 2 Research Objectives, Motivation, Novelty and Methodology

2.1 Goal

The goal of this research is to fabricate a novel adsorbent made of GO/rGO attached on natural zeolite substrates for the removal of variably charged organic model compounds and POPs in aqueous solutions.

2.2 Objectives

The research evaluates novel particles by GO/rGO coated on the zeolite substrate and their subsequent enhancements for the removal of organic model compounds and emerging POPs from water with batch and fixed-bed column experiments. Zeolite serves as the substrate and low-cost core components for increasing the contact area of GO, while thin-layered GO/rGO on the surface of zeolite serve as adsorbents. It can be used as single particle type or a multiplexed filter with the ability to remove a wide range of organic contaminants. The objectives of this thesis are:

Objective 1: Develop a practical and convenient approach to coat GO sheets on the surface of natural zeolite. Ex-situ hybridization of graphene-based materials, spin coating, vacuum coating and drying coating, was developed, studied and compared by their adsorption performance and stability;

Objective 2: Evaluate the influence of pH, temperature, and flow rate in adsorption performance by performing column test experiments in laboratory scale;

Objective 3: Compare the adsorption behavior of anionic, cationic, and non-ionic surfactants on GO coated natural zeolite in order to determine the effect of the surfactants on organic model compounds removal;

Objective 4: Modify natural zeolite surface to enhance the interaction between zeolites and GO for increasing loading and stability of GO attached on zeolites;

Objective 5: Reduce GO on the natural zeolite to increase the adsorption capacity for organic model compounds and POPs.

Objective 6: The modeling of adsorption mechanism of Reduce GO on the natural zeolite for organic model compounds removal.

2.3 Motivation

As described above, the adsorption phenomenon of graphene-based materials is due to the surface forces (H bonding, electrostatic interactions, van der Waals forces, *etc.*). Single-layered GO suspensions demonstrate high adsorption capability for POPs due to its homogeneity and large surface area. [96] The hydrophilicity of GO, which is provided by a variety of oxygen functional groups on the surface, carboxyl, hydroxyl, and epoxy group, leads to high solubility. [97] The exclusive use of layered GO sheets with no substrate is not applicable because residues would remain in the water. It is of concern as GO has moderate toxicity toward human and wildlife. [98]

Previously, scientists were focusing on synthetic methods for appropriate configurations of the graphene-based materials, such as bulks, hydrogels, membranes, magnetic nanoparticle composites. It is aimed to avoid resultant residues of graphene-based materials in water purification. [111-120] However, the use of graphene-based bulks, membranes hydrogels were limited

by multiple layered structures. The application of magnetic nanoparticles composites with graphene-based materials could not avoid the agglomerations in the aqueous solutions. So, it could not be used in the fixed-bed water treatment system.

Meanwhile, the increase of adsorption capacity of universal adsorption composites is the result of the sum of the capabilities of its sources. The introduction of graphene-based materials reduces the surface area of substitutes and dramatically increases the porosity and surface area of the adsorbents. They can drastically increase the adsorption capacity and broaden the adsorption ability of adsorbents. For example, even 1wt% graphene-based materials attached to a substrate can dramatically increase the adsorption capacity.

Natural zeolite, as environmentally and economically acceptable material, has a unique three-dimensional porous structure which provides a broad application in industries. It is compact and requires cheap and straightforward maintenance in full-scale water treatment processes. It can be easily modified by techniques such as acid treatment, ion exchange, and surfactant functionalization. [121] In this thesis, the natural zeolite is used as a substrate for supporting the GO/rGO sheets on the surface. It has not been reported as a substrate for graphene-based materials for POPs removal.

2.4 Novelty

The proposed idea of loading graphene-based product on natural zeolite and utilizing it as a single particle for the removal of pollutants from water has never been reported. It should be noted that, so far, no commercial product is capable of simultaneous and effective removal of a broad range of organic compounds. The technology platform of the proposed innovative material also allows

targeting a single compound or a broad range of compounds depending on the application and modification on the functionalization of the particle.

1. A new method for coating GO on natural zeolites surface using drying process.

A simple and effective coating method for fabrication of graphene composites is required for the industrial application. In chapter 3, a facile dry coating method of GO coated on natural zeolite have been reported for the first time. It was compared with the spin coating and vacuum coating methods. Moreover, the loading of GO on natural zeolites, its surface adsorption properties, performance evaluation and experiment condition have also been reported for the first time.

2. Using surfactants to enhance the interaction between the zeolite and GO.

Adsorbent surface modification of zeolite and graphene-based materials by surfactants has been comprehensively investigated for dye removal, respectively. [122-123,124] They focused on the improvement of the adsorption capacity for a specific adsorbate and the interaction between the surfactants and surface of zeolite or graphene-based materials. However, a broad range of adsorption for dyes and POPs and the interactions between zeolites and graphene-based materials have not been reported. A strong interaction between GO and the zeolite can lead to a higher loading of GO which can lead to a better adsorption performance. Meanwhile, it can reduce the desorption of GO from the zeolite. In chapter 4, variable-charge surfactants are used as an agent to increase the interactions between GO and the zeolites. The study on the effect of variable-charge surfactants on the stability of adsorbents and the adsorption performance of anionic, cationic and non-ionic organic model compounds have been reported for the first time.

3. Using 3-aminopropyltriethoxysilane (APTES) to enhance the attachment of GO on zeolites surface and increase the coating layers of GO.

In chapter 5, APTES was introduced to modify the zeolites surface from negative to positive charges for the first time, which enhance the bonding between the GO and the zeolite by electrostatics instead of hydrophilicity. It was inspired by the studies of APTES modification of SiO_2. [125,126,127] The aims of surface modification are: increasing the loading of graphene-based materials on the zeolites surface to improve their adsorption properties and enhance the bonding between the graphene-based materials and zeolites to avoid desorption.

4. *In-situ* partial reduction of GO on the natural zeolite by a physical method(microwave) and chemical method (vitamin C).

RGO, with sturdy π-π stacking on the surface, has a better adsorption ability than GO. In this study, two methods for *in-situ* reduction of GO on natural zeolite: by using microwave heating and vitamin C, were studied and evaluated. The *in-situ* reduction of GO on zeolites surface can improve the adsorption capability of adsorbents by environmental-friendly approaches and reduce the cost of reduction. In 2010, Chen et al. reported that reduction of GO to graphene could be achieved with the assistance of microwaves in the organic solvents. [130] In the same year, Zhou Li et al. synthesized the well-controlled go by dry microwave treatment of a free-standing GO film without using reducing agents. [131] Later, the microwave treatment for GO reduction was applied on graphene-based composites including GO based metal nanocomposites, GO with polymers or carbon nanotubes, and GO surface modification. [132] However, the GO reduction on the macrostructure materials haven't reported. In 2012, M.J. Fernández-Merino et al. reported vitamin C has an excellent reduction ability as an ideal substitute for hydrazine in GO suspensions reduction. [134] A simple, safe and effective approach open the perspective of using the go in practical application in large-scale production. This approach applied in a fundamental study of GO, GO composites nanomaterials synthesis. In chapter 5, it has shown that two approaches, *in-*

situ microwaved and vitamin C reduction of GO on zeolites surface, are reliable and promising large-scale production approaches to fabricate rGO attached to zeolites surface.

In general, to achieve the goal of this research, coating method, surfactants modification and the improvement of the adsorption performance of the adsorbents have been studied. Figure 2.1 shows the outline of this thesis.

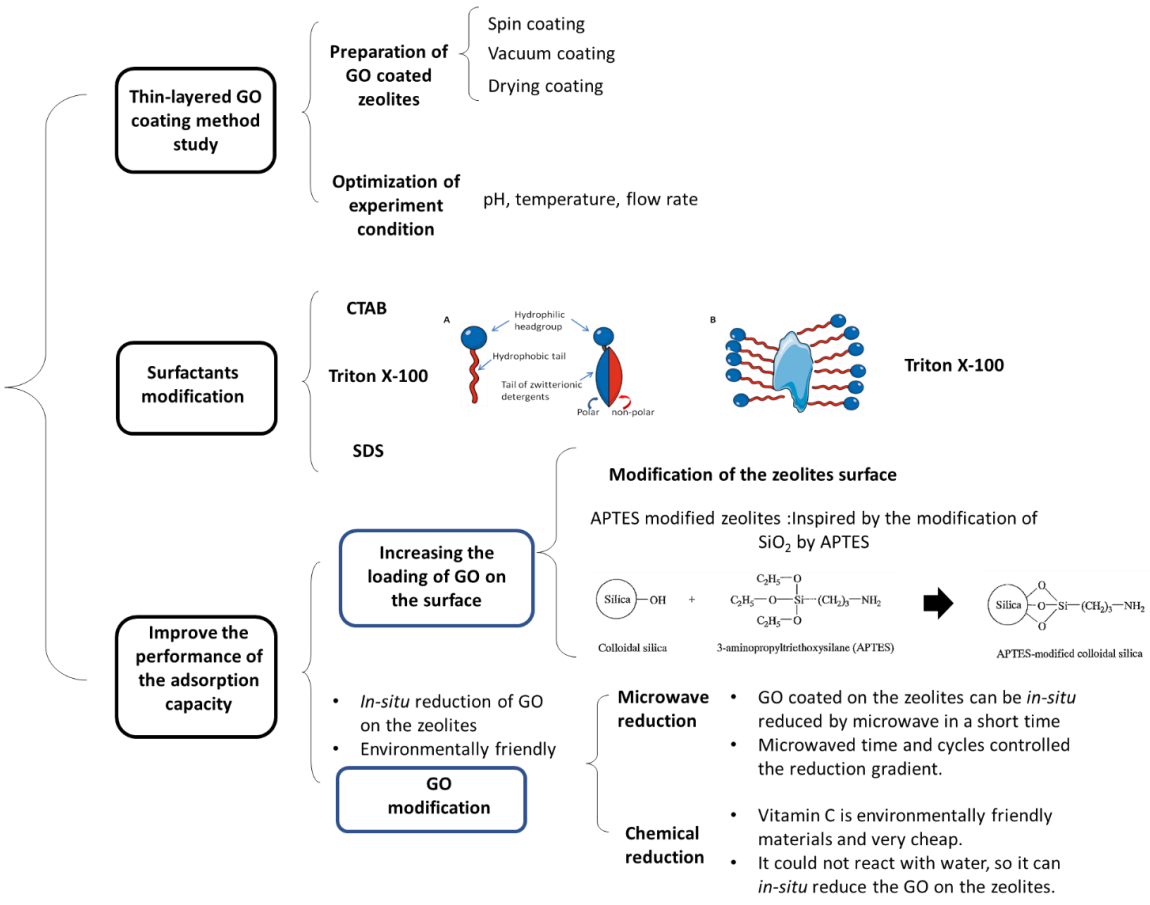

Figure 2.1 Outline of the thesis.

2.5 Experimental

2.5.1 Adsorption experiment

Column experiment

The column experiment was conducted in glass columns of 21 cm length and 2 cm internal diameter. A fixed-bed was created by placing a piece of gauze at the bottom of the column, dry loading the media into the column to a bed height of 13 cm and placing a piece of gauze at the bottom of the column, shown in Figure 2.2. Before filtration, the column was connected to a peristaltic chemical metering pump, and the pH of the adsorbents was adjusted to 7 with 0.1 M NaOH, then rinsed with 1L deionized water. A 1ml of 40mg L^{-1} organic model compounds and POPs solutions were prepared to test the removal efficiency of adsorbents, individually. The solution flowed into column (downward flow) at a rate of 5 mL min^{-1}.

The saturation experiment was studied by the same concentration of adsorbate. To observe reactions with actual POP contaminants, 200µg L^{-1} BPA, PFOA and PCB solutions were prepared. The following equations were used for the calculation of the removal efficiency and adsorption capacity of the absorbents.

$$Removal\ efficiency\ (\%) = \frac{(C_0 - C_f)}{C_0} \times 100\% \quad (1)$$

$$Adsorption\ capacity\ (mg/g) = \frac{(C_0 - C_t) \times V}{m} \quad (2)$$

All the experiments were performed in triplicate, and data were presented as mean ±SD (standard deviation). The removal efficiency and adsorption capacity were calculated by the equations above (1) and (2), where C_0 (mg L^{-1}), C_f and C_t (mg L^{-1}) are the initial, final and outlet concentration for dyes and POPs, V (L) is the solution volume and *m* (g) is the weight of GO or rGO.

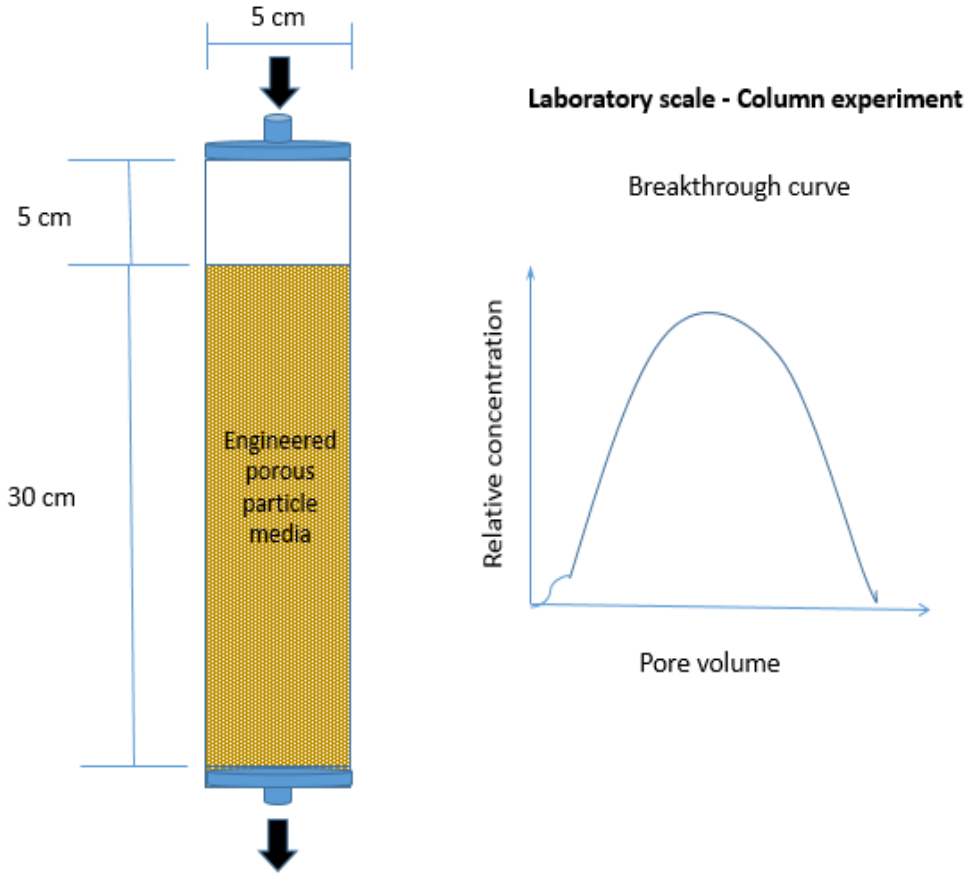

Figure 2.2 The column condition in laboratory scale (supplied by Dr. Marcia R. Silva)

Batch adsorption

A 1 g of adsorbent was added to 100 ml of organic model compounds solution of the desired concentration at pH 6.0 in 250 ml reagent bottles and were agitated at 150 rpm for 48 h at room temperature (25 ± 2 °C) in a mechanical shaker. The concentration of dyes was measured by times. The equilibrium (q_e) was calculated by the equation (1) and (2). The batch adsorption study was replicated thrice for each of the adsorbents. Schematic diagram of batch experiment is shown in Figure 2.3.

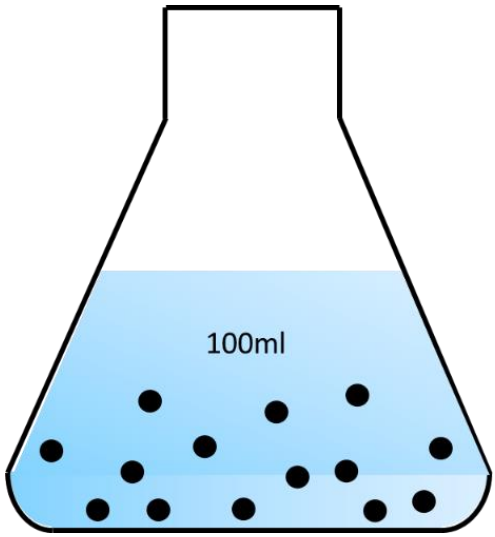

Figure 2.3 Schematic diagram of batch experiment.

2.5.2 Desorption of GO and rGO from the natural zeolite

To measure desorption of graphene-based materials from zeolite, 10 g of samples were immersed in 100 ml water and placed on a shaker table for 24 hours at 200 rpm. The solid was removed by filtration through 0.2 μm filters (Whatman) using a vacuum pump and rinsed the adsorbents by deionized (DI) water for three times. The weight loss of adsorbents was measured to determine the stability of GO and rGO on the zeolites surface.

2.5.3 Thermal regeneration

Thermal regeneration of the adsorbents was carried out in an electric furnace. According to the literature, rGO has an excellent thermal stability under 550 ^{o}C and the melting points of PCB, BPA, and PFOA are lower than 500 ^{o}C. So, the samples were placed in the electric furnace at 500 ^{o}C under an N_2 atmosphere for 1 hour with at 10 ^{o}C min^{-1}. The removal efficiency of dispersed blue 26 (melting point at 217 ^{o}C) was used to test the regeneration ability of our samples.

2.6 Analytical Methods

Raman spectroscopy (Raman) was carried out using a Horiba XploRA Plus Raman microscope with a 532 nm HeNe laser with three accumulations of 10 seconds each. Infrared (IR) spectra were collected with a Shimadzu Vector Fourier transform spectrophotometer at a resolution of 4 cm^{-1} with 40 scans per spectrum. X-ray photoelectron spectroscopy (XPS) spectra of samples were obtained using an HP5950A ESCA spectrometer with monochromatic Al Kα radiation as the X-ray source. Zeta potential was measured using a zetasizer nano ZS (ZEN3600, Malvern), using water as background. The morphologies of as-prepared samples were characterized by scanning electron microscopy (SEM) and energy-dispersive X-ray spectroscopy (EDS), performed on a Hitachi S-4800 equipped with a Bruker EDS detector. EDS element mapping was checked under 200 kV accelerating voltage with an image resolution of less than 0.08 nm and energy resolution of 0.35 eV.

The concentration of methylene blue and disperse blue 26 was detected by a UV visible spectrophotometer (UV-1800) Thermo Scientific. The concentration of sodium fluorescein was determined by the Synergy H4 multi-mode plate reader. The pH of solutions was measured by a pH meter model OAKTON 700. Quantification of total BPA and PFOA was carried out by liquid chromatography coupled with tandem mass spectrometry through a turbo spray interface operating in the negative ion mode. The mobile phase consisted of water and methanol at a flow rate of 0.4 mL min^{-1}. The elution program was as follows: linear gradient from 40% to 60% of methanol for 20 min and then reverting to initial conditions allowing 10 min for column stabilization. The eluates from the analytical column were diverted by the switching valve to waste, except for the elution window from 9 to 11 min. The injection volume was 10 µL, and the temperature for the analytical column was set at 35 °C. [134,135] Quantification of PCB was detected with GC-MS

(Shimadzu GCMS-QP2010 plus). The extraction of PCBs from water samples using method 3510 (separatory funnel) extraction method for subsequent analysis by SW-846 EPA Method 8082A. [142]

Chapter 3 A study of fabrication methods of graphene oxide coated on the natural zeolite

3.1 Introduction

The fabrication methods of graphene-based inorganic composites including nanoparticles were summarized by Zhang et al. in 2012. [136] Enormous efforts have been made to enhance the properties for a comprehensive application like electronics, storage, and water purification and so on. Metals like Au, Pt, Ni; oxides like TiO_2, SnO_2, MnO_2, SiO_2 have been composed with graphene-based materials. [110-121] The fabrication methods can be classified as *ex-situ* hybridization and *in-situ* crystallization. The graphene-based sheets can encapsulate or coat on the surface of the material through *ex-situ* hybridization. The *ex-situ* hybridization of graphene derivations and materials are usually by van der Waals' force, covalent and non-covalent bonding and electrostatic adsorption through merely mixing of GO solutions and materials. It is considered as a simple and practical approach to fabricate graphene-based composites. The *in-situ* crystallization of graphene-based composites can be achieved through chemical reduction, electroless deposition, electrochemical deposition, self-assembly, sol-gel method, thermal evaporation, and hydrothermal methods. [136]

This chapter aims to develop a practical and convenient approach to coat GO sheets on the surface of the natural zeolite. The proposed idea of loading graphene-based materials on the natural zeolite and utilizing it as a single particle for the removal of POPs from water have never been reported. Three *ex-situ* hybridization methods including spin coating, vacuum coating and dry coating method were developed and studied. Characterization of the adsorbents was done using FT-IR, SEM, zeta potential, Raman, EDX and BET studies. The loading of GO on zeolites surface,

physical stability and the adsorption performance of the samples made by these three methods were systematically studied. It should be noted that, so far, no commercial product is capable of simultaneous and effective removal of variably charged organic compounds. The removal efficiencies of organic pollutants including BPA, PCB, and PFOA were also examined by column experiments. Finally, the optimization of operation conditions including pH value, flow rate and temperature was determined by column experiments.

3.2 Experimental

3.2.1 Materials

Australian natural zeolite (diameter: 0.7-1 mm, chemical composition: 68.26% SiO_2, 12.99% Al_2O_3, 4.11% K_2O, 2.09% CaO, 1.37% Fe_2O_3, 0.83% MgO, 0.64% Na_2O, 0.23% TiO_2, Zeolite Australia Ltd.), GO (ACS Materials), granular activated carbon (coconuts) (GAC, General Caron corporation), the dyes, which are disperse blue 26 (Crescent chemical), methylene blue (Electron Microscopy Sciences), and sodium fluorescein (Pfaltz &Bauer), are chosen as the representations for neutral, cationic, and anionic organic model compounds. Bisphenol A (BPA, ≥99%, Sigma-Aldrich), perfluorooctanoic acid (PFOA, 96%, Sigma-Aldrich), polychlorinated biphenyl (PCB, Aroclor 21, 200µg mL^{-1}, Sigma-Aldrich).

3.2.2 Clean zeolite

Raw zeolite was cleaned before fabrication. 40 g of raw zeolite was added into a large beaker and filled in with 500 mL of DI water. Beaker was then placed in the sonicator and set the frequency as 37 kHz for 15 minutes. This step was repeated for ten times. (The zeolite was rinsed by 500ml for each time) The sonicated zeolite was immersed in 200 mL DI water in a large beaker and microwaved at low power for 15 minutes to bring the DI water to a low boil. This step was repeated

for ten times. The beaker was refilled with 200 ml DI water before microwave treatment. Finally, clean zeolite was rinsed and dried in the oven at 100 ^{o}C for 24 h.

3.2.3 Spin coating, vacuum coating and drying coating method

1.0 mg mL^{-1} and 2.5 mg mL^{-1} GO aqueous solution was made by sonication of the solutions for at least 2 hours at 40~60 ^{o}C. Spin coating method: 15ml of 1mg $\cdot mL^{-1}$ aqueous solution of GO was poured on top of 15 g clean zeolite and was set to spin at 600 rpm for 5 min to cause uniformly spreading of the solution onto the zeolite. Then it was sped up to 800 rpm for 5 min to thin the solution layer, and finally the spin coated GO on the zeolite (SCGZ) was kept at 1600 rpm for 5 min to dry the samples. Vacuum coating method: 15g of clean zeolite was mixed with 15ml of 2.5mg $\cdot mL^{-1}$ aqueous solution of GO. Then the mixture was poured into a filtration apparatus with a filter membrane (diameter 0.45 μm), and the vacuum was held for 10 minutes. Finally, vacuum coated GO on the zeolite (VCGZ) was placed in an oven at 100^{o}C for 24 h. Dry coating method: 15 ml of 2.5 mg mL^{-1} GO solution was added to the beaker containing 15 g of clean zeolite and shaken on a shaker for 120 mins at 150 rpm. Finally, dry coated GO on the zeolite (DCGZ) was dried at 100^{o}C for 24h. All the samples were rinsed with ethanol for three times and by water three times to remove the extra GO on zeolites surface. The theoretical loading of GO on the zeolite was listed in Table 3.1.

Table 3.1 Method of investigation of GO coated on the zeolite

Methods	Process	Machine	Theoretical loading of GO
Spin coating	Zeolite was added in a petri dish with GO solution, then was spanned at a certain speed.		1 mg g^{-1}
Vacuum coating	Zeolite was immersed in the GO solution, then dried by vacuum system.		2.0 mg g^{-1}
Dry coating	Zeolite was immersed in the GO solution and, shaken on the orbital shaker for 2hours.		2.5 mg g^{-1}

3.3 Results and Discussion

3.3.1 Characterization

The morphology of the natural zeolite (a), SCGZ (b), VCGZ (c), and DCGZ (d) was determined by SEM shown in Figure 3.1, respectively. The rough and porous structure of the natural zeolite and SCGZ can be seen clearly in Figure 3.1 (a) and (b). It is hard to find large GO sheets on SCGZ due to a lower loading of GO (1 mg mL^{-1}). After the combination with GO and the zeolite by vacuum and dry coating methods, GO presents the sheet-like structure with a smooth surface on the zeolite which has a much more continuous surface, shown in Figure 3.1 (c) and (d). [137] EDS elemental mapping of carbon for DCGZ revealed that the carbon layers were partially uniformly dispersed on the surface of zeolite, as shown in Figure 3.1(e) and (f).

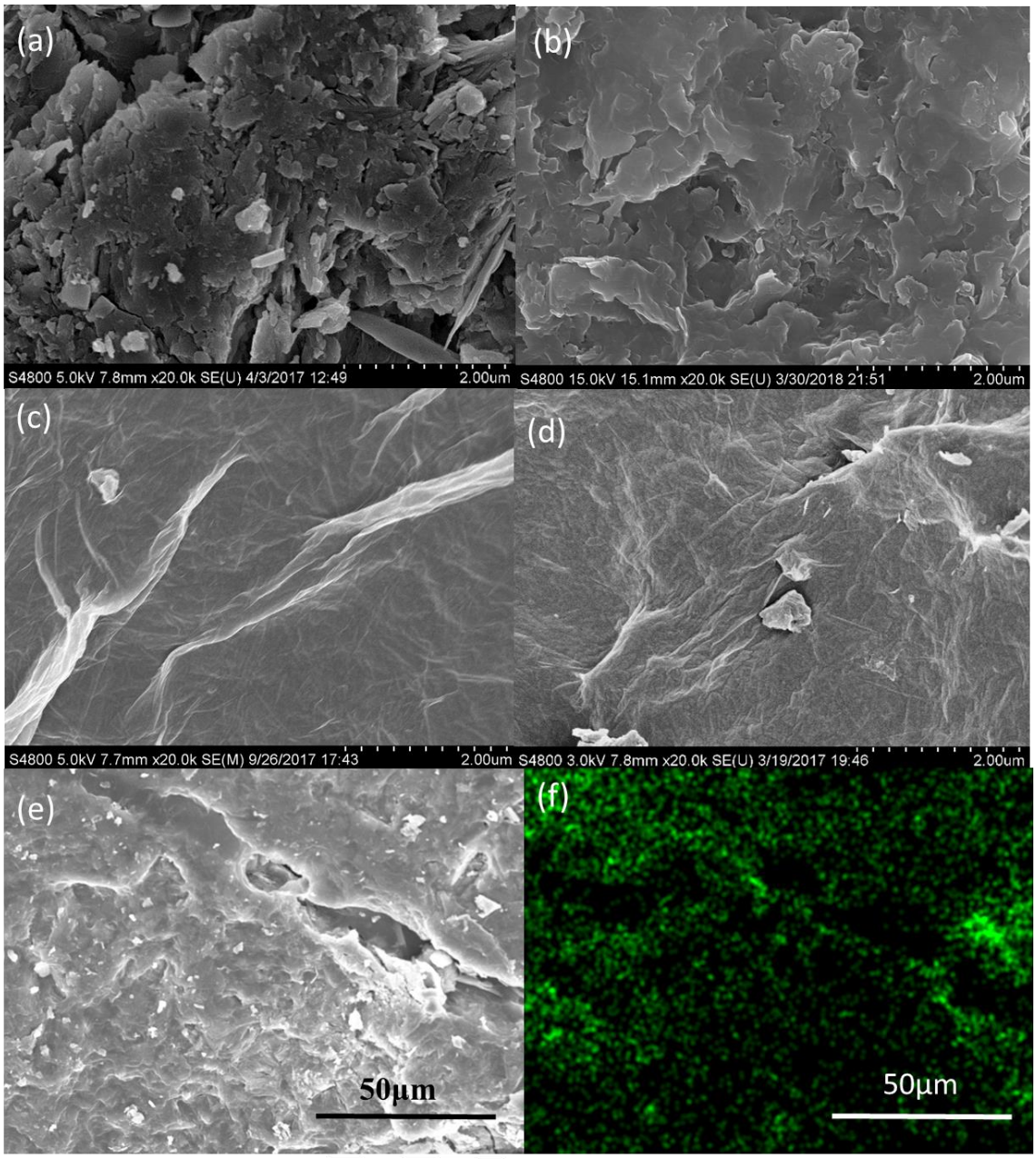

Figure 3.1 SEM images of natural zeolite (a), SCGZ (b), VCGZ (c), DCGZ (d), and EDX element mapping of carbon for DCGZ is shown in the (e) and (f).

The Raman and FT-IR spectra of the DCGZ are shown in Figure 3.2. The Raman mapping is used to map the sample surface with lateral resolution as good as 1 µm. This micro-scale Raman mapping is used to check GO distribution on zeolites surface. The micro-scale Raman map of the

DCGZ shows two peaks: The G-band of GO appears at 1594 cm^{-1} and that of D band at 1341 cm^{-1}. Figure 3.2 also shows the FT-IR spectra of DCGZ. In the range of DCGZ, the broadband at 3427 cm^{-1} can be assigned to the stretching vibration of the -OH groups situated on the surface of GO. The peak at 1725 cm^{-1} corresponds to the -COOH functional groups and the appearance of a peak at 1631 cm^{-1} is owing to the skeletal vibration of unoxidized graphitic domains. The peak at 1393 cm^{-1} is attributed to the -OH deformation peak and bending vibration of interlayer water. The C-O (epoxy) and the C-O (alkoxy) stretching vibration peak of GO appear at 1231 and 1061 cm^{-1}, respectively.

Physical properties of clean zeolite, GAC (coconuts), SCGZ, VCGZ and DCGZ are summarized in Table 3.2. The surface areas, volumes and pore sizes were calculated by the Density Functional Theory (DFT) approach. It shows that the specific pore volume and surface area follows the trend: GAC > DCGZ > VCGZ > SCGZ > clean zeolite. GAC as a successfully commercialized adsorbent, has a remarkable 0.42 $cm^2\ g^{-1}$ specific pore volume and 1231 $m^2\ g^{-1}$ specific surface area. Also, it displays that the loading of GO on zeolites surface has a strong impact on pore structure. The higher of loading of GO, the higher specific pore volume and surface area it exhibits. Compared with the clean zeolite, the specific pore volume and surface area of DCGZ were increased from 3.79×10^{-2} to 0.11 $cm^3\ g^{-1}$ and 14.7 to 159.4 $m^2\ g^{-1}$, respectively. It demonstrates that GO coating layers increases the pore volume and surface area significantly and it may result in the improvement for the organic model compounds and POPs adsorption capacity.

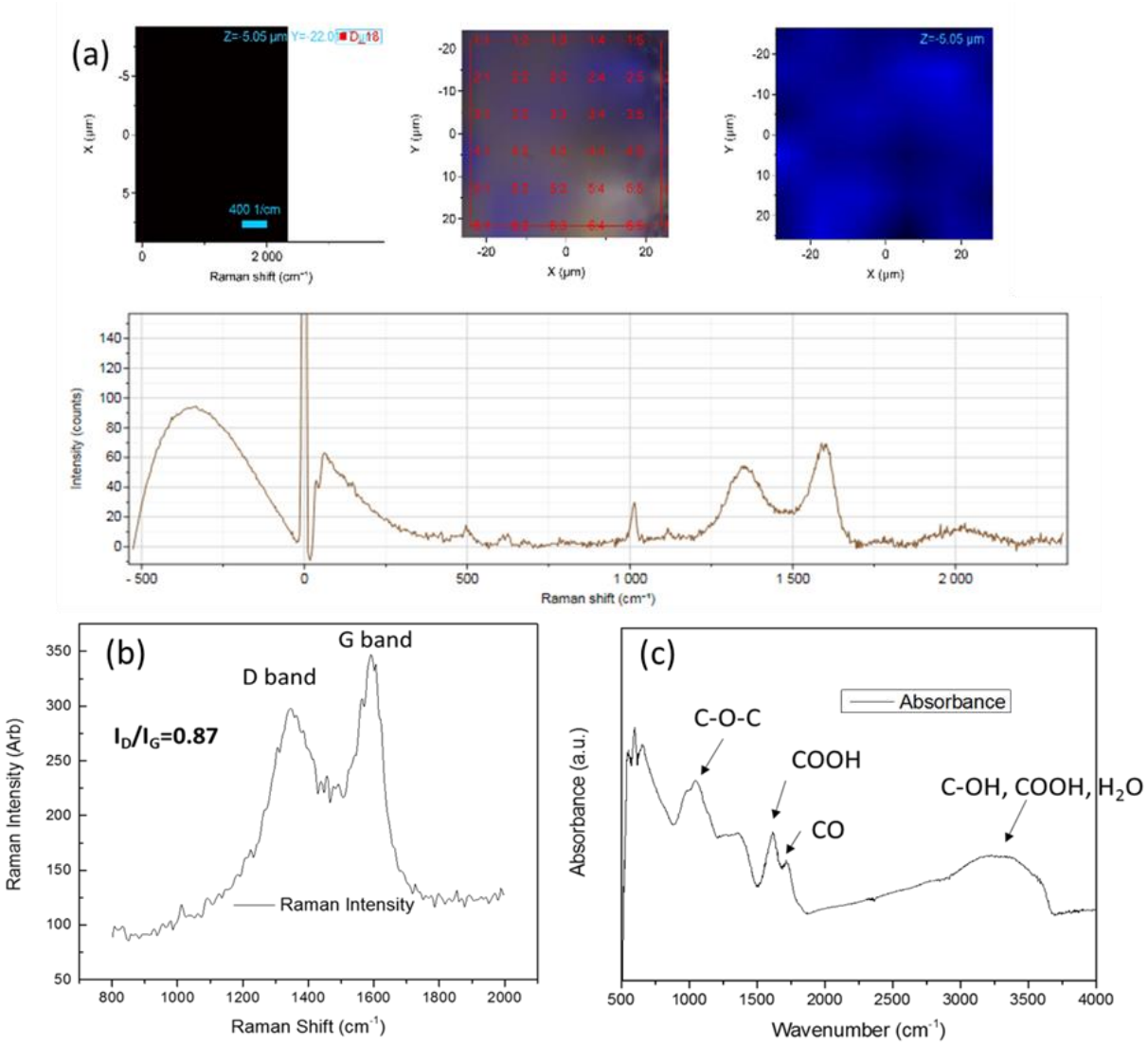

Figure 3.2 Micro-scale Raman mapping of the DCGZ. The blue color corresponds to high intensity of GO, Z is the depth 5.05 µm and the area is 400 µm^2 (a). Raman spectra and FT-IR of DCGZ (b, c).

Table 3.2 BET surface and pore structure characteristics of adsorbents

Samples	Pore structure		
	V_{DFT} ($cm^3 g^{-1}$)	S_{DFT}($m^2 g^{-1}$)	Pore size (Å)
Clean zeolites	3.79×10^{-2}	14.7	9.4
GAC	0.42	1231	5.11
SCGZ	5.14×10^{-2}	45.32	7.37
VCGZ	9.31×10^{-2}	89.4	5.21
DMGZ	0.11	159.4	5.95

The surface charges of clean zeolite, SCGZ, VCGZ, and DCGZ in aqueous solutions were further examined by zeta potential measurements at different pH values ranging from 2.0-11.0. It is used for explanation of the interactions between GO and the zeolite, as well as predicting the adsorption capability of our adsorbent for variably charged POPs adsorption. As shown in Figure 3.3 (a), the zeta potential values of GO are from -14 to -53 mV at pH range from 2 to 11, which has also been reported by Yang Shubin et al.. [137] The negative charges originated from the ionization of the carboxylic acid and phenolic hydroxy groups located on the GO. The values of zeta potential for clean zeolite are negative, too. The mechanism of coating GO sheet on the zeolites surface is mainly the interactions of the interlayered hydrogen bonds for facilitating GO sheet adherence to the zeolites surface. [137]

The values of zeta potential for targeted organic model compounds and POPs are shown in Figure 3.3 (b). It reveals that the values of the zeta potential of methylene blue and PCB are similar and in the range from 15 to -9.5 mV from pH 2 to 11. The values of the zeta potential of sodium fluorescein flows the trend of the values for PFOA. Moreover, the values of the zeta potential of disperse blue 26 are comparable with the ones of BPA. These can be explained by the similar molecule structure or charges of organic model compounds and POPs. The molecule structures of

methylene blue disperse blue 26 and sodium fluorescein are shown Figure 3.3 (d). Finally, the values of the zeta potential for clean zeolite, SCGZ, VCGZ and DMGZ are shown in Figure 3.3 (c). It shows that the value of zeta potential of the samples depends on the loading of GO coated on the zeolites surface. The higher the loading of GO, the lower the value of zeta potential.

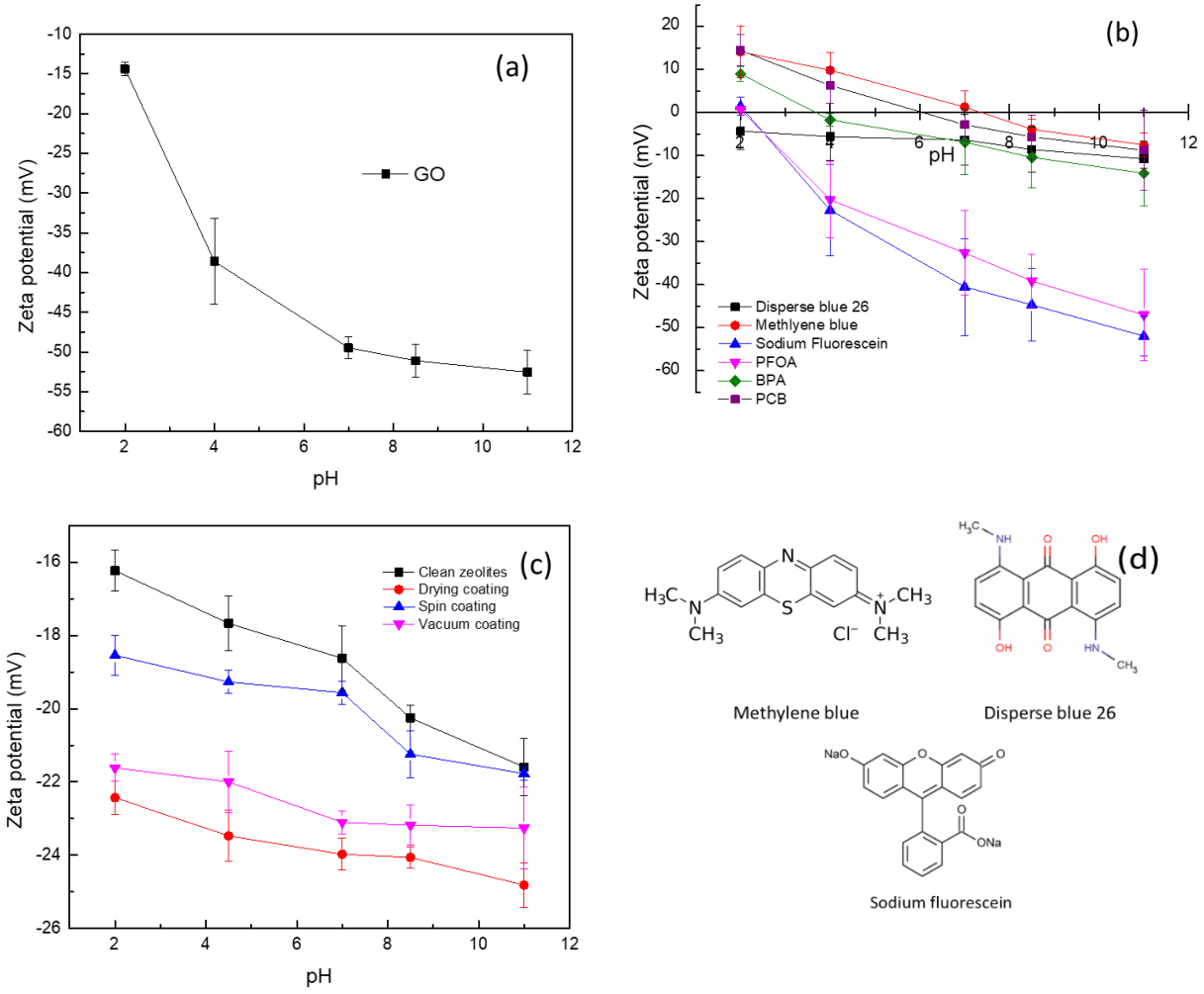

Figure 3.3 Zeta potential *vs.* pH for GO (a), organic model compounds (b), clean zeolite and GO coated zeolites by different coating methods (c) at pH range from 2 to 11. The molecule structures of methylene blue disperse blue 26, sodium fluorescein (d).

3.3.2 Desorption experiment

Desorption experiment was conducted to study the stability of different coating methods. It is as known that an inappropriate coating method could cause the loss of GO when the solution is fluxing through the adsorbents. Herein, stronger bonding and higher loading of GO are desired to gain a better adsorption performance and stability during water treatment process. In Figure 3.4 (a), it displays the decrease of the GO loading for spin, vacuum and dry coating methods after shaking for 24 hours. Even though the theoretical loading of GO on SCGZ is approximate 1 mg g^{-1}, it was reduced to approximate 0.7 mg g^{-1} and the removal efficiency of disperse blue 26 remained as low as 45.2%. VCGZ lost approximately 0.7 mg g^{-1} (56%) of GO on the zeolites surface. From Figure 3.4 (b), VCGZ has the darkest solution of dissolved GO which was desorbed from zeolites surface. It is results from the high loading of VCGZ (2 mg mL^{-1}) and a weak interaction between GO and the zeolite. The vacuum coating method gives a short contact time for GO and the zeolite. And GO sheets can be easily accumulated on the zeolites surface and formed a multiple layered structure which can be easily detached from zeolites surface. DCGZ displayed better performance than the others. The removal efficiency was reduced from about 67% to 62.2%. Meanwhile, the loading of GO reduced to approximate 1.7 mg g^{-1}. Based on this experiment, the dry coating method performed a stronger interaction between GO and the zeolite which benefits from longer contact time and proper distribution during the shaking and drying process.

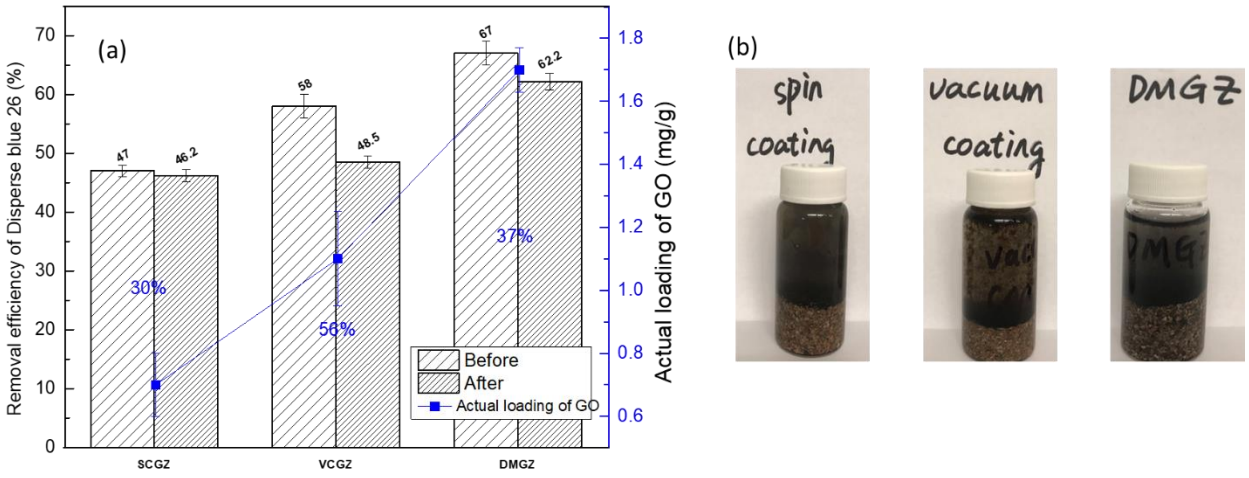

Figure 3.4 The removal efficiencies of before and after desorption experiment for dispersed blue 26 by different coating methods (a), and the images of 10g samples in 20 ml water solution after desorption experiments.

3.3.3 Organic model compounds adsorption experiments

Figure 3.5 presents the removal efficiencies and adsorption capacity of variably charged organic model compounds. 40 mg L^{-1} of organic model compounds was used and adjusted the value of pH to 7. The removal efficiency and saturation curves were obtained by column test experiments under a continuous flow rate of 5 ml min^{-1} at room temperature. The amount of organic model compound was determined by the total pore volume of the column, which is equivalent to Ww (weight of water)- Wz (weight of zeolites) at the same volume. We set the activated material for our adsorbent is GO sheets, and the amount of adsorbent is the loading of GO on the natural zeolite. The objective of the fixed-bed column test is to design a laboratory scale experiment to test the adsorption ability of adsorbents. It is assumed that the amounts of coating GO are approximate 0.7 mg g^{-1}, 1.1 mg g^{-1}, and 1.8 mg g^{-1} for SCGZ, VCGZ, and DCGZ, respectively. (Proved in the desorption experiment in section 3.3.2).

The adsorption performance of clean zeolite, GAC, SCGZ, VCGZ, and DCGZ, are shown in Figure 3.5. It shows the removal efficiency of variably charged organic model compounds, anionic methylene blue, non-ionic disperse blue 26, and cationic sodium fluorescein, respectively. Clean zeolite displays a weak adsorption performance which has only 8%, 92% and 35% removal for disperse blue 26, methylene blue, and sodium fluorescein, respectively. While DCGZ shows higher removals for organic model compounds than SCGZ and VCGZ due to the higher loading of GO on zeolites surface. It also indicates that the DCGZ removal efficiencies of disperse blue 26 and methylene blue are close to the GAC, which are 69% and 99.4%, respectively. It is noted that cationic methylene blue is more favorably adsorbed onto DCGZ and GAC due to the electrostatic interactions. According to the previous analyses, the values of zeta potential of sodium fluorescein, GAC and DCGZ are negatively charged. The removal efficiency of DCGZ for sodium fluorescein reaches to 87.5% which is a significant improvement compared with SCGZ and VCGZ. However, it is still less than the removal of GAC, which is 96.4% removal for sodium fluorescein.

The adsorption capacities of clean zeolite, GAC, SCGZ, VCGZ, and DCGZ are shown in Figure 3.5 (b). When compared with clean zeolite, SCGZ, VCGZ and DCGZ show a higher adsorption capacity for variably charged organic model compounds. The results indicate that the negative charged GO sheets play a crucial role in adsorption. It is worthy to mention that the adsorption capacity of DCGZ is over ten times than GAC. Especially for methylene blue, the adsorption capacity reaches 2872 mg g^{-1}. It reveals that even a small amount of GO sheets attached to the zeolite can achieve a high adsorption capacity. It proves that GO sheets have a remarkable adsorption capability for variably charged organic pollutants due to the strong surface force include H bonding, electrostatic interactions, and van der Waals forces.

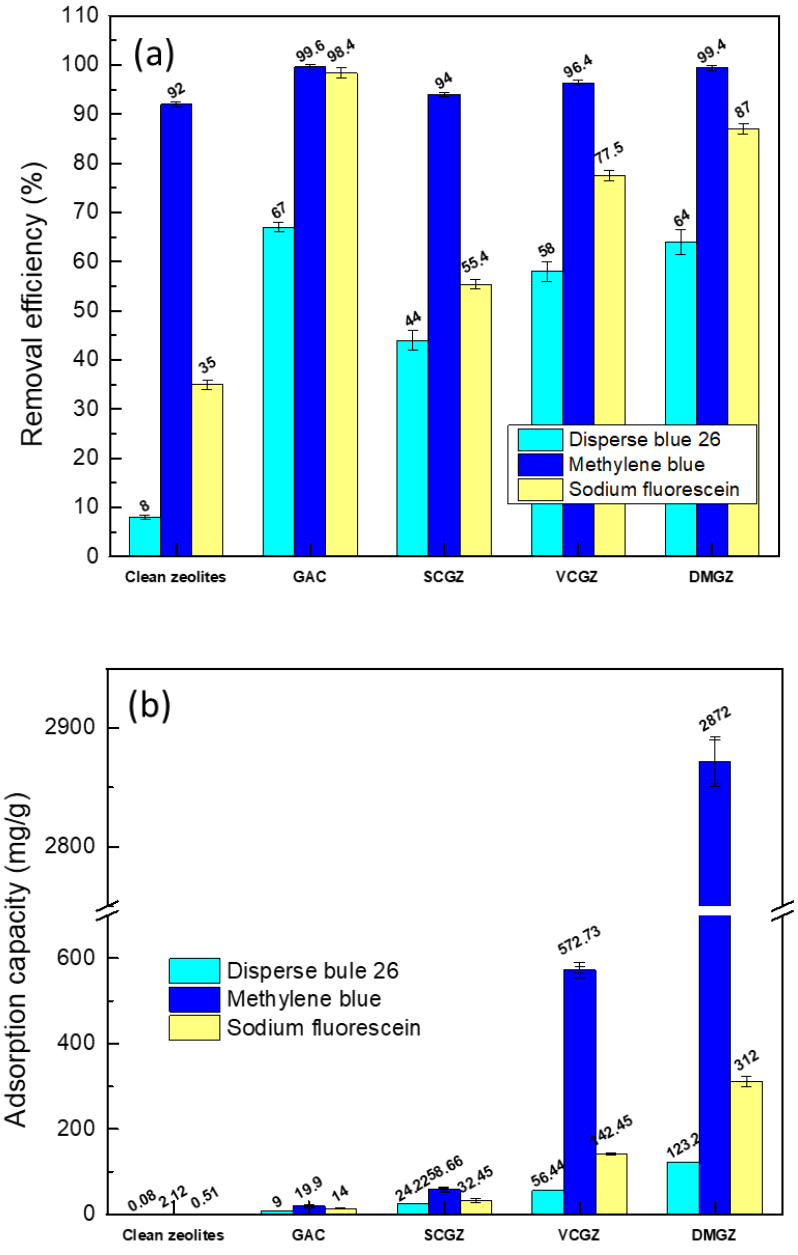

Figure 3.5 The removal efficiency (a) and saturation experiment (b) of variably charged organic model compounds for clean zeolite, GAC, SCGZ, VCGZ and DCGZ. The experiment condition is pH=7~9, flow rate=5ml min^{-1}, 1ml of the 40mg L^{-1} organic model compounds.

3.3.4 POPs adsorption experiment

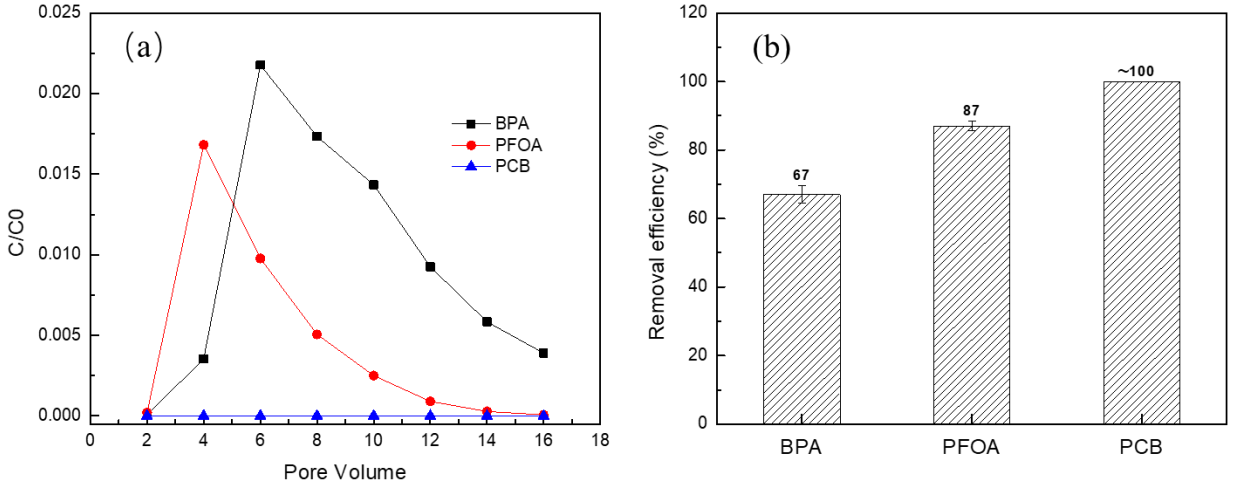

Figure 3.7 The removal efficiency of BPA, PFOA and PCB. The experiment condition is active materials pH=7~9, the amount of GO=1.8 mg g^{-1}, flow rate=5 ml min^{-1}, the solutions of BPA, FPOA and PCB are 1ml and the concentration are 40 mg L^{-1}.

Due to the large surface area and super adsorption capacity of graphene-based materials, the mechanism study of adsorption of BPA, PCB and PFOA on GO sheets has been reported in recent years. [138] It was assumed that the removal efficiency of BPA, PCB and PFOA by DCGZ should be comparable as disperse blue 26, methylene blue and sodium fluorescein, respectively, because of their analogous molecular structure and charges. In Figure 3.7, the column test shows that the removal efficiency of BPA and PFOA are 64% and 84.3%, respectively. The result of the removal efficiency of PCB by DCGZ is almost 100%, which is highly possible due to the negative surface charge of DCGZ. The experiment reveals that non-ionic POPs (BPA) can adsorb less readily on the DCGZ than charged POPs (PFOA and PCB). The adsorption mechanism of PCB on GO surface is mainly because of electrostatic interactions, while the π-π stacking of GO also plays a vital role in BPA and PFOA adsorption.

3.3.5 Optimization of operation conditions

Meanwhile, optimization experiments for investigating the best condition for adsorption was also conducted by using DCGZ, shown in Figure 3.6. The disperse blue 26 was selected as the organic model compound. The pH of water solution, the temperature and flow rate are considered as the critical factors in the removal efficiency and adsorption capacities for the column test.

Solution pH is considered as the most critical parameter in the adsorption process because it can directly influence the GO surfaces and the degree of ionization of pollutants. In Figure 3.6 (a), it shows that with increasing pH under acidic conditions, the removal efficiency of disperse blue 26 decreases gradually. The maximum removal efficiency was observed at pH =7. With the increasing pH values from 7 to 10, the removal efficiency for DCGZ decreased. This shows that the pH has a critical impact on the adsorption process, where higher pH of water solution leads to the lower removal efficiency of the neutral organic model compound. It can be attributed to the function groups and pH values of GO sheets. According to the obtained results, pH for DCGZ was about 7. When the pH of the solution is higher than the pH of DCGZ, the surface of GO becomes negatively charged and can adsorb cations by the electrostatic reactions. On the other hand, when pH of the solution is higher than the pH of adsorbent, the surface of GO becomes positively charged and absorbs anions. Considering the negative charge of disperse blue 26 at alkaline conditions (phenol), the adsorption rate decreased due to the negatively charged GO surface. In addition, at alkaline pH, the degradation of -OH groups of phenolic compounds, such as disperse blue 26 and BPA,

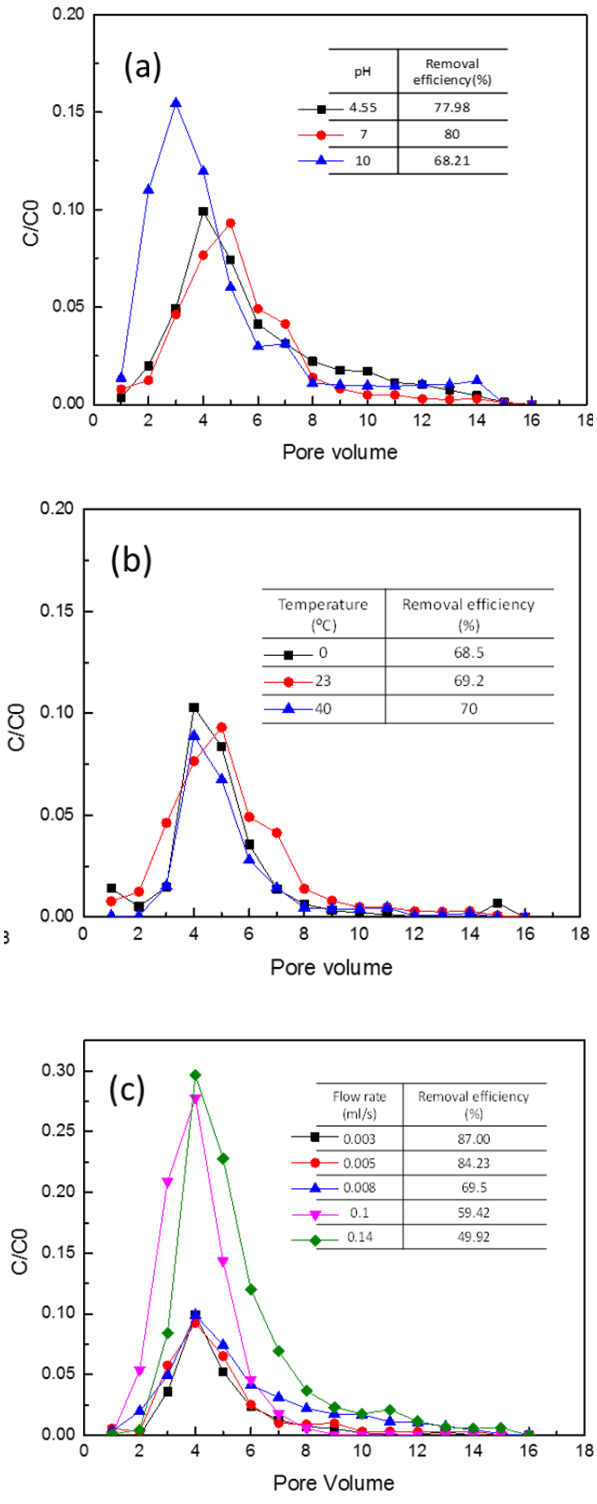

Figure 3.6 The optimization experiment for disperse blue 26 in different pH, temperature and flow rate. The experiment condition is pH=7~9, flow rate=5 ml min^{-1}, the amount of GO (DMGZ) =1.7 mg g^{-1}, 1 ml of the 40 mg L^{-1} disperse blue 26. The optimization experiment for disperse blue in different pH,

temperature and flow rate. The experiment condition is pH=7~9, flow rate=5 ml min^{-1}, the amount of GO (DMGZ) =1.7 mg g^{-1}, 1ml of the 40 mg L^{-1} disperse blue 26.

prevents the formation of hydrogen bonds on the GO surface between adsorbed molecules in solution and GO. As a result, adsorption efficiency is decreased. In contrast, because the zeta potential of dispersed blue 26 at acidic conditions (pH=4.5) is similar with pH at neutral condition (pH=7), the removal efficiencies of disperse blue 26 be close to each other.

However, the temperature from 0 to 40 ^{o}C shows less influence on the adsorption, which the removal efficiencies are approximately 69% for dispersed blue 26. Also, the flow rate condition test shows that the higher the flow rate, the lower the removal efficiency. It is attributed the short residence time between the disperse blue 26 and GO. Finally, according to the water treatment system in practice, the flow rate was set up at 4.8~5 ml min^{-1}. In summary, the optimized operation experimental condition is: pH=7~9, flow rate= 4.8~5 ml min^{-1} and the temperature between 0~40^{o}C.

3.4 Conclusion

In summary, GO sheets coated on the natural zeolite substrate was prepared via spin, vacuum, and dry coating methods. SEM, EDS, FTIR and Raman results showed that the GO sheets were successfully attached to the zeolites surface. The analyses of zeta potential revealed the interactions between the zeolite, GO and adsorbents. From the adsorption performance, it can be concluded that the dry coating method for fabrication of GO coated on natural zeolite is an effective and straightforward approach. DCGZ has a better physical stability and less desorption of GO from the zeolites than the others. The removal and adsorption capacities of variably charged organic model compounds for GO coated on the zeolites were described, which reveals that the adsorption performance strongly depend on the loading of GO. The adsorption mechanism for

organic model compounds and POPs by DCGZ included electrostatic and physical interactions due to the functional groups and π-π stacking on GO surface. Optimization of column experiment suggested the best operation conditions are: pH=7~9, flow rate= 4.8~5 ml min^{-1} and the temperature between 0~40 ^{o}C.

Chapter 4 The effect of surfactants on the graphene oxide coated on zeolites surface

4.1 Introduction

Surfactants are classified as anionic, cationic, and nonionic with negative, positive and no charged groups, respectively. They are usually amphiphilic containing hydrophobic groups and hydrophilic groups. Surfactants have been studied as agents for graphene-based material dispersion in aqueous solution or the surface modification of graphene-based materials. The different mechanisms of ionic and non-ionic surfactants in stabilizing graphene dispersions are explained by the theory for colloidal stability. [141,142] The effect of surfactants and their concentrations on graphene-based materials has been examined in many studies. [138,139,140]

Besides that, they have been used to enhance the interaction between graphene-based materials and substrates. [140,142] Cationic surfactants functionalize the surface of substrate by exchanging adsorbed cations on the anionic substrate surface. The adsorption of cationic surfactants on SiO_2 surfaces have been reported that it is consistent with the wettability change of the film surface. [143] Extensive studies reported impressive adsorption capacities of cationic CTAB modified SiO_2, Al_2O_3, clays or AC for the removal of dyes, benzene, phenol, and chlorobenzenes. [144,145,146,147] Anionic surfactants are applied for dispersion and exfoliation of graphene-based materials sheets in aqueous solution. Seo et al used anionic SDS as a surfactant to fabricate three-dimensional GO sponge to remove cationic dyes. They demonstrated that the addition of SDS could improve the anion-cation interaction between GO and dyes. [153] Additionally, nonionic surfactants are used to stabilize the dispersion of graphene-based materials in aqueous solution and to improve the surface hydrophilicity for substrates. They are used for graphene-based composites in heavy metal

adsorbents, semi-conductors, nanofibers and so on. [148,149,150,151] Typically non-ionic surfactants include alkyl polyglycoside, decyl glucoside, lauryl glucoside, PEG-10 sunflower glycerides, and Triton X-100. [152]

In this chapter, variable-charge surfactants cationic CATB, nonionic Triton-X 100 and anionic SDS were selected to enhance and stabilize the bonding between GO and zeolite. The molecular structures of the surfactants are shown in Figure 4.1. The zeta potential was used to study the surface charge modification of GO and zeolite. Batch adsorption experiments for variably charged organic model compounds were conducted to investigate pH and concentration under various conditions. The objective of this study is to determine an appropriate surfactant which can enhance the bonding between GO and the zeolite to improve the adsorption performance for POPs and stability of the adsorbents.

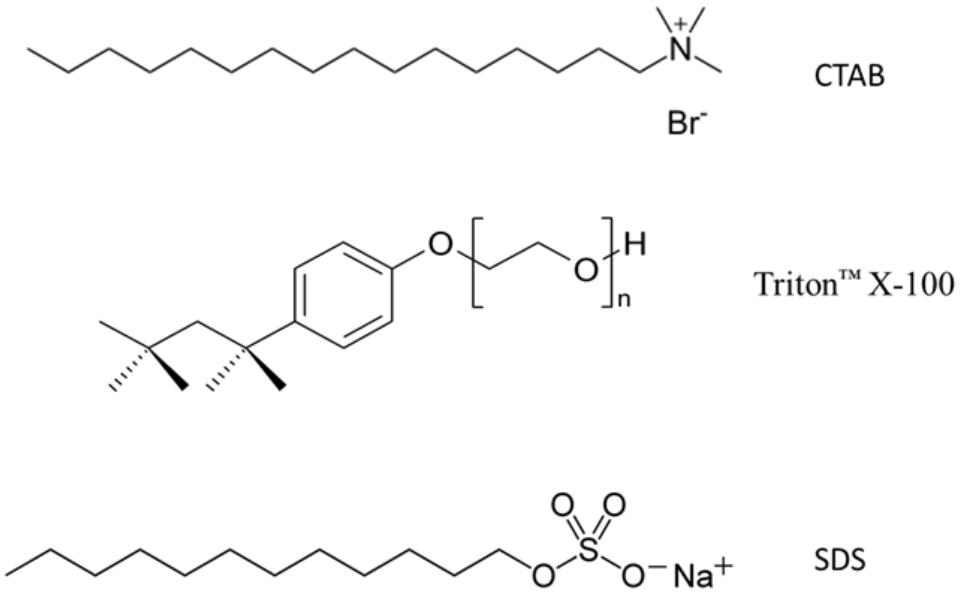

Figure 4.1 The molecule structures of CTAB, Triton X-100 and SDS.

4.2 Experimental

4.2.1 Materials

Australian natural zeolite, (clinoptilolite, diameter: 0.7-1 mm, chemical composition: 68.26% SiO_2, 12.99% Al_2O_3, 4.11% K_2O, 2.09% CaO, 1.37% Fe_2O_3, 0.83% MgO, 0.64% Na_2O, 0.23% TiO_2, Zeolite Australia Ltd.), graphene oxide (ACS Materials), Triton X^{TM}-100, Hexadecyltrimethylammonium bromide (CTAB, 95%, Sigma -Aldrich), Sodium dodecyl sulfate (SDS, ACS reagent, ≥99.0%, Sigma-Aldrich). Dyes, which are disperse blue 26 (Crescent Chemical), methylene blue (Electron Microscopy Sciences), and sodium fluorescein (Pfaltz &Bauer), were chosen as the representations for nonionic, cationic, and anionic organic model compounds.

4.2.2 Materials preparation

CTAB/zeolite and CTAB/DCGZ

10 ml of 0.25 mg·ml^{-1} CTAB was mixed with 15g of natural zeolite and shaken on shaker at 150 rpm for 60 min. Afterwards, the CTAB/zeolite was dried at 100 ^oC for 6 hours. 25 ml of 2.5 mg·ml^{-1} GO was mixed with CTAB/zeolite and shaken on the shaker for 120 mins at 150 rpm. The product was dried at 100 ^oC for 24 h, then rinsed by ethanol once followed by DI water rinse for three times to remove the extra GO on the surface of zeolite before use.

SDS/DCGZ

1.5 ml of 5 wt% SDS in aqueous solution was added in 25 ml of 2.5 mg mL^{-1} GO aqueous solution and sonicated for 120 mins. Then the SDS/GO solution was mixed with 25g of clean zeolite and shaken on the shaker for 120 mins at 150 rpm. The product was dried at 100^oC for 24h, then rinsed by ethanol and water for three times to remove the extra GO on the surface of zeolites before use.

Triton X-100/DCGZ

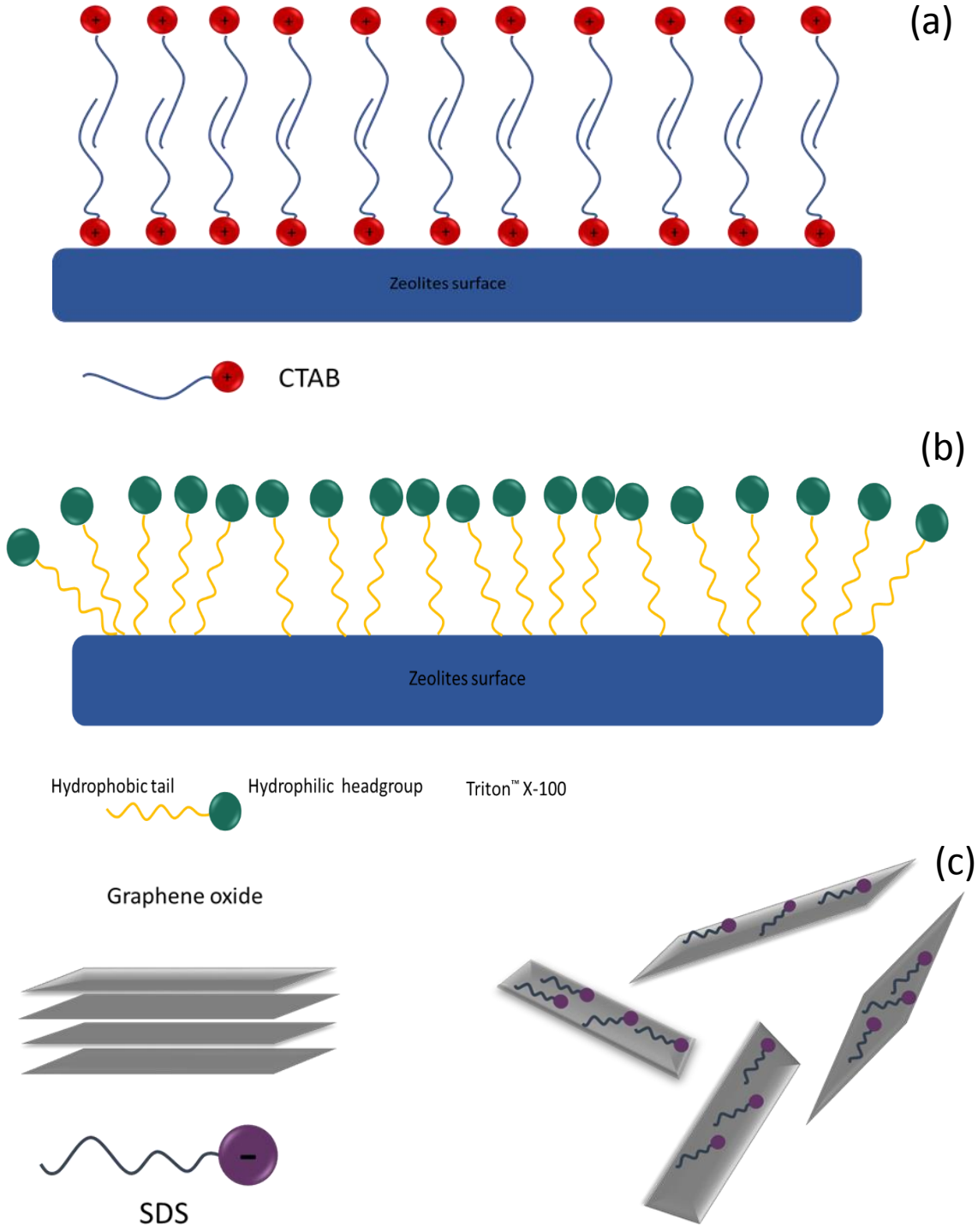

Figure 4.2 The schematic diagrams of CTAB(a), Triton X-100(b) interaction with the zeolite, and SDS interaction with GO(c).

One drop of Triton X-100 was added into 25 ml of 2.5 mg mL^{-1} GO aqueous solution and sonicated for 120 mins. Then the Triton X-100 solution was mixed with 25 g clean zeolite and shaken on the shaker for120 mins at 150 rpm. The product was dried at 100 ^{o}C for 24 hours, then rinsed by ethanol and water for three times to remove the extra GO from the surface of zeolite before use.

The schematic diagrams of the interaction of CTAB, Triton X-100, and SDS with GO and the zeolite are shown in Figure 4.2 (a), (b), and (c), respectively.

4.2.3 Batch experiment

Adsorption capacity studies were conducted by batch experiments and column tests using the organic model compounds in aqueous solution. Batch experiments were carried out to determine the adsorption performance of organic model compounds onto the adsorbents in a 250 mL glass flask. The sample was immersed in 100 mL of a specific concentration of organic model compounds and was shaken at 150 rpm for 48 hours to reach adsorption equilibrium. The study was conducted at room temperature to represent conditions that are typical in the industrial setting. The pH of the solution was adjusted with a 0.1 M solution of NaOH and a 0.1 M solution of HCl. The effect of various factors on the rate of adsorption process was assessed by varying contact time, concentration of organic model compounds, and pH of the solution. All experiments were carried out in triplicate, and the average values were taken for analyses.

4.3 Results and discussion

4.3.1 Synthesis and characteristics of CTAB/DCGZ, Triton X-100/DCGZ, and SDS/DCGZ

The synthetic illustration process of functionalization for CTAB/DCGZ, Triton X-100/DCGZ, and SDS/DCGZ are illustrated in Figure 4.2. Surface modification of the natural zeolite by cationic surfactant CTAB has been used via dry coating method. CTAB modified the anionic zeolites

surface by evaporation. CTAB/DCGZ, Triton X-100/DCGZ and SDS/DCGZ was easily obtained using the dry coating method. Figure 4.1 shows the values of zeta potential for DCGZ with variable charge surfactants at pH values ranging from 2 to 11. The values of zeta potential for SDS/DCGZ appears to be the most negatively charged and the values of zeta potential of Triton X-100/DCGZ shows slightly higher than the values of SDS/DCGZ. The values of zeta potential of CTAB/DCGZ are substantially higher than the other samples which is not surprising considering the cationic surface of the modified zeolite. CTAB is expected to modify zeolites surface to positive charge and enhance the electrostatic interaction between the zeolite and GO sheets. The values of zeta potential for SDS/DCGZ were the lowest observed due to the anionic nature of SDS. It is expected to induce a negative charge on the GO sheets, which leads to electrostatic repulsion between the surfactant molecules and the GO sheets. The primarily separated layers of GO may appear due to the repulsion between the negatively charged GO sheets, and the intercalation of SDS within the basal planes of GO which may weaken the π–π stacking interaction. [154] The values of zeta potential of Triton X-100/DCGZ are similar with the DCGZ shown in Chapter 3. Nonionic Triton X-100 added in the GO solution results in a stable GO suspension due to the enhancement of hydrophilicity between GO layers, this also enhances the interaction between the zeolite and GO.

SEM images of CTAB/DCGZ, SDS/DCGZ and Triton X-100/DCGZ at a low magnification resolution are presented in Figure 4.4 (a), (d), and (g) respectively. The continues GO coating area was observed on the surface of zeolites for all these samples. Moreover, EDX mapping in Figure 4.4 (b, c, e, f, h, i) of carbon layers also show the lateral size of the GO sheets on the order of 10 µm to 200 µm. The selected area of SEM mapping area indicates that the GO sheets uniformly deposited on the zeolites surface with these surfactants, these fragments are overlapping and forming only a few layers of GO sheets on the zeolites surface. One possible explanation might

be that and adsorption capacity of variable charge organic compounds were investigated on the samples with a variation of concentration.

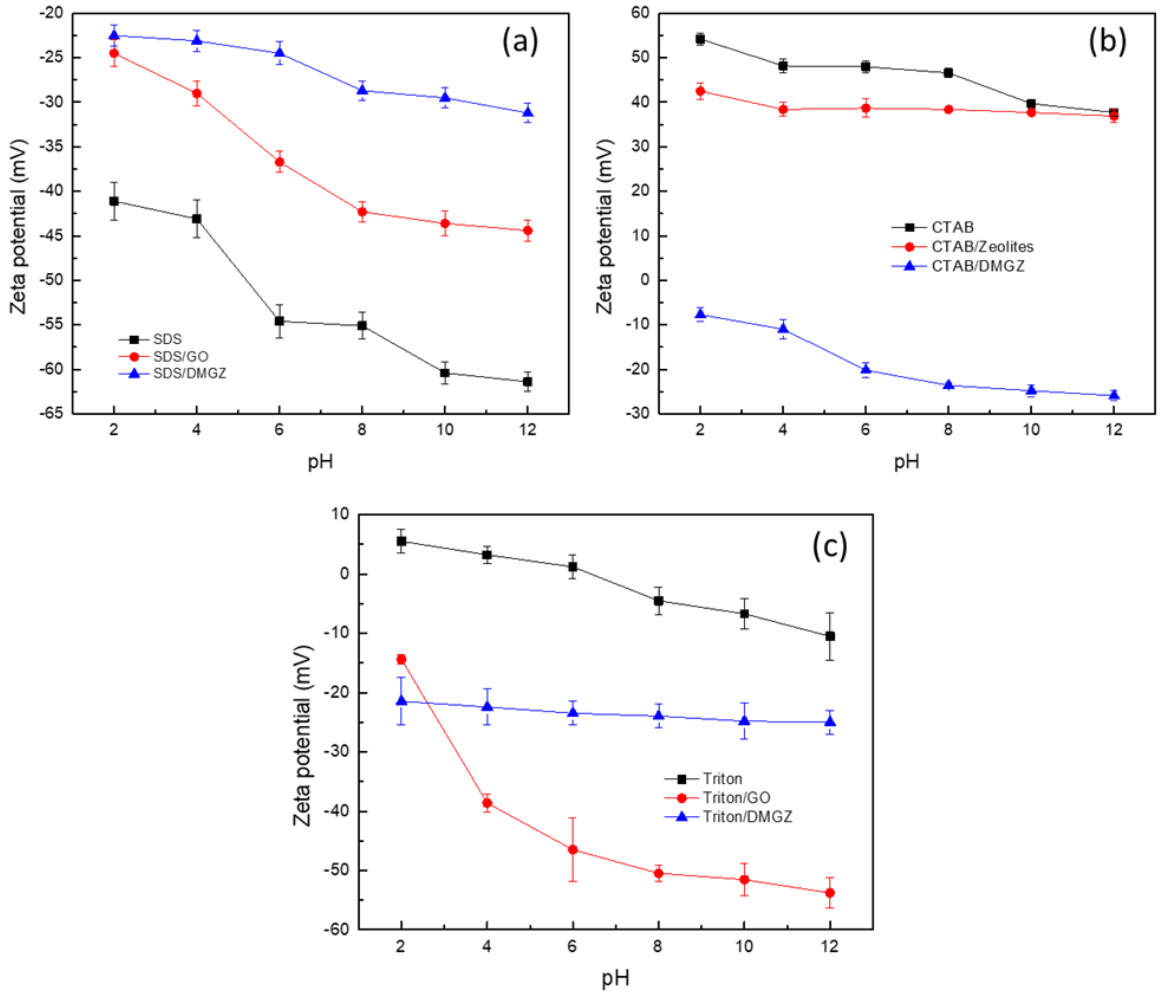

Figure 4.3 Zeta potential of SDS and SDS modified samples (a), CTAB and CTAB modified samples, and Triton X-100 and Triton X-100 modified samples in the range of pH from 2 to 12.

Table 4.1 shows the EDX analysis of DCGZ samples. The C/O ratio of DCGZ is 0.19 and after modified by SDS and Triton X-100, it increases to 0.20 and 0.21 respectively. Compared with these two samples, the C/O ratio of CTAB/DCGZ increases to 0.55 which may be due to the higher loading of GO coating on the surface of the zeolite. By adding the surfactants, the surface charge

Table 4.1 EDX analysis of surfactants added samples

Samples(wt%)	C	O	Si	Al	C/O
DMGZ	10.90±4.50	57.37±2.12	29.17±1.24	17.45±0.37	0.19
SDS/DMGZ	15.14±6.63	74.33±10.27	8.50±5.22	2.04±4.23	0.20
CTAB/DMGZ	32.00±5.54	58.26±10.45	5.14±4.47	4.60±6.69	0.55
Triton X-100/DMGZ	12.59±2.01	47.01±5.45	27.46±1.24	15.72±0.37	0.21

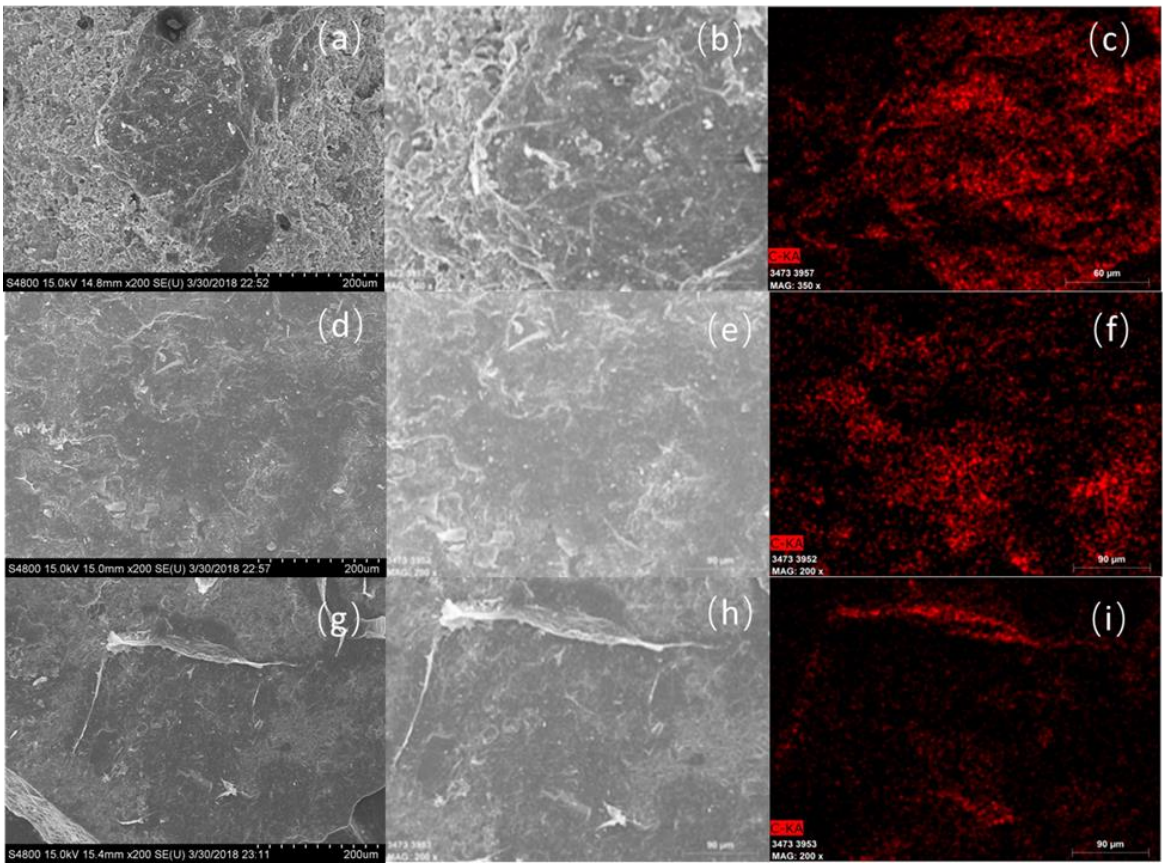

Figure 4.4 SEM images of CTAB/DCGZ(a), SDS/DCGZ(d) and TritonX-100/DCGZ(g) at 200K resolution. The EDX mapping of carbon for CTAB/DCGZ(b,c), SDS/DCGZ(e,f) and TritonX-100/DCGZ(h,i)

of the GO sheets has been modified, and the exposed surface can serve as advanced adsorbents to attract the target organic model compounds. Based upon this hypothesis, the removal efficiency and adsorption capacity of variable charge organic compounds were investigated on the samples with a variation of concentration.

4.3.2 Desorption experiment

To investigate the stability of the GO sheet deposition onto the zeolite surface in aqueous solution, the desorption experiment was conducted by shaking 10g of adsorbents in 20 ml DI water for 24 hours at 150 rpm. Samples were rinsed with DI water three times and then the samples were dried at 100 ^{o}C for 24 hours before measuring their weights. All the adsorbents were shaken for 24 hours and the desorption results are displayed in Figure 4.5 (b). It is observed that severe desorption of GO sheets from the zeolite is obtained by SDS/DCGZ. The quantitative analyses of the GO detached from the zeolite surface was calculated and reported in Figure 4.5 (a). The calculation shows that all the desorbed samples exhibit lower removal efficiencies as compared to the non-shaken samples, especially the SDS/DCGZ which had lost about 48 wt% of GO on the zeolites surface. It is due to the decreased loading of GO on the zeolites surface. Results from the zeta potential analysis show that a reasonable conclusion is that the surface charge repulsion between zeolite and GO plays a vital role in desorption. The CTAB/DCGZ and the Triton X-100/DCGZ maintain 90 wt% and 86 wt% loading of GO on the zeolite surface respectively. These results are due to the electrostatic attraction and hydrophilicity between GO and zeolite. The stability of the GO on the zeolites surface is: CTAB/DCGZ >TritonX-100/DCGZ>DCGZ>SDS/DCGZ.

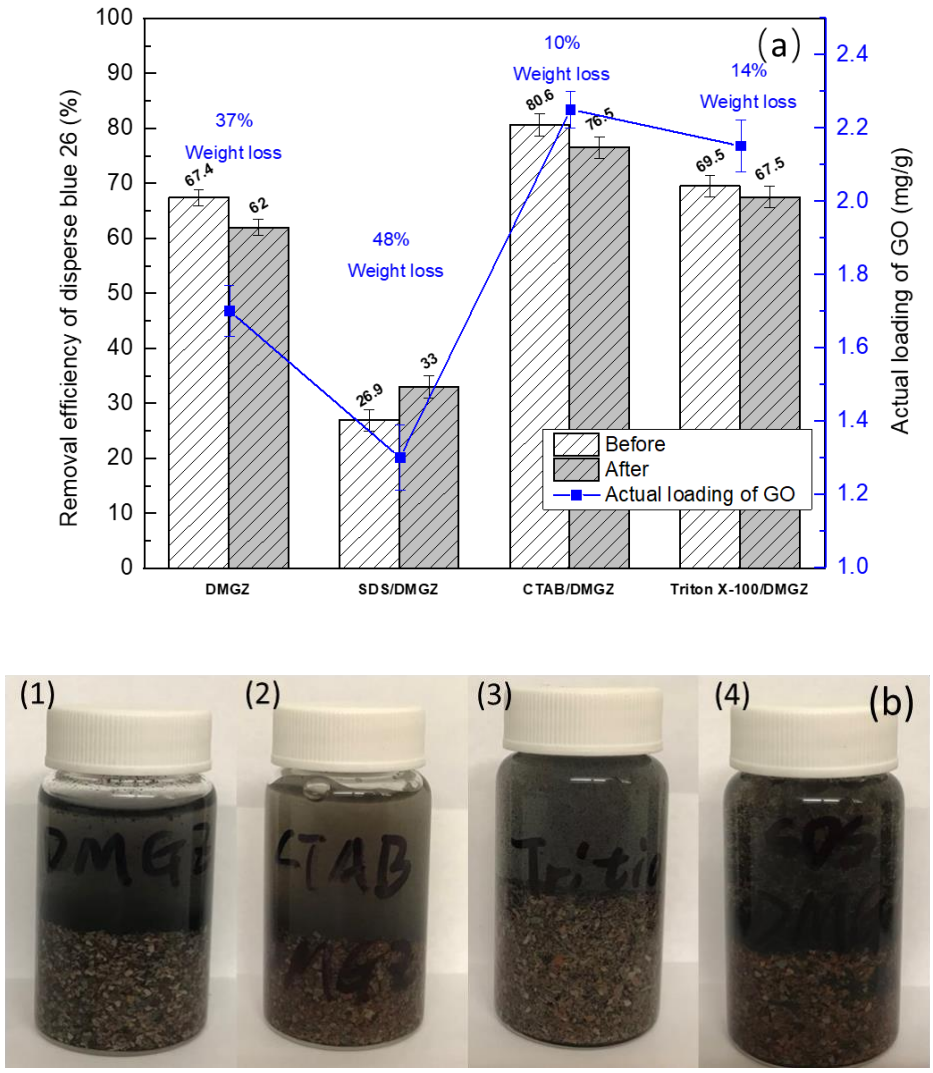

Figure 4.5 The removal efficiency of before and after desorption experiment for dispersed blue 26 by variable surfactants (a), and the images of 10 g DMGZ (1), CTAB/DMGZ (2), Triton X-100/DMGZ (3) and SDS/DMGZ (4) in 20 ml water solution after desorption experiments (b).

4.3.3 Organic model compounds adsorption experiment

To determine the adsorption capability of CTAB/DCGZ, TritonX-100/DCGZ, and SDS/DCGZ, the removal efficiencies for organic model compounds were examined by individual column tests. Study on their adsorption capacity was observed by batch experiment. Based on the analysis of the zeta potential and desorption experiments, the assumption is that CTAB/DCGZ and SDS/DCGZ may have a good adsorption performance on anionic and cationic organic model compounds, respectively. The TritonX-100/DCGZ may have a unique ability to have a broad adsorption ability than CTAB/DCGZ and SDS/DCGZ.

The removal efficiencies of nonionic disperse blue 26 and anionic sodium fluorescein are shown in Figure 4.6 (a), they follow the trend: CTAB/DCGZ >Triton X- 100/DCGZ> DCGZ>SDS/DCGZ. In Figure 4.6 (b), the equilibrium concentration of disperse blue 26 was obtained after 24 hours, and the adsorption capacities were approximately 354 $mg \cdot g^{-1}$, 246 $mg \cdot g^{-1}$ and 186 $mg \cdot g^{-1}$ for CTAB/DCGZ, TritonX-100/DCGZ, and SDS/DCGZ respectively. Rapid adsorption for sodium fluorescein was observed in Figure 4.6 (d), and the adsorption capacities were reached within 6 hours and were approximately 444 mg g^{-1}, 164 mg g^{-1} and 70 mg g^{-1} for CTAB/DCGZ, TritonX-100/DCGZ and SDS/DCGZ respectively. The anionic sodium fluorescein can be adsorbed to the surface of the GO sheets due to the electrostatic attraction between the negatively charged organic model compound, and the positively charged CTAB modified GO surface. Similarly, the adsorption capacity for methylene blue was measured after 24 hours and followed the trend: SDS/DCGZ >Triton X-100/DCGZ> CTAB/DCGZ which are 354 mg g^{-1}, 290 mg g^{-1} and 186 mg g^{-1} in Figure 4.6 (c). Interestingly, the Triton X-100/DCGZ presented 96% of removal efficiency for sodium fluorescein which was higher than 87% of DCGZ. Besides that, its adsorption capacity for methylene blue is much higher than the adsorption capacity of

CTAB/DCGZ. It implies that the enhancement of GO hydrophilicity leads to increase the adsorption sites on GO surface while keeps a broaden adsorption range of organic model compounds.

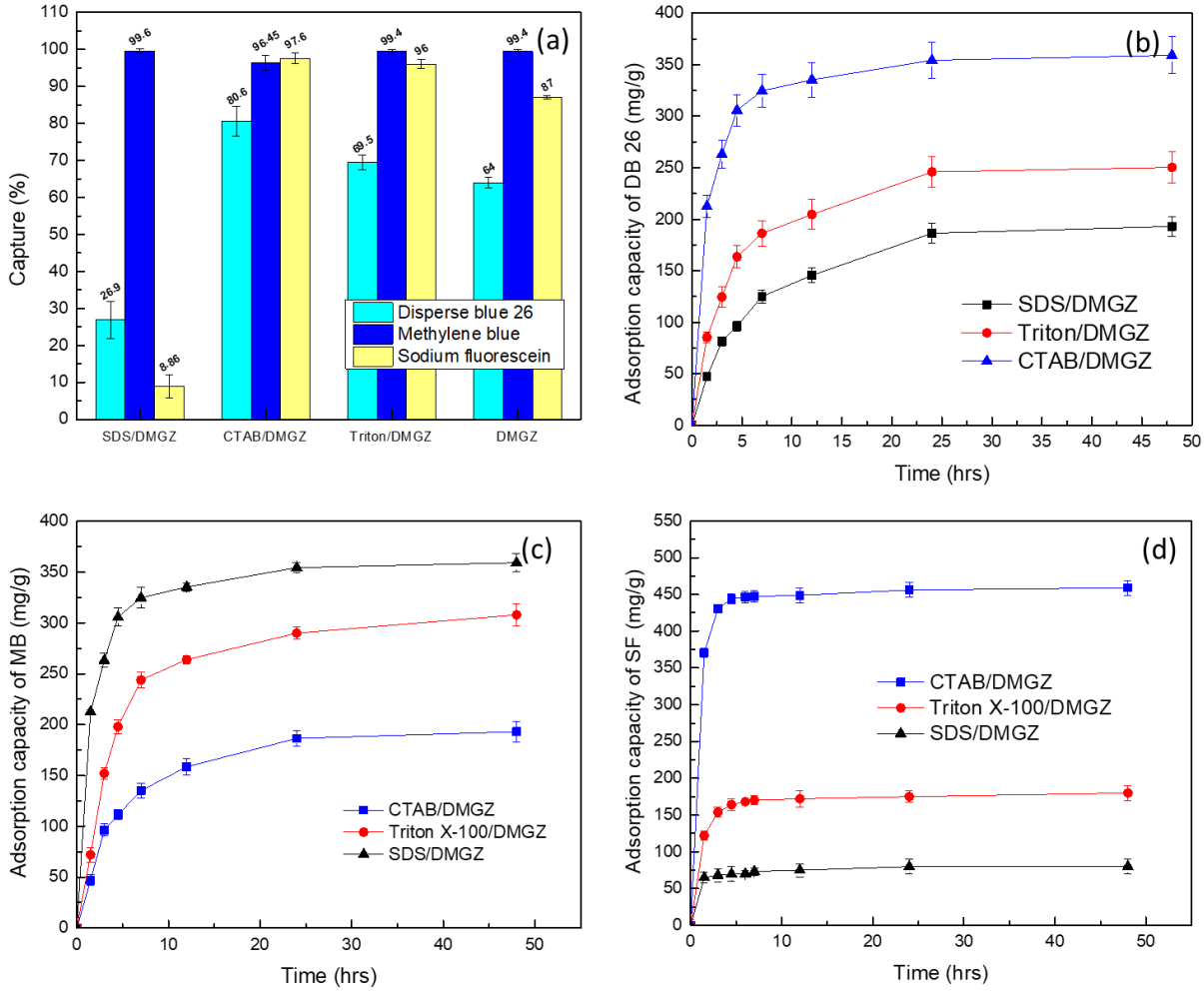

Figure 4.6 Column test for the removal efficiency of organic model compounds for CTAB/DCGZ, Triton X-100/DCGZ, and SDS/DCGZ (a), batch experiment for adsorption capacity of disperse blue 26(b), methylene blue(c), and sodium fluorescein(d) for each adsorbent. The pH of organic model compounds solution=7, flow rate (column test) = 5ml min^{-1}, the amounts of samples for column test and batch experiment are 9 g and 1 g respectively, and the concentration of organic model compounds for column test and batch experiment 40 mg L^{-1} (1ml) and 10 mg L^{-1}, respectively.

Finally, to investigate the effect of adsorbent dosage for variably charged model compounds, different concentrations of organic model compounds ranged from 1 mg L^{-1} to 40 mg L^{-1} were taken and examined after 24 hours at pH=6 at room temperature. To the best of my knowledge, many research studies have been focusing on the GO adsorption kinetic models and isothermal study. They have proved that it follows the pseudo-second order kinetics model. [155,156,157,158] In this thesis, we focus on the adsorption performance in practical application.

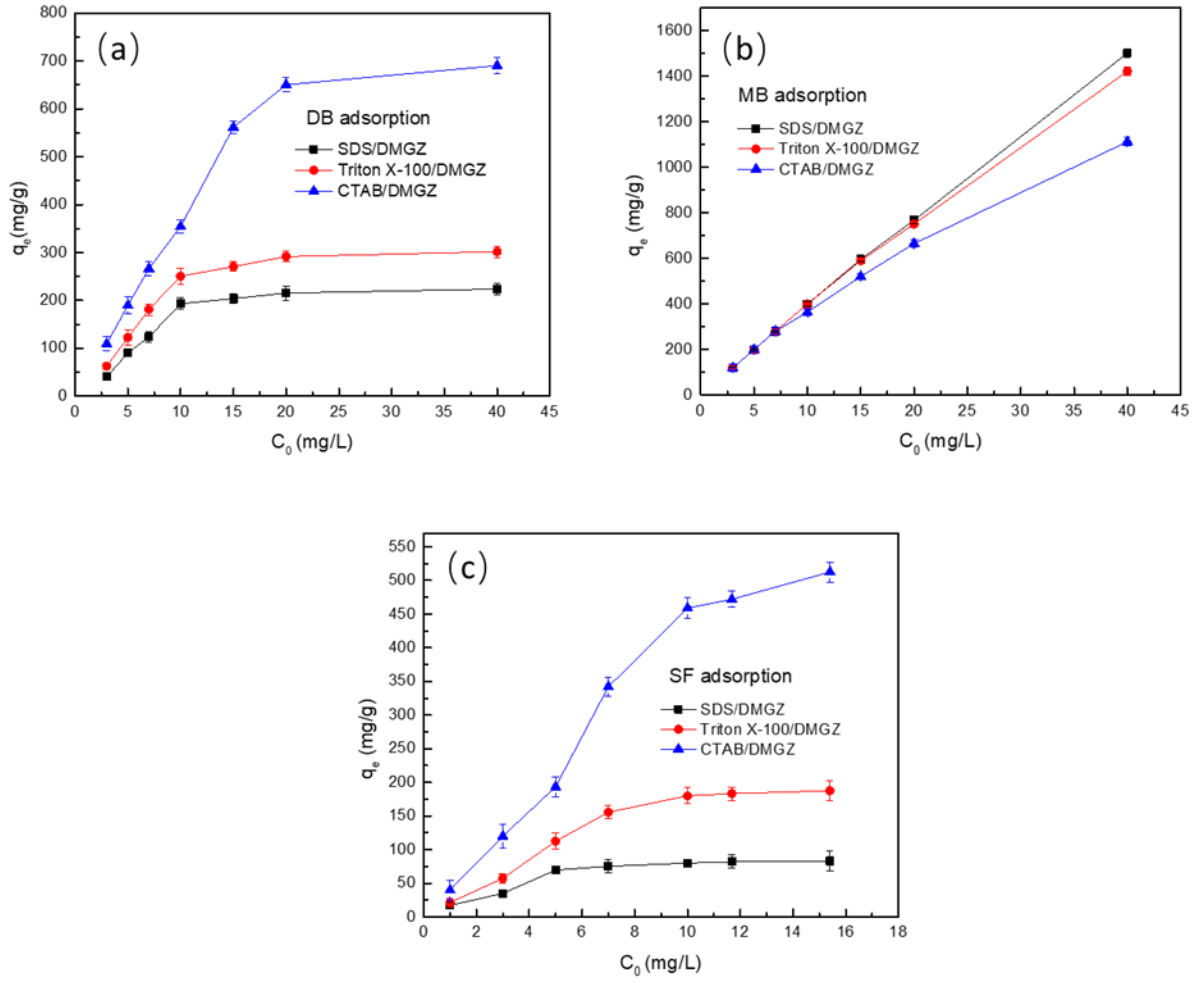

Figure 4.7 Effect of organic model compounds concentration on amount of CTAB/DCGZ, Triton X-100/DCGZ, and SDS/DCGZ by batch experiment.

To determine an appropriate surfactant for GO coated on zeolite, both column tests and batch experiments were carried out. The results demonstrated that neither anionic SDS or cationic CTAB were appropriate candidates due to the limitation of adsorption for variably charged organic model compounds and POPs. Triton X-100, a nonionic surfactant, induced significant adsorption increases for three variably charged organic model compounds. Only 14 wt% of GO detached from the zeolite surface under extreme conditions. It should be considered as an excellent surfactant to enhance the interaction of GO-zeolite and GO-POPs.

4.4 Conclusion

In this chapter, cationic CATB, nonionic Triton-X 100, and anionic SDS were selected as agents to enhance the attachment of GO onto the zeolite. The effect on the removal of organic model compounds was examined. The conclusions from the results of the desorption experiments and adsorption studies for variably charged organic model compounds are:

The characterization by zeta potential has shown an observable physical interaction between GO and zeolites with the adding variable charge surfactants.

(1) SDS/DCGZ and CTAB/DCGZ display strong adsorption capabilities for cationic and anionic model compounds for complimentary charges. Meanwhile, they show weak adsorption abilities to same charged organic model compounds.

(2) The 48 wt% GO (mass) desorbed from the zeolites surface by SDS, and the stability of the GO sheets on the zeolite surface follows the trend: CTAB/DCGZ >TritonX-100/DCGZ>DCGZ>SDS/DCGZ. The desorption experiment suggests that CTAB/ DCGZ and Triton X-100/DCGZ are good candidates for water treatment process.

(3) The batch experiment study agrees with the prediction obtained by surface charge analyses.

Based on the column tests, desorption experiments, and batch experiments Triton X-100/DCGZ shows good physical stability and adsorption capabilities for variable-charge organic model compounds. Non-ionic Triton X-100 is a promising surfactant to enhance the interaction between GO and the natural zeolite.

Chapter 5 APTES modification of natural zeolite and *in-situ* reduction of graphene oxide

5.1 Introduction

Single-layered GO suspensions demonstrate high adsorption capacity due to its homogeneity and large surface area. [159] However, its use as either suspended GO solution or dispersed nano-sized graphene-based materials is not practical for large-scale operation due to the issues with their removal and the resultant residues. The hydrophilicity of GO provided by a variety of oxygen functional groups on the surface, carboxyl, hydroxyl and epoxy group, leads to high solubility.[160] GO has been found moderately toxicity toward human cell lines and zebrafish.[161] Previously, scientists have been focusing on synthesis method or configuration of the graphene-based materials such as microspheres, hydrogels, membranes, magnetic nanoparticle composites to avoid their removal and the resultant residues in water purification. [162,163,164] However, the use of the graphene-based membrane or graphene composite hydrogels were limited by multiple layered structures.

This work aimed to demonstrate that a thin-layered graphene-based product with high capacity could be engineered for POPs removal and that it could also be easily regenerated and reused. Australian natural zeolite, clinoptilolite zeolites ((Na_3K_3) $(Al_6Si_{30}O_{72})$ $\cdot 24H_2O$), which are readily available, economically acceptable and have excellent chemical stability were selected as support materials. Many studies have reported their exceptional ion-exchange and adsorption properties in water treatment. Here, we reported a thin-layered rGO synthesized by *in-situ* reduction on an engineered natural zeolite used as the support material. Environmentally friendly vitamin C was selected as a reducing agent for the controlled reduction of the adsorbed GO to oxidize graphene

partially. APTES (3-aminopropyltriethoxysilane) was used to modify the charge of the zeolites surface to increase GO loading and improve the stability of GO coated zeolites composite. Non-ionic disperse blue 26, anionic sodium fluorescein, and cationic methylene blue were selected as organic model compounds. The adsorption capacity of GO was evaluated by a column test by elution. Evaluation of the removal efficiency and adsorption characteristics of BPA, PFOA, and PCB were also examined. The investigation of a single multi-purposed adsorbent for POPs with different charges was studied for the first time. In addition to the well-controlled stable studies, we also determined the desorption of graphene-based material on the modified zeolite and thermal regeneration ability in simulated engineering systems.

5.2 Experimental

5.2.1 Materials

Australian natural zeolite, (clinoptilolite, diameter: 0.7-1 mm, chemical composition: 68.26% SiO_2, 12.99% Al_2O_3, 4.11% K_2O, 2.09% CaO, 1.37% Fe_2O_3, 0.83% MgO, 0.64% Na_2O, 0.23% TiO_2, Zeolite Australia Ltd.), graphene oxide (ACS Materials), dyes, which are disperse blue 26 (Crescent chemical), methylene blue (Electron Microscopy Sciences), and sodium fluorescein (Pfaltz &Bauer), were chosen as the representations for neutral, cationic, and anionic particles. L-Ascorbic acid (Vitamin C, Sigma-Aldrich, 99%), Bisphenol A (BPA, ≥99%, Sigma-Aldrich), Perfluorooctanoic acid (PFOA, 96%, Sigma-Aldrich), Aroclor 1242 (PCB, analytical standard, Ultra scientific).

5.2.2 *In-situ* reduced GO coated zeolite

i) Method 1----Microwave reduced GO

10 g of active material (2.5 mg ml^{-1} DCGZ) was added in the 20 ml container. It was then microwaved at 500 W, 6.425 GHz±1.150GHz, for each cycle; the sample was heated for a specific time. After each heating, the microwave was stopped to let the sample cool down to room temperature. The heating-and-cooling cycle was repeated for a certain number of cycles until the rate of temperature rise fell back to the room temperature.

ii) Method 2 ---- Sol-gel method reduced GO

To reduce the GO sheets on the surface of zeolite, two different mixing approaches have been investigated. The first method encompasses mixing 5 g adsorbent with 250 mg Vitamin C directly, then add 10 ml water, react at 95 ^{o}C in the water bath for a specific time. The second method consists of adding 5 g graphene-based materials coated on modified natural zeolite substrate (GBMZS) into Vitamin C solutions at a concentration of 50 mg ml^{-1}, then react at 95 ^{o}C in the water bath for a specific time.

5.2.1 Fabrication of GO coated APTES modified zeolites and recoated GO zeolites

20 g of clean zeolite (the treatment was shown in the chapter 3) was added to 15 ml anhydrous ethanol along with 5 ml APTES which was shaken for 6h. Next 70% ethanol was used to rinse the modified zeolite, which was placed in the oven at 100 ^{o}C for 24 hours. Afterwards the sample was mixed with 15 ml of 2.5 mg mL^{-1} GO solution to with one drop of Triton X-100 added. Samples were then shaken the on the orbital shaker for 120 mins at 150 rpm. The product was dried at 100 ^{o}C for 24 hours, then rinsed by ethanol for 3 times and by water 3 times for removal the extra GO on the surface of the zeolite. Lastly, the GO coated zeolite samples were placed in an oven at 100 ^{o}C for 24 h before using. Table 1 shows the summary of the series of adsorbents in this chapter and Figure 5.1 shows the schematic illustration of APTES modified rGO coated on the zeolites.

Table 5.1 Summary of the series of adsorbents

Samples	Materials	Fabrication	Theoretical loading of GO/rGO (mg g^{-1})
CZ	Clean zeolite	Clean zeolite Process 1[a]	0
AMZ	APTES modified acid treated zeolites	APTES modified process	0
DCGZ	Dry method GO coated zeolites	Drying method coated process	1.8[a]
GAMZ	GO coated APTES modified zeolites	Drying method GO coated APTES modified acid zeolites	2.5[a]
FRGAMZ	4 times recoated GO coated APTES modified zeolites	Four times GO recoated APTES modified zeolites	10[a]
FRrGAMZ	4 times recoated reduced GO coated APTES modified zeolites	*In-situ* Vitamin C reduced GO four times coated APTES modified zeolites	10[a]

[a] The theoretical loading of GO/rGO, calculated from the desorption experiment assuming a 100% adsorption capacity of GO/rGO on the functionalized zeolites surface.

The recoated GO onto the natural zeolite was added to 15 ml of 2.5 mg ml^{-1} GO solution in the beaker containing the 15 g of GO coated APTES modified zeolite. Then it was shaken on the shaker for 120 mins at 150 rpm. The product was dried at 100°C for 24 hours.

5.2.2 Thermal regeneration

Thermal regeneration of the adsorbents was carried out in an electric furnace. According to the literature, rGO has excellent thermal stability at 550 °C, and the melting points of PCB, BPA, and PFOA are lower than 500 °C. The samples were placed in the electric furnace at 500 °C under N_2 atmosphere for 1 hour with at 10 °C min^{-1}. The removal efficiency of disperse blue 26 (melting point at 217 °C) was used to test the regeneration ability of FRrGAMZ.

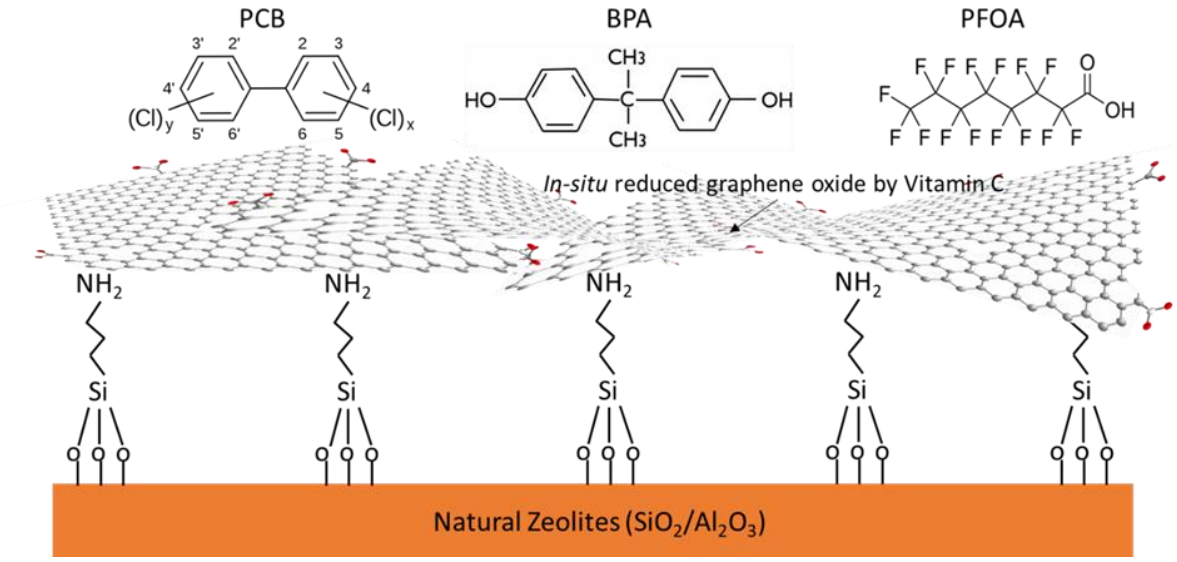

Figure 5.1 The schematic illustration of APTES modified rGO coated on the zeolites surface.

5.3 Results and Discussion

5.3.1 Study of increasing GO loading with surface modification of zeolite

Many research studies focus on the kinetics and isothermal adsorption mechanism of graphene-based products by batch experiment. [165,166, 167,168] While graphene has a large surface area, it has been used ineffectively in water purification. It is desired to fabricate single or few layers graphene-based products which are stable, capable, and easily separated from water. To obtain multilayered sheets or thin-layered graphene-based materials, GO was coated onto the zeolite selected as the support material for deposition and confirmed in previous chapters. The zeta potential measurement was examined to understand the interaction between the zeolite and graphene-based materials. According to the zeta potential shown in Figure 5.2 (a) and (b), both charges of zeolite and GO are negative. Those negative charges originated from the ionization of the C=O, O-C=OH and -OH are from the functional groups of GO and zeolites surface. It is highly

likely that hydrophilicity caused by hydrogen bonding between -OH or -COOH groups on the GO surface and associated -OH groups on zeolite, provided the driving force to form the coating layer on the zeolite surface rather than electrostatic attraction.[169] APTES was used to generate ionic bonding between the zeolite and GO by the interaction of amine groups with oxygen-containing groups to gain a higher loading of GO.[167] In Figure 5.2 (a), it can be seen that surface charge of AMZ switched from negative to positive (17.5 mV at pH=2 and 12.4 mV at pH=11). The results imply that the driving force for the coating layer buildup is primarily due to the electrostatic attraction between the AMZ surface and GO. Therefore, to obtain a higher loading, the drying method coating procedure was performed in a stepwise manner. In this study, we prepared one-time GO coating samples DCGZ and GAMZ, and four-time GO coating samples FRGAMZ and FRrGAMZ to study the influence of loading of GO on the surface of zeolites. (See Table 5.1) The theoretical loading of graphene-based materials was calculated under the assumption that the total amount of GO present was adsorbed to zeolite surface. The theoretical loading of GO increased from 2.5 mg g^{-1} for GAMZ to 10 mg g^{-1} for FRGAMZ, and the zeta potential switched from positive to negative. It demonstrates qualitatively that the GO coating layers are formed by the stepwise adsorption of zeolite and GO.

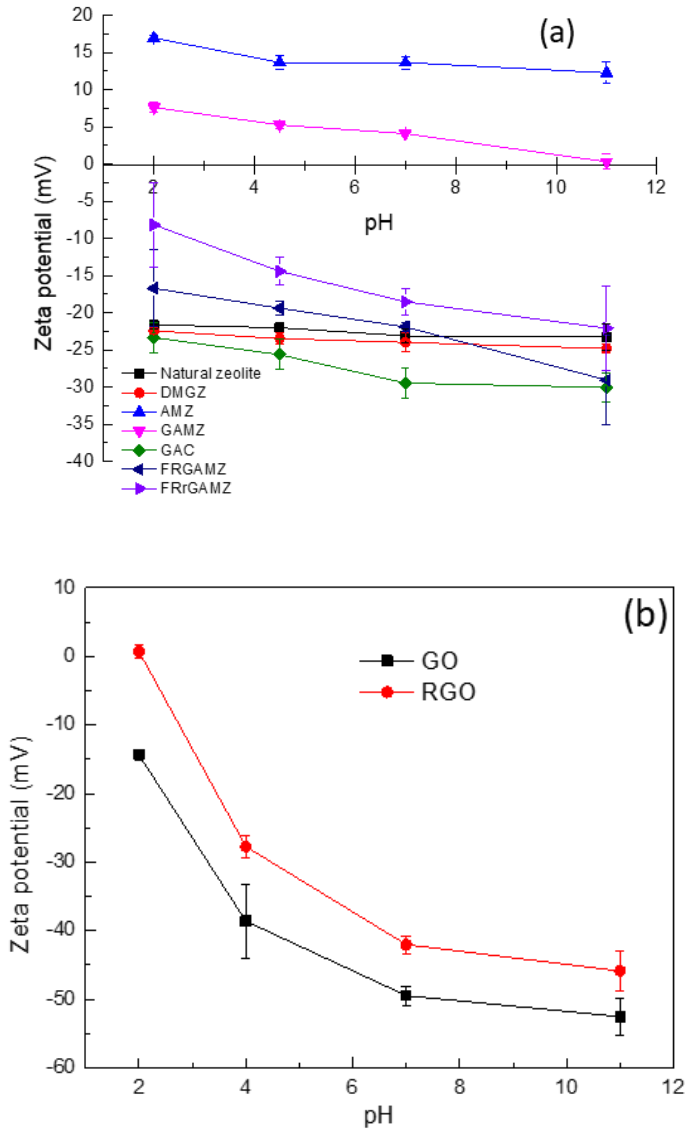

Figure 5.2 Zeta potential of multifunctional adsorbents (a), GO and rGO (b).

XPS was employed to probe the chemical feature of the graphene-based materials and the modified zeolite. To provide the detailed surface composition, XPS C1s core level spectrum were resolved into four peaks representing different chemical environments using a sum of Lorentzian Gaussian functions. The resolving results for commercial GO, natural zeolite, and DCGZ, are presented in Figure 5.3 (a). Briefly, the C1s XPS spectrum of commercial GO indicates a considerable degree of oxidation with four components that correspond to carbon atoms in different functional groups:

sp^2 C, C=O, and O-C=O, the binding energy of the peaks at 284.5, 287.4, and 288.5 eV respectively, which are fitted and assigned according to literature values. [170] Also, the peaks, sp^2, C–O at 285.25 eV and O-C-O bonds are found in natural zeolite which comes from hydrocarbon impurities typically obtained during sample preparation. XPS C1s core level scan spectra of DCGZ were resolved into four peaks, sp^2 C at 284.6 eV, C=O at 287.64 eV, O-C=O 288.25 eV, and C–O at 287.0 eV. The first three peaks are assigned to GO, while the last three are contributed by natural zeolite, which indicates that the GO was successfully coating on the zeolite surface. The AMZ displays a weak and broad N 1s XPS peak between 395 eV and 406 eV. As shown in Figure 5.3 (b), the presence of the three peaks at 398.76, 401.1, and 402.2 eV in the N 1s spectrum provides direct evidence of the successful grafting of APTES onto the surface of the zeolite. The peak at 399.8 eV is attributed to the free terminal amine groups on the APTES, whereas the peaks at 401.1 and 402.2 eV probably resulted from protonated amine NH^{3+} or hydrogen bonded NH_2. [171]

Direct observation of the GO adsorption on the zeolites surface was provided by SEM: the morphology of the surface of natural zeolite (a, b), AMZ (c), DCGZ (d), GAMZ(e), FRGAMZ(f) are displayed in Figure 5.4. The natural zeolite and AMZ featured porous, sharp-edged and rough surface with mean diameter in the 10-20 µm range. SEM images obtained from GO coated zeolite are essentially identical to those of the uncoated zeolite. The presence of GO coating layer on the zeolite surface results in the zeolite surface smoothness. Single or few layers coating was shown in Figure 5.4 (d) for DCGZ, which is the evidence that GO sheets were coupled to the zeolites. After modification by APTES, GAMZ, the surface was partially coated by GO which means that the surface of the zeolite was not saturated by GO adsorption. Zeolites can interact with GO sheets through physisorption and electrostatic binding. This finding is corroborated by EDX element mapping measurements shown in Table 5.2. SEM images of low and high loading GO on the

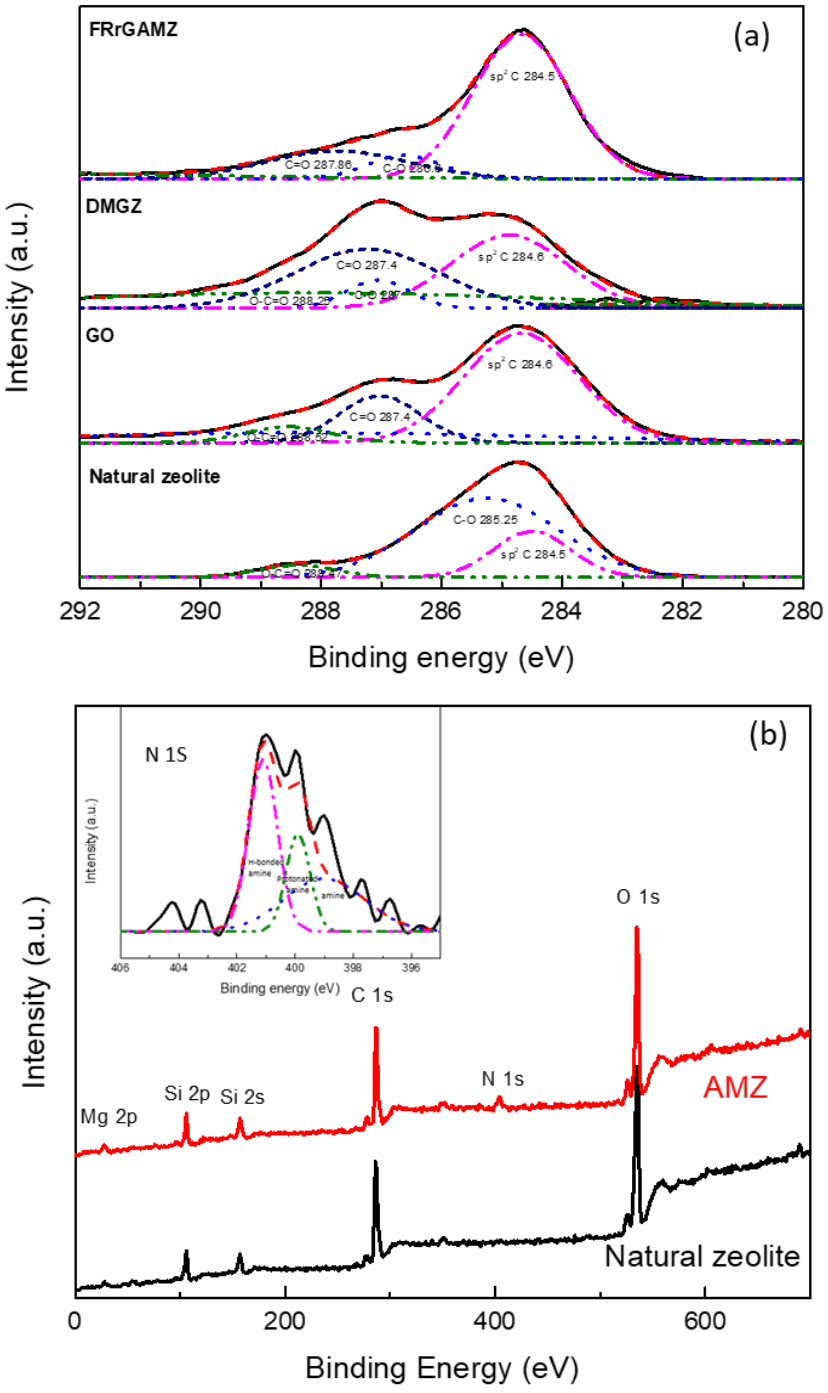

Figure 5.3 High-resolution XPS scans for C1s peaks of GO, natural zeolite, DCGZ and FRrGAMZ(a), and N1 peaks of AMZ (b).

zeolite (DCGZ & FRGAMZ) cross section was observed in Figure 5.4 (f, g), respectively. This observation indicates that thin-layered GO of DCGZ was coated on the zeolites surface around 1 to 1.5 µm. While after the four-time coating, the thickness of GO layers increased to 2 to 3 µm. The binding of the zeolite to GO maintains the interaction between them. EDX was conducted to quantify and elucidate the chemical compositions of GO with zeolite. The C, O, Si and Al were selected as the general elements. It is shown that with increased coating times, the ratio of C/O atomic ratio has increased from 0.06 for natural zeolite to 0.49 for FRGAMZ, while the pure C/O of pure GO is 3.1. [172]

For all samples, BET and DFT specific pore volume and surface areas, V_{BET}, V_{DFT}, S_{BET} and S_{DFT} gave in Table 5.3. The V_{BET} and S_{BET} values were calculated for assuming mesoporous geometry. The V_{DFT} and S_{DFT} values were calculated using the regularized density functional theory model assuming microporous geometry. Comparing the values of the few layered DCGZ with GAMZ calculated by BET and DFT, both pores volume and surface area were reduced. It is possible to conclude that the strong bonding of the GO coating layer reduced the specific surface area contributed from GO sheet. After four times recoating, the pore volume (BET) increases to 8.5×10^{-2} cm^3 g^{-1} while the pore volume (DFT) is lower than DCGZ. However, these specific surface areas are approximately equal. It indicated that multiple coating layers were formed on the zeolites surface while the specific active surface area was the same or even reduced. It is highly possible to lead to a decrease of adsorption capacity of GO.

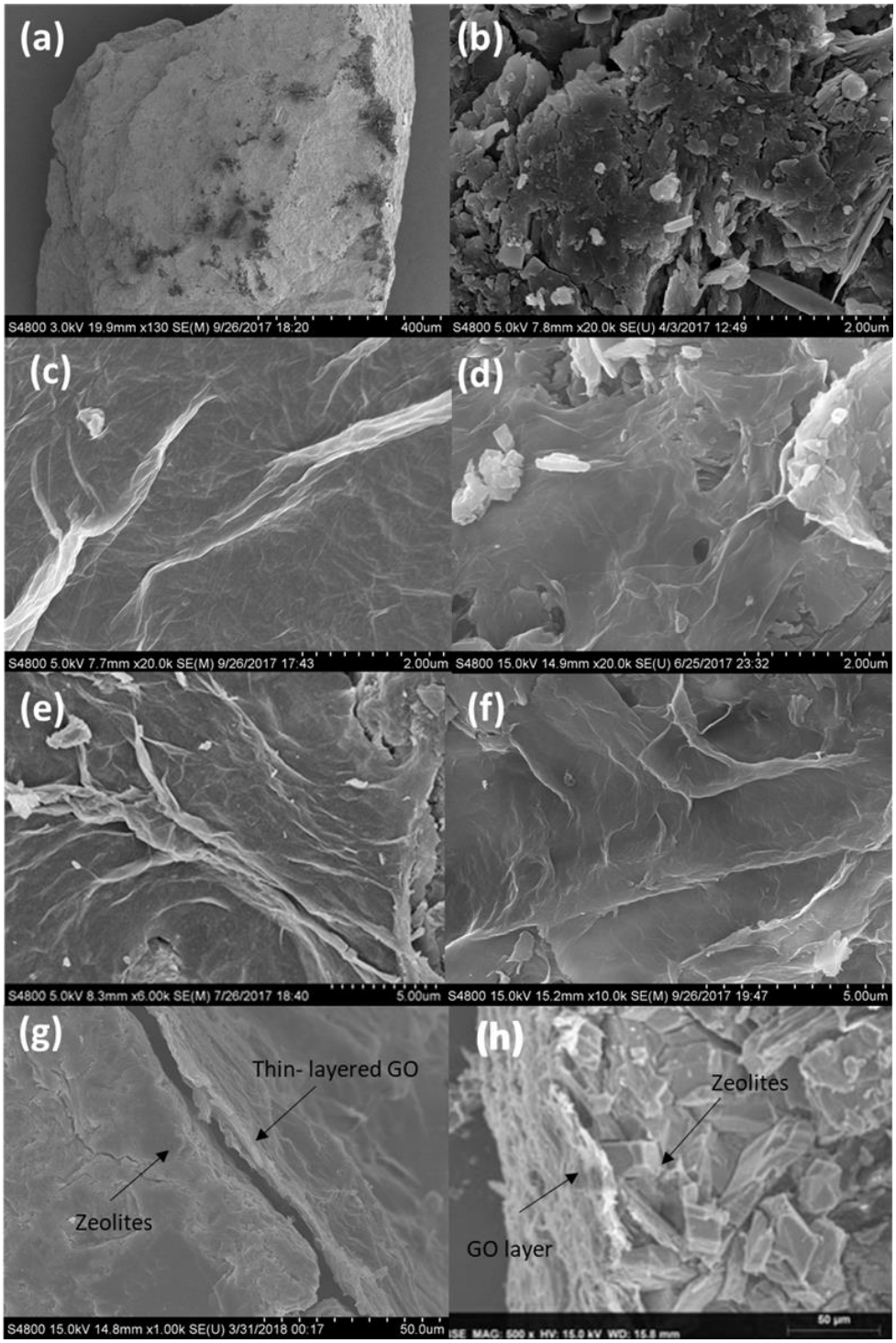

Figure 5.4 SEM images of adsorbents. The surface of natural zeolite (a, b), DCGZ (c), GAMZ(d), FRGAMZ(e) and FRrGAMZ(f). The surface and the cross-sections of DCGZ and FRrGAMZ (g) and (h).

Table 5.2 EDX analysis of chemical compositions

Samples(wt%)	C	O	Si	Al	C/O
Natural Zeolite	3.25±0.86	55.25±3.80	35.98±1.86	5.71±2.46	0.06
DMGZ	12.59±2.01	47.01±5.45	42.46±1.24	0.72±0.37	0.21
GAMZ	16.12±3.59	45.21±1.84	35.98±2.55	2.79±0.02	0.36
FRGAMZ	23.05±5.09	47.52±6.13	29.01±9.50	1.22±0.29	0.49
FRrGAMZ	42.80±3.02	38.28±4.10	17.43±1.84	1.49±0.67	1.12

An appropriate assumption for this phenomenon can be explained by the bonding intensity between that GO and zeolites. Before the zeolite surface modification, the thin GO coating layers have a weak interaction with zeolites surface, which led to a more substantial microporous volume and surface area. The gap between GO layers and zeolites can be seen in the SEM image of the cross-section of DCGZ in Figure 5.4 (g). After modification, the thin GO layers have a robust electrostatic attraction with the modified zeolite surface. Thus, the specific volume and active surface area of GO was reduced. Even though increasing the GO layers by repeating the coating steps, it could not contribute to improving the specific volume and surface area which is possible lead to a decrease of adsorption capacity of GO. The assumption of the surface structure of DCGZ and GAMZ.is shown in Figure 5.5.

Table 5.3 BET and DFT specific volume and surface of all samples

Samples	Pore structure			
	V_{BET} ($cm^3\ g^{-1}$)	V_{DFT} ($cm^3\ g^{-1}$)	S_{BET} ($m^2 g^{-1}$)	S_{DFT} ($m^2\ g^{-1}$)
CZ	7.09×10^{-3}	3.8×10^{-2}	15.08	14.7
DCGZ	3.1×10^{-2}	0.1	101.6	159.4
GAMZ	2.7×10^{-2}	2.4×10^{-2}	51.0	109.6
FRGAMZ	8.5×10^{-2}	7.6×10^{-2}	101.6	159.3
FRrGAMZ	6.8×10^{-2}	6.1×10^{-2}	60.8	94.8

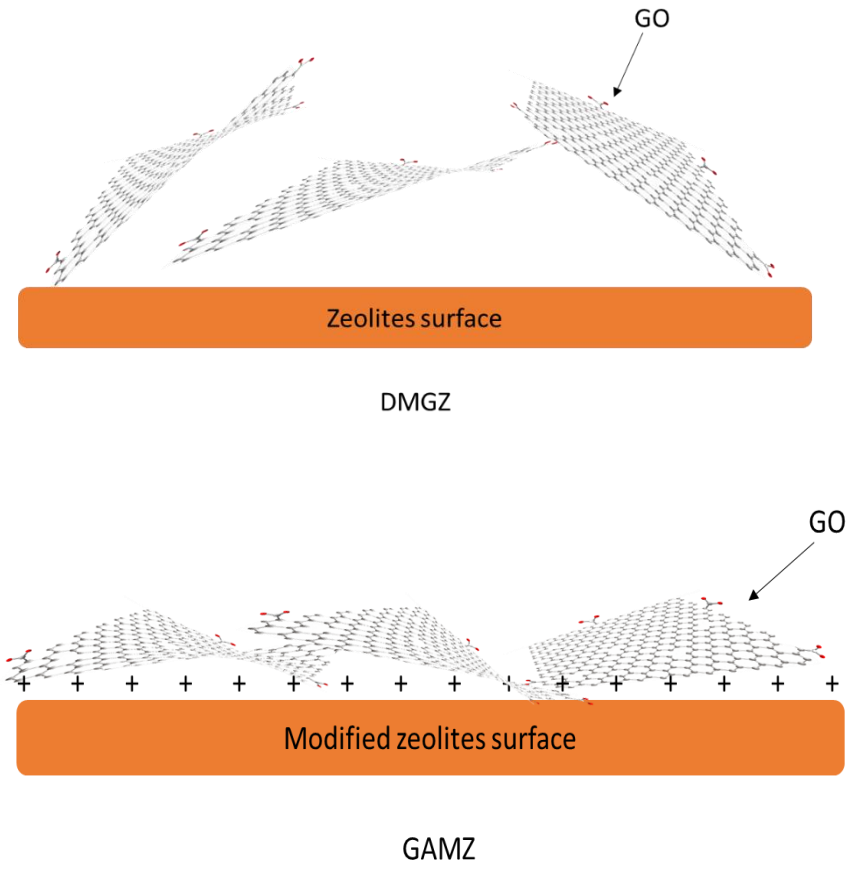

Figure 5.5 Schematic illusion of surface structure of DCGZ and GAMZ.

5.3.2 *In-situ* GO reduction on zeolite

In-situ reduction of GO on the support material is desirable for water purification process due to the insolubility of rGO with water and its incompatibility with zeolites surface. Chemical reduction is effective at moderate temperatures but involves considerable care, multiple steps, and some of the reagents are toxic. [172] Vitamin C was introduced as a reducing reagent to in-situ reduce the GO on zeolites. The desorption of rGO from zeolite is not desirable for economic and environmental reasons. [173] As previously mentioned, the interaction between zeolites surface and GO are mainly attributed to their hydrophilicity. The functional groups of GO, such as -COOH, -OH, offer negative charges so that GO can be adsorbed on the zeolites surface tightly. The oxygen functional groups in GO sheets can be removed and the conjugated graphene network reestablished by vitamin C reduction. [174]

In Figure 5.6, Raman spectra of DCGZ and FRrGAMZ displayed two prominent peaks at 1340 cm^{-1} and 1585 cm^{-1} corresponding to the well-documented G and D bands, respectively. [175] The I_D/I_G intensity ratio of DCGZ was calculated to be 0.87. After four-times coating, FRGAMZ was reduced at 90 ^oC for 1 hour with 50 mg g^{-1} vitamin C solution, and the I_D/I_G intensity ratio was dramatically increased to 1.37, suggesting that the reaction of vitamin C formed a greater extent of reduction and a more substantial number of defects over the graphene sheets. Also, to control the degree of *in-situ* reduction of GO on zeolite, the influence of the concentration of vitamin C and reaction time were studied and are shown in Figure 5.7. The results show that the extent of GO *in-situ* reduction was well-controlled by the above factors, and the optimized reduction conditions were used for further research. Meanwhile, surface and cross-section morphology of FRrGAMZ are shown in Figure 5.4 (g, h) providing evidence that few layers of rGO were coating on the modified zeolites surface.

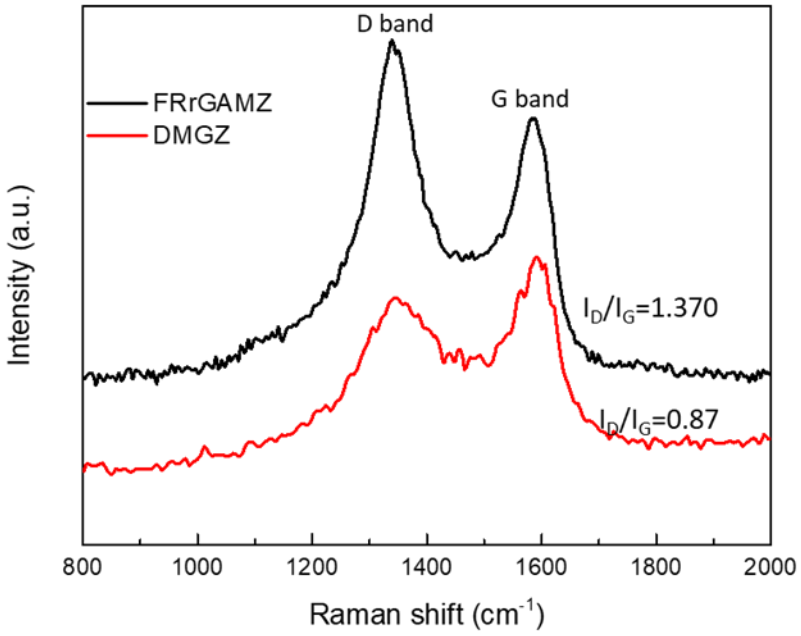

Figure 5.6 Raman spectra of DCGZ and FRrGAMZ.

Interestingly, adding vitamin C method can also affect the reduction gradient of GO, which is shown in Figure 5.7 (c). Mixing the vitamin C powder with GAMZ directly leads to a higher extent of reduction, while the ratio of I_D/I_G can only reach to 1.19 by adding the vitamin C solution. Possible explanation is that the local concentration of vitamin C obtained by method 1 is higher than the one by method 2. The higher the concentration of vitamin C, the more reduction extent of GO can be achieved. Herein, we used the method 1 for further research.

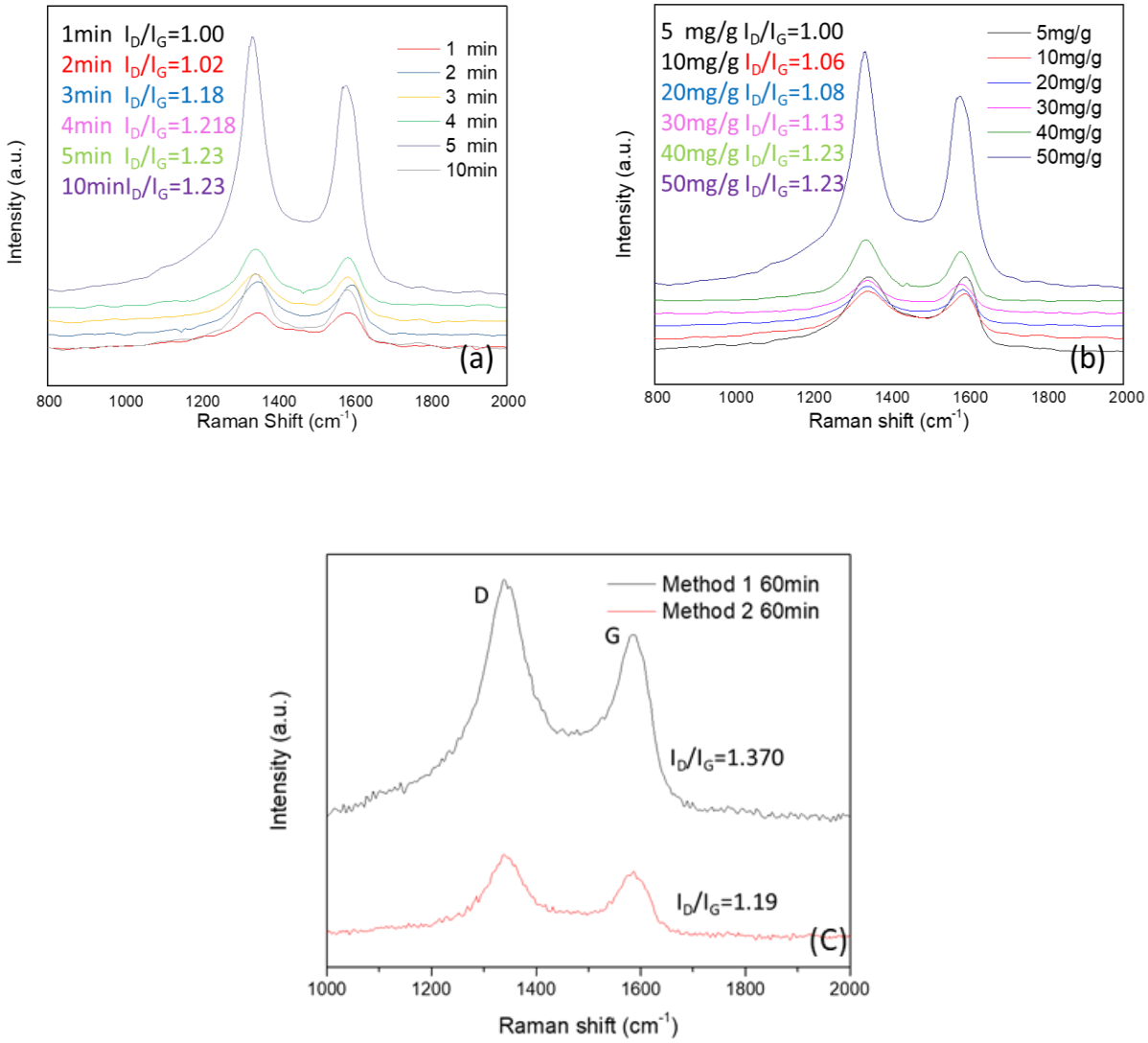

Figure 5.7 Raman spectra of *in-situ* reduction of GO by being reduced for 1 to 10 min (a), different amount and adding methods via vitamin C. (a, b) The adding method 1: was mixing 50 mg g^{-1} vitamin C powders with adsorbents directly, then adding 1ml g^{-1} (adsorbent) water at 90°C in water bath for 60 min. The adding method 2: was mixing 50 mg ml^{-1} vitamin C solution with adsorbents, then react at 95°C in water bath for 60min. (c)

In addition to constituting a well-controlled *in-situ* reduction of GO on zeolites surface, information provided by XPS analysis of C1s spectra of FRrGAMZ shows that the peak change is contributed from C=O and O-C=O groups. After treated by vitamin C, the C=O bonding shifts from 287.4 eV to 287.86 eV, and the intensity of C=O and O-C=O peaks is reduced dramatically which indicates the loss of oxygen and conversion to new chemical species. Theoretically, the oxygen-containing functional groups on the GO nanosheets are the only resource of C=O on the zeolite, so the peak area percentages of C=O to the total peak area of all chemical bonds can be used to indicate the reduction degree of GO. The remaining C=O group and C-O peak contributed from rGO and zeolite respectively suggested that the reduction of GO was partially reduced. The zeta potential in Figure 5.2 (b) also shows that the value of zeta potential of rGO is higher than GO due to the lack of functional groups on the surface. Therefore, the value of zeta potential of rGO with modified zeolite is higher than that of GO with the modified zeolites. For example, the value of zeta potential of FRrGAMZ (-8.2 eV) is lower than the one of FRGAMZ (-16.8 eV) at pH=2, which indicates that the in-situ reduction procedure occurred on zeolite readily by adding vitamin C. The EDX analysis in Table 5.2 shows that the ratio of C/O increased from 0.49 for FRGAMZ to 1.12 for FRrGAMZ, confirming the decomposition of the functional groups of GO on the zeolite surface. BET analysis in Table 3 also shows a reduction of microporous volume and specific surface area. This method provides a quantitative evaluation of *in-situ* reduction of GO on zeolite by vitamin C.

5.3.3 Organic model compounds adsorption experiment

To examine the removal efficiency and adsorption capability of the adsorbents, non-ionic disperse blue 26, cationic methylene blue and anionic sodium fluorescein were selected in this study. Figure 5.8 (a, b) shows the results of the removal efficiency and adsorption capacity of the variably

charged organic model compounds which is compared with the commercial GAC. Adsorption experiments shows that thin-layered graphene-based materials have higher removal efficiency capability than GAC. In order to prove that the CZ does not contribute significantly to adsorption capacity for organic model compounds, the adsorption experiment of CZ was conducted. It shows that the adsorption capacity of the column test is only 0.26 mg g^{-1}, 0.51 mg g^{-1} and 2.12 mg g^{-1} for disperse blue 26, sodium fluorescein and methylene blue, respectively. (See Chapter 3).

Compared with the adsorption capacity of graphene-based materials shown in Figure 3.5 (b), the contribution from clean zeolite is insignificant. In Figure 5.8 (a), it shows that the removal efficiency of disperse blue 26 increased from 69.5% for DCGZ to 94.5% for GAMZ. The zeta potential in Figure 5.2 (a, c) provides that charge of disperse blue 26 is higher than GAMZ but less than methylene blue in the pH range between 2 to 11. Thus, the mechanism of adsorption of disperse blue 26 for GAMZ should be resulted from the large surface area with active sites of GO and π-π stacking interaction between organic model compounds and GO. With the increasing of GO loading, the removal efficiency of disperse blue 26 reaches up to 99.4% for FRGAMZ. Especially, FRrGAMZ shows a remarkable removal efficiency of 99.9% for disperse blue 26, which should be benefited from both high loading and partially in-situ reduction of GO.

Similarly, the removal efficiency of anionic dye increased from 96% for DCGZ to 99.9% for FRrGAMZ. For cationic methylene blue, all the adsorbents showed an excellent removal efficiency which was over 99% because of π-π electron donor-acceptor interactions and electrostatic attraction between positively charged dye ions and negatively charged adsorbents. Another explanation for the excellent removal is that the unique porous structure of natural zeolites gives an excellent cationic exchange and sorption properties confirmed by numerous studies so far. [137] For anionic sodium fluorescein, the removal efficiency of DCGZ is less than commercial GAC

probably due to the strong electrostatic repulsion from GO. With the increasing amount of GO, the π-π stacking interaction and large surface area play a vital role in the adsorption. Moreover, the partial reduction of GO by vitamin C improved the adsorption capacity of sodium fluorescein. In Figure 5.8 (a), the order of removal efficiency of variably charged organic model compounds was FRrGAMZ> FRGAMZ > GAMZ >DCGZ.

The adsorption capacities of graphene-based materials attached on natural zeolite were obtained and are shown in Figure 5.8 (b). They display remarkable adsorption capabilities of variably charged organic model compounds much higher than GAC. To the best of my knowledge, the single adsorbent applied for adsorption of multiple charged organic model compounds was reported for the first time.

The breakthrough curves for organic model compounds are presented in Figure 5.8 (c, d, e). For disperse blue 26, faster attainment of exhaustion was observed for natural zeolite at 80 mins and DCGZ at 120 mins. As the loading of GO increased, smoother breakthrough curves were obtained. The maximum adsorption capacity obtained is 192 mg g^{-1} for GAMZ. This experiment was performed up to 140 mins, which was much higher than that of most of the reported adsorbents, such as multi-walled carbon nanotubes (77.5 mg g^{-1} neutral red), AC (48.7 mg g^{-1} for congo red) and metal oxide (105 mg g^{-1} neutral red). [175,176,177] It is worth pointing out that the adsorption capacity of GAMZ is higher than DCGZ, possibly because it is related to the increased electrostatic interactions with the surface of GO which is due to a more homogenous coating and relatively more active sites per mass. Compared with GAMZ, the adsorption capacity of disperse blue 26 for higher loading FRGAMZ was decreased from 192 mg g^{-1} for GAMZ up to 117 mg g^{-1} up to 140 min, because its active sites per mass were reduced as a result of the multiple layers caused by

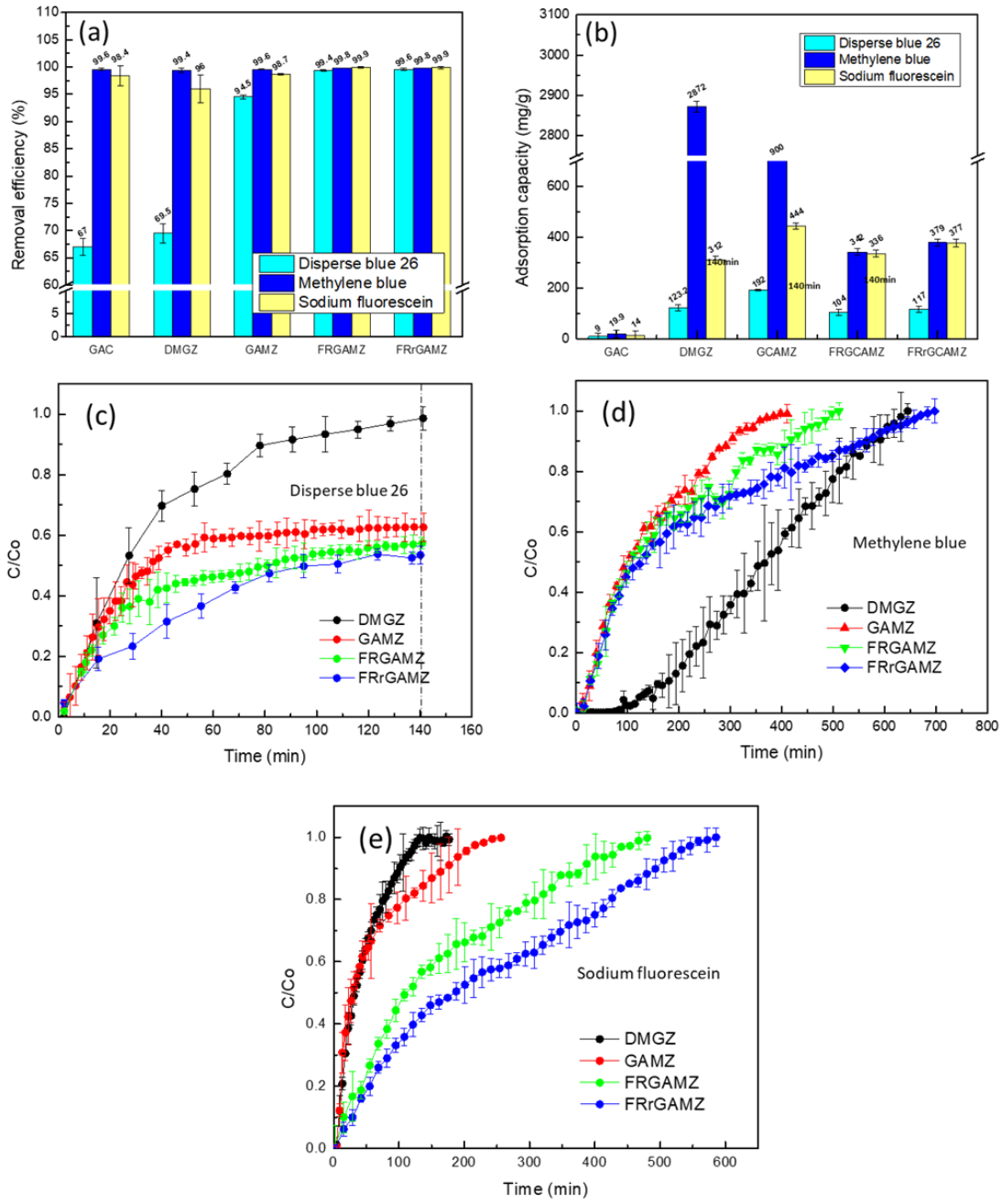

Figure 5.8 The removal efficiency and adsorption capacity of organic model compounds by different engineered zeolites (a, b), the exhaustion experiment for disperse blue 26(c), methylene blue(d), and sodium fluorescein(e). The pH of organic model compounds solution=7, flow rate= 5ml min^{-1}, the amount of GBMZS=9g, and the concentration of organic model compounds is 40mg L^{-1} (1ml).

multiple coating steps. However, decreased adsorption capacity caused by increasing layers of GO reduces the active sites per mass.

Additionally, FRrGAMZ which was reduced from FRGAMZ has a higher adsorption capacity due to the partially reduced GO. Similarly, the adsorption experiment of cationic organic model compounds, methylene blue, exhibited a remarkable adsorption capacity shown in Figure 5.8 (d). It was noted that the DCGZ has a higher adsorption capacity of 2872 mg g^{-1} than the others. This result indicates that the remarkable performance toward cationic adsorbates is probably correlated to the electrostatic interaction between the large surface area of single or few layers of GO with negatively charged natural zeolite and the positively charged dye. The positively charged GAMZ shown in Figure 5.8 (a) maintains an incredible adsorption capacity for methylene blue which achieves approximately 900 mg g^{-1}. Its remarkable adsorption is due to the large surface area and single or few layers of GO loading. As coating layers increase on the surface, the adsorption capacity of methylene blue decreases from 900 mg g^{-1} to 342 mg g^{-1} for FRGAMZ due to the decrease of specific coating layers of GO on the zeolites surface.

In Figure 5.8 (e), the breakthrough curves of anionic sodium fluorescein show that the DCGZ reaches the saturation point at 145 mins, while the GAMZ reaches approximately 240 min. With the increasing loading and reduction of GO, the maximum saturation reaches up to 600 min for FRrGAMZ. The increased adsorption sites in the presence of rGO improved the adsorption capacity for organic model compounds. The adsorption capacity decreases slightly from 444 mg g^{-1} for GAMZ to 377 mg g^{-1} for FRGAMZ. It can be explained by the increased coating layers and decreased specific surface area of GO on zeolites. In general, the high capacities for variably charged organic model compounds for the robust multifunctional adsorbent are due to the increased adsorption sites, π-π stacking of rGO and electrostatic interaction to adsorbates.

5.3.4 POPs adsorption

In 1976, United States Congress banned PCBs domestic production, and United States EPA suggests that PCB exposures below the oral reference dose (RFD) of 20 ng kg^{-1} day^{-1}.42 USFDA estimated that the daily BPA exposure level for adults in 2007 was about 0.16 μg kg^{-1} day^{-1}. [178] In addition, the Office of Water estimated a cancer slope factor of 70 μg kg^{-1} day^{-1} for PFOA based on testicular tumors and confirmed its lifetime. [179]

To evaluate the removal ability of our adsorbent for removing POPs from water, 40 mg/L of PCB, BPA and PFOA solutions were introduced to FRrGAMZ by independent column tests. As shown in Figure 5.9 (a), FRrGAMZ has high removal efficiencies to adsorb these POPs, especially for PCB which has 100% removal due to its relatively positively charged property shown in Figure 5.9 (a). Also, lower removal efficiency for BPA and PFOA is possibly due to the hydrophobicity and presence of negative charge, whereas, it maintains 94.5% and 96.1% removal respectively. It is, as discussed above, because of the large surface area and π-π stacking of rGO. To investigate adsorption ability, the experiment was also conducted with 200 μg L^{-1} POPs for 24 hours shown in Figure 5.9 (b). Neutral pH value and flow rate for 5ml min^{-1} were selected to simulate the water treatment condition.

These results indicate that rGO can provide excellent adsorption for PCB which are relatively positively charged when compared to the adsorbent. It also shows that over 82% of BPA and PFOA in the solutions can adsorb onto the FRrGAMZ after 24 hours. These results are consistent with organic model compound adsorption studies for disperse blue 26 and sodium fluorescein removal discussed in Chapter 3. The long-term POPs adsorption experiments show that our adsorbent has a good adsorption ability for different charged organic contamination.

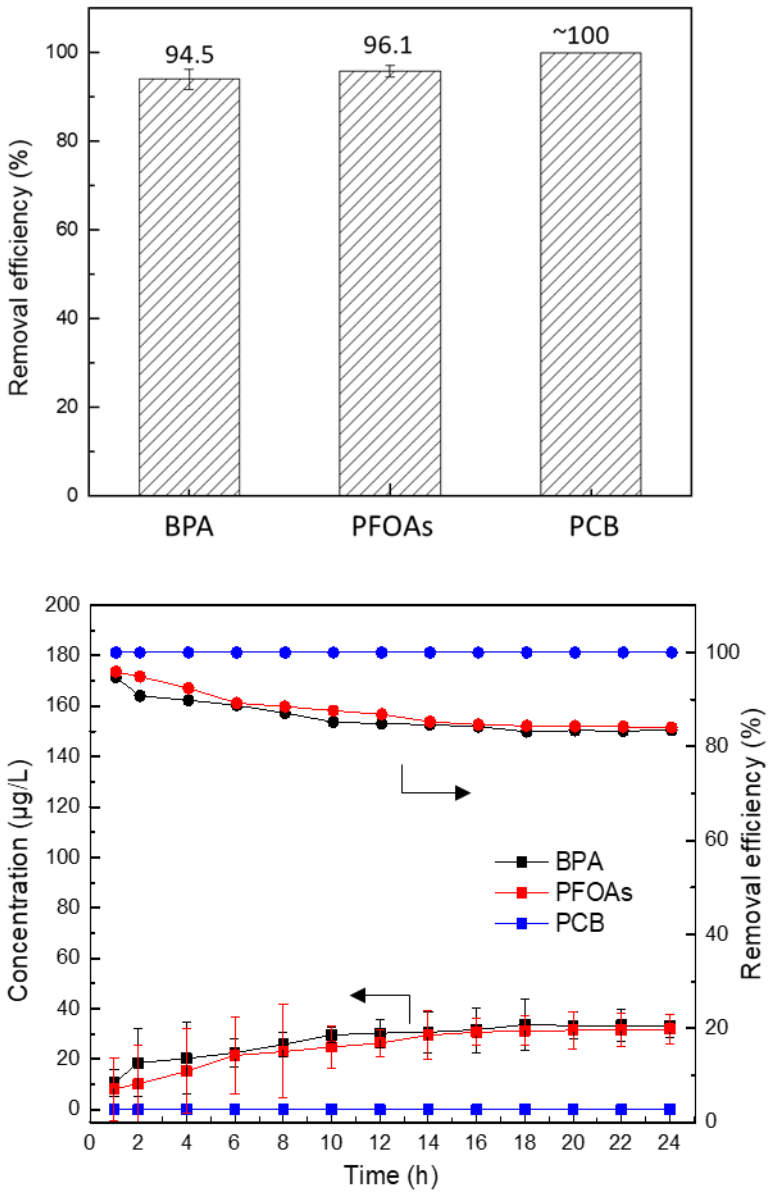

Figure 5.9 The removal efficiency of POPs (40 mg L^{-1},1ml) by FRrGAMZ (a) and long-lasted 200 μg L^{-1} of POPs adsorption. The pH of POPs solution=7, flow rate=5 ml min^{-1}, the amount of FRrGAMZ= 9 g.

5.3.5 Desorption experiment and thermal regeneration

To test the stability of the robust multifunctional adsorbent for large scale application, the desorption and thermal regeneration experiment were also explored. The relative weight loss of

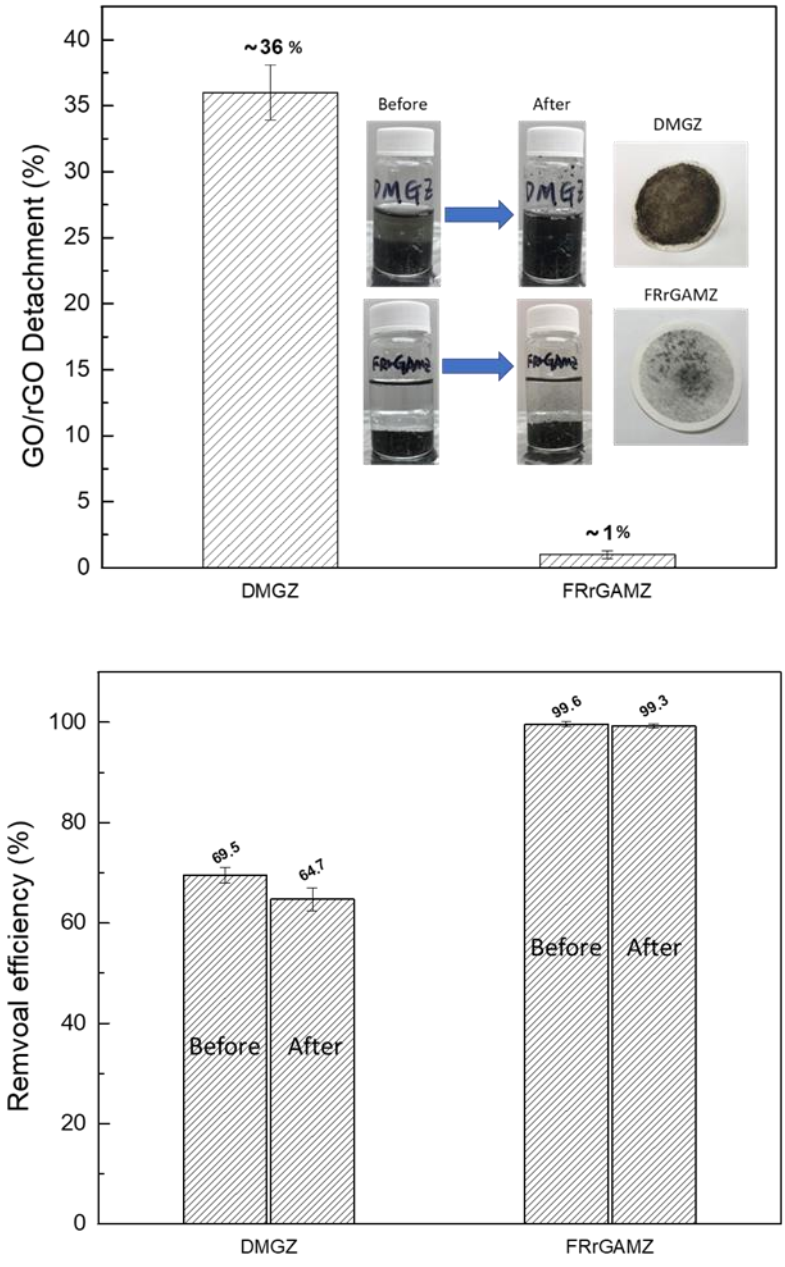

Figure 5.10 The relative weight percent of GO/rGO detached from zeolites (a) and the removal efficiency of disperse blue 26 before and after desorption experiment for DCGZ and FRrGAMZ (b). The

pH of disperse blue 26 solutions = 7, flow rate= 5 ml min^{-1}, the amount of DCGZ and FRrGAMZ= 9 g, and the concentration of disperse blue 26 is 40 mg L^{-1} (1 ml).

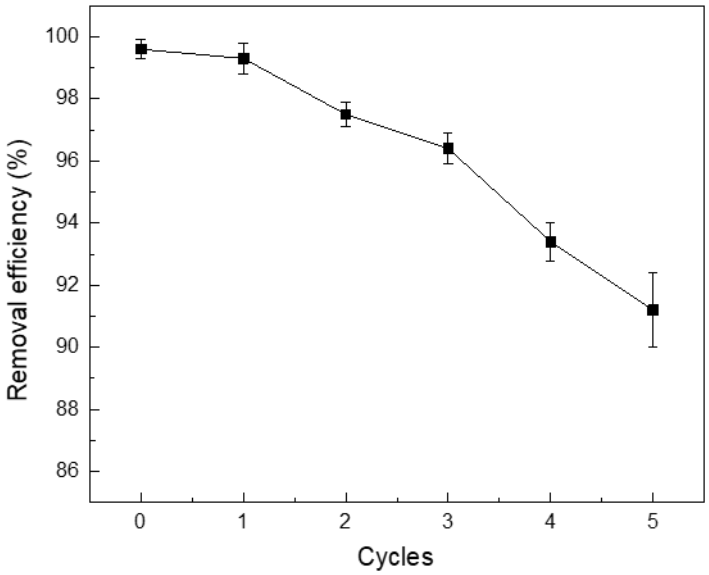

Figure 5.11 The removal efficiency of disperse blue 26 for thermal regeneration of FRrGAMZ under N_2 at 550 ^oC for 1hrs. The pH of disperse blue 26 solutions =7, flow rate= 5 ml min^{-1}, the amount of FRrGAMZ= 9 g, and the concentration of disperse blue 26 is 40 mg L^{-1} (1 ml).

GO/rGO detached from zeolites and removal efficiency of disperse blue 26 were measured and shown in Figure 5.10. It has been reported by many studies that the desorption of graphene-based materials from the surface of support material are mainly caused by the weak driving force between them. [171,180.181] After shaking at 200 rpm for 24 hours, about 36% of GO was detached from DCGZ and the removal efficiency of disperse blue 26 reduced from 69.5% to 64.7%. While 1% weight loss of rGO was detached from the FRrGAMZ, 99.3% removal was maintained. This is attributed to the well-controlled partially reduction of GO by vitamin C, and the strong interaction between zeolite and rGO. To determine the thermal regeneration ability, FRrGAMZ was tested by heating under N_2 at 550 ^oC for 1 hour and tested by non-ionic disperse blue 26 was selected as

adsorbate. The result shows that the removal efficiency reduced with cycle numbers and maintained over 91% after five cycles in Figure 5.11. The decrease of removal efficiency may be caused by the loss of active sites of rGO.

5.4. Conclusion

In summary, a thin-layered rGO with natural zeolite as a substrate was developed as a novel adsorbent for POPs removal from water. We overcame the limited GO loading firstly by modifying the natural zeolite surface by APTES to increase the loading of GO and to limit the desorption of graphene-based materials from the surface. Secondly, the reduction extent and gradient of the adsorbed GO on zeolites surface was successfully controlled by environmentally friendly vitamin C and microwave in-situ to enhance the adsorption capacity for POPs. The thin-layered rGO provided a reliable and effective way to remove POPs from water. The high adsorption capacities were attributed to the more active sites on the rGO. It is easily recycled and exhibits good regeneration ability which is beneficial to reduce the cost. These results prove that the thin-layered rGO coated on zeolites can be used for various types of water contaminants and is a promising candidate for water purification.

Chapter 6 Adsorption mechanism study of FRrGAMZ for organic model compound removal

6.1 Introduction

The adsorption mechanism of graphene-based materials for dyes and organic pollutants have been study in recent years. Ramesha et al. have prepared exfoliated GO and rGO for the adsorption of various charged dyes such as methylene blue, methyl violet, rhodamine B, and orange G from aqueous solutions. [182] Yang et al. and Zhang et al. have reported that GO sheets as an adsorbent for removal of methylene blue from aqueous solutions. [183,184] To understand the transportation of adsorbates by diffusion on the graphene-based materials, kinetic modeling plays a significant role in providing an explanation of reaction pathways. An appropriate kinetics model assumption can provide the rate of adsorption to understanding the adsorption mechanisms and behavior for designing the adsorption and filtration system in the water treatment process application. The equilibrium of adsorbate adsorption is also an important parameter to provide an approximate exhaustion conditions at the end of the adsorption process. Isothermal study is to plot the amount of adsorbate on the adsorbent as a function of its concentration (if liquid) at constant temperature. It is worth to be mentioned that even a good fit between experimental data and isotherm-type does not necessarily imply that the underlying mechanism is identical to the one suggested by the model. [185]

The aim of this chapter is to study the adsorption mechanism of FRrGAMZ for the removal of organic model compounds. Methylene blue was selected for the present investigation as adsorbate. From the previous study, the adsorption experiment results indicate that the mono or few layered

GO or rGO sheets have more specific active sites than GO or rGO bulk. The few layered FRrGAMZ has a good adsorption capacity for organic model compounds than GAC.

Herein, two hypotheses were listed as following: 1) The overall sorption rate is limited by the rate of organic model compounds diffusion in the pores of few-layered rGO (intraparticle diffusion model). It has been investigated by several experimental study, e.g. Wu et al., Jin et al. and Ahsaine et al., which proved that the pseudo-second-order kinetics model was fitted to the adsorption experimental results.[186,187,188] 2) There is a limited number of sorption sites on few layered rGO, and that the sorption speed is proportional to the number of unoccupied sites as well as to the concentration of the dyes in contact with the solid phase. From the literature research, experiments have shown that the Langmuir isotherm yielded better agreement with experimental results. [186,187,188]

6.2 Experimental

6.2.1 Materials

Australian natural zeolite, (clinoptilolite, diameter: 0.7-1 mm, chemical composition: 68.26% SiO_2, 12.99% Al_2O_3, 4.11% K_2O, 2.09% CaO, 1.37% Fe_2O_3, 0.83% MgO, 0.64% Na_2O, 0.23% TiO_2, Zeolite Australia Ltd.), graphene oxide (ACS Materials), Triton X^{TM}-100, Vitamin C (Sigma-rich, 99%), methylene blue (Electron Microscopy Sciences).

6.2.2 Batch experiment

Adsorption capacity studies were conducted by batch experiments and column tests using the organic model compounds in aqueous solution. Batch experiments were carried out to determine the adsorption performance of organic model compounds onto the adsorbents in a 250 mL glass flask. The sample was immersed in 100 mL of a specific concentration of methylene blue and was shaken at 150 rpm for 48 hours to reach adsorption equilibrium. The study was conducted at room

temperature to represent conditions that are typical in the industrial setting. The pH of the solution was adjusted with a 0.1 M solution of NaOH and a 0.1 M solution of HCl. The effect of various factors on the rate of adsorption process was assessed by varying contact time, concentration of organic model compounds, and pH of the solution. All experiments were carried out in triplicate, and the average values were taken for analyses.

6.3 Mathematical modeling

6.3.1 Kinetic study of adsorption mechanism of FRrGAMZ

The kinetic models are adopted to describe the mechanism of the adsorption process. From the literature research, the adsorption mechanism of graphene-based materials was usually fitted to the pseudo-second-order kinetics model described by the following equation (6.1). [189,190,191]

$$\frac{t}{q_t} = \frac{1}{k_1 q_e^2} + \frac{1}{q_e} t \qquad (6.1)$$

where q_t is the adsorption capacity by time, q_e is the adsorption capacity at equilibrium, and k_1 (g mg^{-1} min^{-1}) is the rate constant for the pseudo-second-order kinetics model. From the equation (6.1), the values of the k_1 and q_e can be calculated from the slope and intercept of the linear plots of t/q_t verses t.

6.3.2 Isothermal study of adsorption mechanism of FRrGAMZ

The equilibrium adsorption data were analyzed by Langmuir isothermal models described by equation (6.2). [192]

$$\frac{C_e}{q_e} = \frac{C_e}{q_m} + \frac{1}{q_m k_L} \qquad (6.2)$$

where C_e (mg/L) is the equilibrium concentration, q_e (mg/L) is the amount adsorbed at equilibrium, k_L (L/mg) is the equilibrium adsorption constant which are related to the heat of adsorption, and q_m(mg/g) is the maximum adsorption capacity for complete monolayer coverage. The values of C_e/q_e versus Ce determine q_m and k_L from the intercept and the slope, respectively. The dimensionless equilibrium parameter R_L is expressed for essential characteristics of Langmuir isotherm model, which is given by the following equation: [193]

$$R_L = \frac{1}{1+k_L C_0} \qquad (6.3)$$

The value of R_L indicates that the type of the isotherm to be either unfavorable ($R_L > 1$), linear ($R_L = 1$), favorable ($0 < R_L < 1$) or irreversible ($R_L = 0$).

6.4 Results and discussion

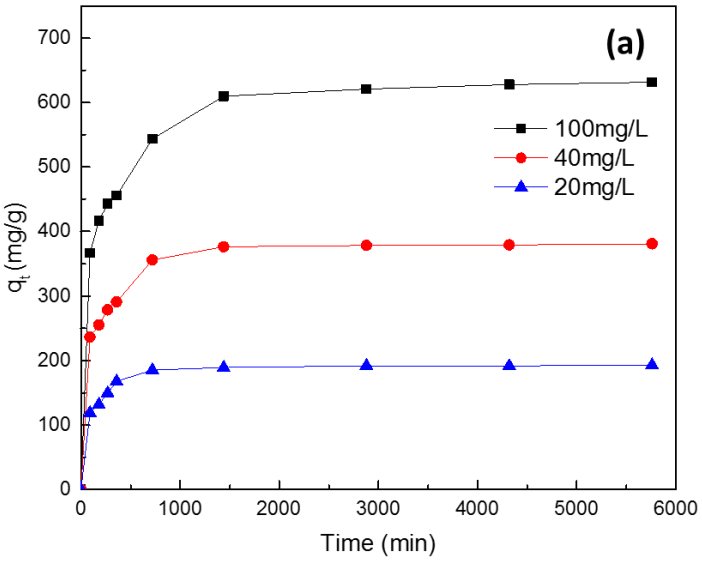

Figure 6.1 The effect of different concentration on adsorption capacity of methylene blue onto FRrGAMZ. The concentrations of methylene blue are 20 mg L^{-1}, 40 mg L^{-1} and 100 mg L^{-1}, respectively. The experiment conditions are at room temperature, at pH=6~7.

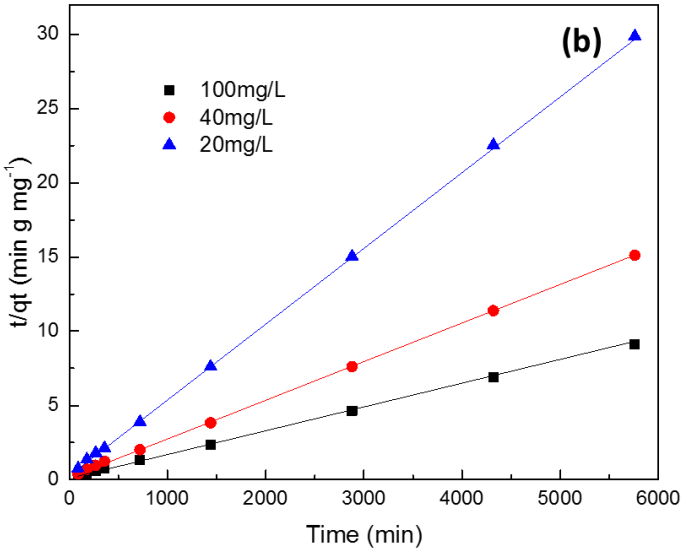

Figure 6.2 Pseudo-second order kinetics of adsorption methylene blue onto FRrGAMZ. The concentrations of methylene blue are 20 mg L^{-1}, 40 mg L^{-1} and 100 mg L^{-1}, respectively. The experiment conditions are at room temperature, at pH=6~7.

Table 6.1 The effect of different initial concentrations of methylene blue onto FRrGAMZ at room temperature.

C_o (mg/L)	$q_{e,\,exp}$ (mg g^{-1})	q_e (mg g^{-1})	k_1 (g mg^{-1} min^{-1})	R^2
20	191.64	192.8	2.522×10^{-5}	0.9997
40	381	384.61	2.766×10^{-5}	0.9995
100	631.52	632.5	3.232×10^{-5}	0.9998

The effect of different concentration on adsorption capacity of methylene blue onto FRrGAMZ is shown in Figure 6.1. The adsorption capacity of methylene blue onto FRrGAMZ increased with the increase of contact time and initial concentration. The higher initial concentration of methylene blue can provide a higher driving force to enhance the sorption of dyes due to the mass transfer resistances between the aqueous solution and solid phases. [198]

The pseudo-second-order kinetics model expressed by equation (6.1) was adopted to examine the mechanism of the adsorption process. The kinetic constants k_1 and correlation coefficients R^2 for the model were calculated and listed in Table 6.1, where calculated from the slope and intercept of the linear plots of t/q_t versus t in Figure 6.2. It was observed that all of the correlation coefficients of pseudo-second-order kinetics model are higher than 0.9995, and the values of calculated $q_{e,cal}$ agree very well with the experimental results $q_{e,exp}$.

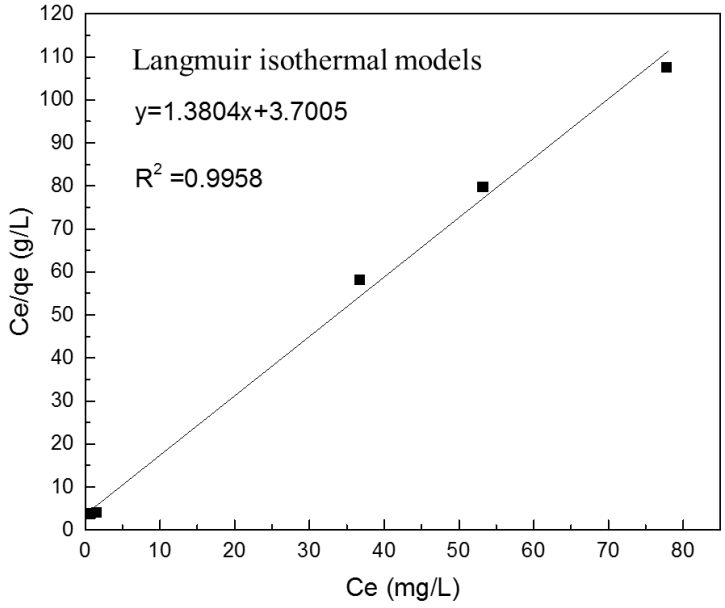

Figure 6.3 Langmuir and adsorption isotherm of methylene blue onto FRrGAMZ at room temperature.

Table 6.2 Parameters and the correlation coefficients of Langmuir isothermal models for the adsorption of methylene blue onto FRrGAMZ at room temperature.

C_o	C_e	q_e	q_m	k_L	R_L	R^2
20	0.72	192.8	724.4	0.3733	0.19	0.9992
40	1.54	384.61			0.06	
100	36.75	632.5			0.03	
120	53.23	667.7			0.02	
150	77.74	722.6			0.02	

Meanwhile, the adsorption data were analyzed using Langmuir isothermal models given by the equation (6.2). The values of Langmuir constants and correlation coefficients R^2 obtained from the linear regression were listed in Table 6.2. The experimental data were well fitted with the Langmuir isotherm model, and all the values of R_L were less than 1, which means that Langmuir model was favorable in this study.

The organic molecules adsorption on to the graphene-based materials has been noted by many authors. The adsorption mechanism can be explained by the electrostatic interactions, H-bonding and π-π stacking on the rGO sheets. [193] It was proved that the essential interaction between the positive charged methylene blue and rGO sheets is electrostatic interactions. While, the other two mechanisms act simultaneously in the adsorption process.

The presence of π-π stacking on the rGO sheets allows the interaction between bulk π systems on the rGO surface and organic molecules with C=C bonds or aromatic rings. Generally, π-π interactions depend on the size and shape of the aromatic system and the substitution unit of molecules. The planar molecules are easy to approach multiwalled carbon nanotubes via a face-to face conformation, which is favorite for π-π interactions between the conjugated aromatic chromophore skeleton and the rGO sheets. On the contrary, the non-planar molecules are kept apart from rGO sheets due to the spatial restriction, resulting low π-π interactions with the rGO sheets. The chemical structures of methylene blue and sodium fluorescein are polar molecules and disperse blue 26 is non-polar molecules. Therefore, this fact suggests that the π-π stacking interactions between the rGO, methylene blue and sodium fluorescein is stronger than rGO and disperse blue 26.

H-bonding, noncovalent forces, can occur between the surface of rGO sheets and organic molecules. The remaining -OH and -COOH on the rGO sheets act as the hydrogen electron donor,

and the oxygen atoms and aromatic rings of the organic compounds act as the elector accepter. The higher number of -OH and -COOH groups remained on the GO sheets, the more active sites for organic molecules adsorption. From the XPS in Chapter 5, it was found that the C-O-C are hardly left on the rGO sheets, which means that the C-O-C group doesn't contribute to the H-bonding of organic molecules. Several studies reported that increased oxygen-containing functional groups on AC decreased the adsorption of chemicals which can form H-bonds. Yu et al. have studied the adsorption of benzene, aniline and naphthylamine on reduced graphene oxides. [194] They found that adsorption mechanism of benzene does not occur via the formation of H-bonding, while the hydrogen bond between reduced graphene oxide and aniline or naphthylamine was weaker, resulting in a lower adsorption capacity. Chen et al. ruled out hydrogen bonding mechanisms in the adsorption of nitroaromatic compounds onto graphene materials. [195] They found that electrostatic interaction between norfloxacin and the adsorbents was one of the major factors controlling the adsorption process. From the adsorption mechanism study and column experiment, it indicates that hydrogen bonding possibly cannot make as significant contribution to overall adsorption process of organic model compounds onto rGO sheets.

An explanation of the zeolites surface modification by APTES and the interaction with GO sheets can be seen in Figure 6.3. The first step in this process is the physisorption of APTES to the zeolites surface through H-bonding and H-bond acceptor on the zeolites surface (SiO_2 and Al_2O_3). Then the positive amine group was introduced by the APTES modification, the charge of zeolites surface was changed from positive to negative. (Proved by zeta potential and XPS) The -OH and -COOH groups on the GO sheets with negative charges can easily react with amine groups to form the GO-NH through the electrostatic attraction which is much stronger than the Van der Waals force and H-bonding. The π-π stacking on the GO sheets also contributed to interactions. Herein, the higher

loading of GO sheets was achieved through the enhancement of interactions between zeolites surface and GO sheets.

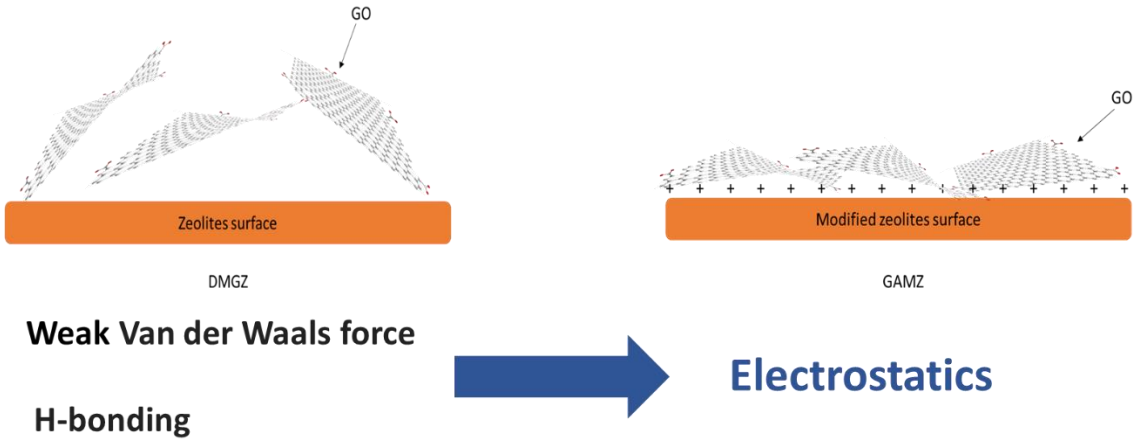

Figure 6.3 The interactions between zeolites surface and GO sheets before and after surface modification by APTES.

6.5 Conclusion

In this chapter, the adsorption mechanism of FRrGAMZ for organic model compound, methylene blue, was studied. It indicated that pseudo-second-order kinetics model and Langmuir isothermal model were fitted to the experiment results. Besides that, the hypnosis of adsorption mechanism was given, which suggested that the electrostatic interactions and π-π stacking between the rGO sheets and organic model compounds are the main adsorption mechanisms.

Chapter 7 Conclusion and Future work

7.1 Conclusion

Water resource contamination by POPs is a serious global environmental problem and has been proven to cause endocrine, reproductive, and nervous system disruption, as well as chronic diseases and cancers. The removal of POPs from drinking water requires a low-cost, efficient, and ecological technology. According to the variety of charges and based on human consumption in the aquatic environment BPA, PFOA, and PCBs were selected in this thesis.

Water treatment technologies have been studied and developed for decades. Adsorption technology using in water treatment is considered faster, cheaper, and universal technique for the removal of toxic contaminants. An ideal adsorbent for this application should be low-cost, recyclable, non-toxic, rapidly adsorbing, regenerate easily. However, there are several limitations to commercial adsorbents, such as AC, which has a short lifetime, selective chemical removal, ineffective against some bacteria and viruses, and so on.

The overall goal of this dissertation is to fabricate and evaluate a thin-layer of GO/rGO attached to the surface of zeolite substrate. The adsorption performance was compared with GAC for the removal of variably charged organic model compounds and POPs in aqueous solution. The coating methods, experimental conditions, surfactants, zeolite surface modification, and *in-situ* reduction of GO was deployed and studied to achieve this goal. We list four objectives and conclusions as followed:

Objective 1 and 2: Development of the dry coating method for GO onto the zeolites surface. Its adsorption capacity and stability were compared to those found in spin coating and vacuum coating

methods. The investigation and optimization of the column test conditions including pH, temperature, and flow rate;

Conclusion for objective 1 and 2: In Chapter 3, the dry coating method is considered as a simple and effective approach and favored for the fabrication of GO coated on the zeolite. SEM, FTIR, and Raman results confirmed the presence of GO layer on the zeolites surface. The analyses of zeta potential for adsorbents, organic model compounds, and POPs predicted the adsorption performance for DCGZ. The desorption experiment showed DCGZ had better physical stability than those produced by the other methods. It revealed that the adsorption performance was strongly depended on the loading of GO onto the zeolites surface. The saturation experiment for dispersed blue 26 by column tests showed that the clean zeolite alone did not contribute much to the adsorption, while only less than 1 wt% GO sheets on the surface had a strong impact on adsorption. GO coating layers played a crucial role in adsorption of the target compounds. The adsorption mechanism for organic model compounds and POPs by DCGZ included electrostatic and physical interactions. This was believed that the functional groups and π-π stacking on the GO surface attract the target molecular onto the surface. Finally, the optimized experimental condition was set: pH=7~9, flow rate= 4.8~5 ml min^{-1} and the temperature between 0~40 ^{o}C.

Objective 3: Comparison of the adsorption behavior of anionic, cationic, and non-ionic surfactants modified by DCGZ in order to determine the effect of the surfactants on the removal of organic model compounds;

Conclusion for objective 3: In Chapter 4, variable charge surfactants, anionic SDS, cationic CTAB and non-ionic Triton X-100, were introduced to enhance the attachment of GO onto natural zeolite. Their influences on the removal of organic model compounds were studied. Desorption experiment also suggested that the CTAB and Triton X-100 modification of zeolites surface were promising

approaches to enhance the interaction between GO and the zeolite. In conjunction with results from multiple analyses of zeta potential, SDS/DCGZ and CTAB/DCGZ displayed strong adsorption capabilities to cationic and anionic model compounds, respectively. While, they showed weak adsorption capabilities to the same charged organic model compounds. Triton X-100/DCGZ showed an excellent adsorption performance for variably charged organic model compounds.

Objective 4, 5 and 6: Modification of the natural zeolite surface for the enhancement of the interactions between zeolite and GO sheets in order to increase the loading and stability of their bonding; *In-situ* reduction of GO onto the surface of the natural zeolite to increase the adsorption capacity for organic model compounds and POPs, and the modeling of its adsorption mechanism.

Conclusion for objective 4, 5 and 6: In Chapter 5 and 6, APTES was introduced to overcome the limitation of GO desorption from zeolites surface and increase the loading of GO for improvement of the adsorption capacity for POPs. This was done to enhance the interaction between the zeolite and GO. Zeta potential, XPS, and EDS proved a successful positively charged surface modification to the natural zeolite. The increased loading of GO on the modified zeolites was achieved by a step-wised dry coating method, and the desorption experiment displayed a strong interaction between GO and the zeolite. Finally, we observed that the only 1wt% rGO desorbed from zeolite compared to approximately 36wt% detachment with DCGZ.

Besides that, the attached GO sheets were in-situ reduced by a microwave treatment and a reducing agent to increase the adsorption capability. Vitamin C is regarded as an environmental-friendly chemical to reduce GO. The I_D/I_G ratio of intensities obtained from Raman spectra revealed that the extent and gradient of GO could be well controlled. The variables of control include microwave time, concentration of vitamin C, and adding method. FRrGAMZ kept 91.5% removal for disperse

blue 26 after five cycles of thermal regeneration. Besides that, the adsorption mechanism of FRrGAMZ for organic model compound, methylene blue indicated that pseudo-second-order kinetics model and Langmuir isothermal model were fitted to the experiment results.

In summary, we fabricated a novel adsorbent made of GO/rGO attached onto the zeolite substrate for the removal of variably charged organic model compounds and POPs in aqueous solutions. The thin-layered GO/rGO sheets were attached onto the natural zeolites surface with a low-cost and straightforward fabrication process. It eliminates the use of harsh chemicals, increases stability, and produces a reusable adsorbent. Its regeneration ability and stability were also reported for the first time. It is a promising candidate as an industrial adsorbent and has outcompeted other adsorbents on the market.

7.2 Future work

Based on current work, the following directions are proposed for future studies.

1. Some specific organic pollutions, antibiotics, such as tetracycline and ciprofloxacin, are increasing attention in recent years. The removal of antibiotics in biological wastewater or drinking water have become a global concern, especially in developing countries. Based on current work, a possible direction is fabricating selective adsorption of specific POPs by the modification of graphene-based materials with functional groups. It can be achieved by using N, S, polymers, and so on. Also, chemicals can react with zeolite as adhesions for zeolites and graphene-based materials to enhance the stability and recyclability.

2. As we know from literature research, graphene-based materials have good adsorption capabilities for heavy metals. This study can be applied to research into the removal of heavy

metals and antibiotics. Also, the mechanism of adsorption for heavy metals, kinetic, and isothermal reviews need to be revealed.

3. Also, the combination of polymer membranes and graphene-based materials with the zeolite may be possible. The hybrid membrane with graphene-based materials may have an excellent mechanical strength and filtration ability, while also acting as a suitable adsorbent for heavy metals and antibiotics.

In conclusion, the improvement in the adsorption performance of graphene-based materials coated onto zeolite substrates need to be further studied. This includes the modification of the surface of GO/rGO, or enhancement of the interactions between the zeolite and GO/rGO. The same methods used for the removal of POPs need to be applied and examined for the removal of heavy metals and antibiotics. Also, use of this material for large scale water filtration must be explored.

References

1. Ferrari, A. C.; Robertson, J. Raman spectroscopy of amorphous, nanostructured, diamond-like carbon, and nanodiamond. *Philosophical Transactions of the Royal Society A: Mathematical, Physical and Engineering Sciences* 2004, *362* (1824), 2477- 2512.
2. Canadian Arctic Resources Committee, *Northern Perspectives: Persistent Organic Pollutants.* Canadian Arctic Resources Committee, 2000.
3. www.sciencebuzz.com/persistent-organic-pollutants.
4. Ng, C. A.; von Goetz, N. The Global Food System as a Transport Pathway for Hazardous Chemicals: The Missing Link between Emissions and Exposure. *Environ Health Perspect* 2017, *125* (1), 1–7.
5. Ghiotti, A., Bruschi, S. Tribological behaviour of DLC coatings for sheet metal forming tools. *Wear* 2011, *271*, 2454–2458.
6. Quitmeyer, A.; Roberts, R. Babies, Bottles, and Bisphenol A: The Story of a Scientist-Mother. *PLOS Biology* 2007, *5* (7), e200.
7. Jones, D. C.; Miller, G. W. The effects of environmental neurotoxicants on the dopaminergic system: A possible role in drug addiction. *Biochemical Pharmacology* 2008, *76* (5), 569-81.
8. Bisphenol An Action Plan; Highlights of CASRN 80-05-7; United Sates Environmental Protection Agency: Office of Water; Health and Ecological Criteria Division: Washington, DC, 2010; www.epa.gov/sites/production/files/2015-09/documents/bpa_action_plan.pdf.
9. Bisphenol A; wwww.yourbabiesinfo.blogspot.co.id/2018/02/bisphenol-a.html
10. National Research Council. Bioavailability of Contaminants in Soils and Sediments: Processes, Tools, and Applications. Washington, DC, 2003; The National Academies Press.

www.nap.edu/catalog/10523/bioavailability-of-contaminants-in-soils-and-sediments-processes-tools-and.

11. Wang, Z.; DeWitt, J. C.; Higgins, C. P.; Cousins, I. T. A Never-Ending Story of Per- and Polyfluoroalkyl Substances (PFASs). *Environmental Science & Technology* 2017, *51*, 2508-2518.
12. Diamanti-Kandarakis, E.; Bourguignon, J.-P.; Giudice, L. C.; Hauser, R.; Prins, G. S.; Soto, A. M.; Zoeller, R. T.; Gore, A. C. Endocrine-Disrupting Chemicals: An Endocrine Society Scientific Statement. *Endocrine Reviews* 2009, *30* (4), 293–342.
13. Schaider, L. A.; Balan, S. A.; Blum, A.; Andrews, D. Q.; Strynar, M. J.; Dickinson, M. E.; Lunderberg, D. M., Lang, J. R., Peaslee, G. F. Fluorinated Compounds in U.S. Fast Food Packaging. *Environmental Science & Technology Letters* 2017, *4*, 105-111.
14. *Maximum Contaminant Level Recommendation for Perfluorooctanoic Acid in Drinking Water*; New Jersey Drinking Water Quality Institute, 2017; http://www.nj.gov/dep/watersupply/pdf/pfoa-recommend.pdf
15. *Statement of Need and Reasonableness: Proposed Amendments to the Rules on Health Risk Limits for Groundwater*. Minnesota Department of Health, 2015; www.leg.state.mn.us/archive/sonar/SONAR-04257.pdf
16. *Drinking Water Health Advisory for Perfluorooctanoic Acid (PFOA)*; United Sates Environmental Protection Agency: Office of Water; Health and Ecological Criteria Division: Washington,DC,2016;www.epa.gov/sites/production/files/201605/documents/pfoa_health_advisory_final-plain.pdf.
17. www.wikipedia.org/wiki/Polychlorinated_biphenyl.

18. White, S. S.; Birnbaum, L. S. An Overview of the Effects of Dioxins and Dioxin-like Compounds on Vertebrates, as Documented in Human and Ecological Epidemiology. *Journal of Environmental Science and Health Part C Environmental Carcinogenesis & Ecotoxicology Reviews* 2009, *27* (4), 197-211.

19. Rudel, R. A.; Perovich, L. J. Endocrine disrupting chemicals in indoor and outdoor air. *Atmospheric Environment* 2009, *43* (1), 170-181.

20. Trudel, D.; Horowitz, L.; Wormuth, M.; Scheringer, M.; Cousins, I. T.; Hungerbuhler, K. Estimating Consumer Exposure to PFOS and PFOA. *Risk Analysis* 2008, *28* (2), 251-69.

21. Jense, A. A. *Health risks of PCB in the indoor climate in Denmark*; Danish Health and Medicines Authority, 2013.

22. Moran, M. A.; Kujawinski, E. B.; Stubbins, A.; Fatland, R.; Aluwihare, L. I.; Buchan, A.; Crump, B. C.; Dorrestein, P. C.; Dyhrman, S. T.; Hess, N. J.; Howe, B.; Longnecker, K.; Medeiros, P. M.; Niggemann, J.; Obernosterer, I.; Repeta, D. J.; Waldbauer, J. R. Deciphering ocean carbon in a changing world. *Proceedings of the National Academy of Sciences of the United States of America* 2016, *113* (12), 3143-3151.

23. Daniels, J. A. Advances in Environmental Research. In *Remediation Technologies for Phosphate Removal from Wastewater: An Overview*; Nova Science Publishers, 2014.

24. Progress Cleaning the Air and Improving People's Health; www.epa.gov/clean-air-act-overview/progress-cleaning-air-and-improving-peoples-health.

25. National Research Council (US) Safe Drinking Water Committee *Drinking Water and Health*; National Academies Press (US), 1980.

26. Thomas, W. J.; Crittenden, B. *Adsorption Technology and Design*; Elsevier, 1998.

27. Park, S.-J.; Seo, M.-K. *Interface Science and Composites*; Academic Press, 2011.

28. Cevallos, O. R. F. Adsorption Characteristics of Water and Silica Gel System for Desalination Cycle. Master of Science Dissertation, King Abdullah University of Science and Technology, Thuwal, Kingdom of Saudi Arabia, 2012.

29. Qu, J. H. Research progress of novel adsorption processes in water purification: A review. *Journal of Environmental Sciences* 2008, *20* (1) 1–13.

30. Barazesh, J. M.; Prasse, C.; Wenk, J.; Berg, S.; Remucal, C. K.; Sedlak, D. L. Trace Element Removal in Distributed Drinking Water Treatment Systems by Cathodic H2O2 Production and UV Photolysis. *Environmental Science & Technology* 2018. *52* (1), 195-204.

31. Qu, X.; Alvarez, P. J. J.; Li, Q. Applications of nanotechnology in water and wastewater treatment. *Water Research* 2013, *47* (12), 3931-3946.

32. Brambilla, G.; Iamiceli, A.; Domenico, A. D. Priority Environmental Chemical Contaminants in Meat. *Safety of Meat and Processed Meat* 2009, 391-424.

33. Bozell, J. J.; Petersen, G. R. Technology development for the production of biobased products from biorefinery carbohydrates. *Green Chemistry* 2010, 12, 539-554.

34. Rashed, M. N. Adsorption Technique for the Removal of Organic Pollutants from Water and Wastewater. In Organic Pollutants – Monitoring, Risk and Treatment; Rashes, M. N., Eds.; *InTech.* 2013; 167.

35. Crini, G. Non-conventional low-cost adsorbents for dye removal: A review. *Bioresource Technology* 2006, *97* (9), 1061-1085.

36. Mumption, F. A. First Reported Occurrence of Zeolites in Sedimentary Rocks of Mexico. *American Mineralogist* 1973, *58*, 287-290.

37. Dupré, N.; Moreau, P.; Vito, E. D.; Quazuguel, L.; Boniface, M.; Bordes, A.; Rudisch, C.; Guillemaud, P. B.; Guyomard, D. Multiprobe Study of the Solid Electrolyte Interphase on

Silicon-Based Electrodes in Full-Cell Configuration. *Chemistry of Materials* 2016, *28* (8), 2557–2572.

38. Kim, J.; Van der Bruggen, B. The use of nanoparticles in polymeric and ceramic membrane structures: review of manufacturing procedures and performance improvement for water treatment. *Eniromental Pollution* 2010, 158 (7), 2335-2349.
39. Mansoori, G. A.; Bastami, T. R.; Ahmadpour, A.; Eshaghi, Z. Environmental Application of Nanotechnology. *Annual Review of Nano Research* 2008, 2 (2), 1-73.
40. Ali, I. New Generation Adsorbents for Water Treatment. *Chemical Reviews* 2012, *112* (10), 5073–5091.
41. Chen, T.; Pan, L.; Loh, T. A. J.; Chua, D. H. C.; Yao, Y.; Chen, Q.; Li. D.; Qin, W.; Sun, Z. Porous nitrogen-doped carbon microspheres as anode materials for lithium ion batteries. *Dalton Transactions* 2014, *43,* 14931-14935.
42. Liu, Y.; Simon, J. D. Metal-ion interactions and the structural organization of Sepia eumelanin. *Pigment Cell & Melanoma Research* 2005, *18* (1), 42-8.
43. Liu, Y.; Simon, J. D. Isolation and biophysical studies of natural eumelanins: applications of imaging technologies and ultrafast spectroscopy. *Pigment Cell & Melanoma Research* 2003, *16* (6), 606-18.
44. Lee, H.; Dellatore, S. M.; Miller, W. M.; Messersmith, P. B. Mussel-inspired surface chemistry for multifunctional coatings. *Science* 2007, *318* (5849), 426-30.
45. Wei, Q.; Zhang, F. L.; Li, J.; Li, B. J.; Zhao, C. S. Oxidant-induced dopamine polymerization for multifunctional coatings. *Polymer Chemistry* 2010, *1* (9), 1430-1433.
46. Ito, S. A Chemist's View of Melanogenesis. *Pigment Cell & Melanoma Research* 2003, *16* (3), 230-236.

47. Jastrzebska, M. M.; Isotalo, H.; Paloheimo J.; Stubb, H. Electrical conductivity of synthetic DOPA-melanin polymer for different hydration states and temperatures. *Journal of Biomaterials Science, Polymer Edition* 1995, *7* (7), 577-586.

48. Yu, X.; Fan, H.; Liu, Y.; Shi, Z.; Jin, Z. Characterization of carbonized polydopamine nanoparticles suggests ordered supramolecular structure of polydopamine. *Langmuir* 2014, *30* (19), 5497–5505.

49. Allen, M. J.; Tung, V. C.; Kaner, R. B. Honeycomb Carbon: A Review of Graphene. *Chemical Reviews* 2010, *110* (1), 132–145.

50. Geim, A. K.; Novoselov, K. S. The rise of graphene. *Nature Materials* 2007, *6*, 183-191.

51. Bolotin, K. I.; Sikes, K. J.; Jiang, Z.; Klima, M.; Fudenberg, G.; Hone, J.; Kim, P.; Stormer, H. L. Ultrahigh electron mobility in suspended graphene. *Solid State Communications* 2008, *146* (9-10), 351-355.

52. Morozov, S. V.; Novoselov, K. S.; Katsnelson, M. I.; Schedin, F.; Elias, D. C.; Jaszczak, J. A.; Geim, A. K. Giant intrinsic carrier mobilities in graphene and its bilayer. *Physical Review Letter* 2008, *100* (1), 016602.

53. Lee, C.; Wei, X. D.; Kysar, J. W.; Hone, J. Measurement of the elastic properties and intrinsic strength of monolayer graphene. *Science* 2008, *321* (5887), 385-8.

54. Balandin, A. A.; Ghosh, S.; Bao, W. Z.; Calizo, I.; Teweldebrhan, D.; Miao, F.; Lau, C. N. Superior thermal conductivity of single-layer graphene. *Nano Letters* 2008, *8* (3), 902-907.

55. Cai, W.; Zhu, Y.; Li, X.; Piner, R. D.; Ruoff, R. S. Large area few-layer graphene/graphite films as transparent thin conducting electrodes. *Applied Physics Letters* 2009, *95*, 123115.

56. Brodie, B. C. Sur le poids atomique du graphite. *Annales de Chimie et de Physique* 1860, *59*, 466-472.

57. Staudenmaier, L. Verfahren zur Darstellung der Graphitsäure. *Berichte der Deutschen Chemischen Gesellschaft* 1898, *31*, 1481-1499.

58. Hummers, W. S.; Offeman, R. E. Preparation of Graphitic Oxide. *Journal of the American Chemical Society* 1958, *80* (6), 1339.

59. Graphene Oxide: Introduction and Market News; www.graphene-info.com/graphene-oxide.

60. Zhu, Y.; Murali, S.; Cai, W.; Li, X.; Suk, J. W.; Potts, J. R.; Ruoff R. S. Graphene and Graphene Oxide: Synthesis, Properties, and Applications. *Advanced Materials* 2010, *22* (35), 3906–3924.

61. Xue, Z.; Cao, Y.; Liu, N.; Feng, L.; Jiang, L. Special wettable materials for oil/water separation, *Journal of Materials Chemistry A*. 2014, 2, 2445-2460.

62. Gupta, V. K.; Carrott, P. J.M.; Ribeiro Carrott, M. M.L.; Suhas Low-Cost Adsorbents: Growing Approach to Wastewater Treatment—a Review. *Environmental Science and Technology* 2009, 39 (10), 783-842.

63. Moreno-Castilla, C.; Rivera-Utrilla, J.; Joly, J. P.; López-Ramón, M. V.; Ferro-García, M. A.; Carrasco-Marín, F. Thermal regeneration of an activated carbon exhausted with different substituted phenols. *Carbon* 1995, 33(10), 1417-1423.

64. Lee, T.; Ooi, C.-H.; Othman, R.; Yeoh, F.-Y. Activated carbon fiber – the hybrid of carbon fiber and activated carbon. *Reviews on Advanced Materials Science* 2014, *36*, 118-136.

65. Gandhi, M. R.; Vasudevan, S.; Shibayama, A.; Yamada, M. Graphene and graphene-based composites: a rising star in water purification – a comprehensive overview. *ChemistrySelect* 2016, *1* (15), 4357.

66. Wang, S.; Sun, H.; Ang, H. M.; Tadé, M. O. Adsorptive remediation of environmental pollutants using novel graphene-based nanomaterials, *The Chemical Engineering Journal* 2013, *226*, 336-347.

67. Shen, Y.; Fang, Q.; Chen, B. Environmental applications of three-dimensional graphene-based macrostructures: adsorption, transformation, and detection. *Environment Science & Technology* 2015, *49* (1), 67-84.

68. Jeong, H.-K.; Lee, Y. P.; Jin, M. H.; Kim, S. E.; Bae, J. J.; Lee, Y. H. Thermal stability of graphite oxide. *Chemical Physics Letters* 2009, *470* (4-6), 225-258.

69. Ibrahim, W. A. W.; Nodeh, H. R.; Sanagi, M. M. Graphene-Based Materials as Solid Phase Extraction Sorbent for Trace Metal Ions, Organic Compounds, and Biological Sample Preparation. *Analytical Chemistry* 2016, *46* (4), 267-283.

70. Chen, B.; Johnson, E. J.; Chefetz, B.; Zhu, L.; Xing, B. Sorption of polar and nonpolar aromatic organic contaminations by plant cuticular materials: role of polarity and accessibility. *Environmental Science & Technology* 2005, *39* (16), 6138-6146.

71. Ramesha, G. K.; Kumara, A. V.; Muralidhara, H. B.; Sampath, S. Graphene and graphene oxide as effective adsorbents toward anionic and cationic dyes. *Journal of Colloid and Interface Science* 2011, *361* (1), 270-7.

72. Liu, F.; Chung, S.; Oh, G.; Seo, T. S. Three-dimensional graphene oxide nanostructure for fast and efficient water-soluble dye removal. *ACS Applied Materials & Interfaces* 2012, *4* (2), 922-927.

73. Zhou, G.; Xu, C.; Cheng, W.; Zhang, Q.; Nie, W. Effects of Oxygen Element and Oxygen-Containing Functional Groups on Surface Wettability of Coal Dust with Various

Metamorphic Degrees Based on XPS Experiment. *Journal of Analytical Methods in Chemistry* 2015.

74. Chen, L.; Hu, P.; Zhang, L.; Huang, S.; Luo, L; Huang, C. Toxicity of graphene oxide and multi-walled carbon nanotubes against human cells and zebrafish. *Science China Chemistry* 2012, *55* (10), 2209-2216.
75. Pandey, N.; Shukla, S. K.; Singh, N. B. Water purification by polymer nanocomposites: an overview. *Nanocomposites* 2017, *3* (2), 47-66.
76. Jang, S.-C.; Haldorai, Y.; Lee, G.-W.; Hwang, S.-K.; Han, Y.-K.; Roh, C.; Huh, Y. S. Porous three-dimensional graphene foam/Prussian blue composite for efficient removal of radioactive ^{137}Cs. *Scientific Reports* 2015, *5*, 17510.
77. Schinwald, A.; Murphy, F. A.; Jones, A.; MacNee, W.; Donaldson, K. Graphene-Based Nanoplatelets: A New Risk to the Respiratory System as a Consequence of Their Unusual Aerodynamic Properties. *ACS Nano* 2012, *6* (1), 736-746.
78. Sanchez, V. C.; Jachak, A.; Hurt, R. H.; Kane, A. B. Biological Interactions of Graphene-Family Nanomaterials – An Interdisciplinary Review. *Chemical Research in Toxicology* 2012, *25* (1), 15-34.
79. Lazar, P.; Karlicky, F.; Jurecka, P.; Kocman, M.; Otyepkova, E.; Safarova, K.; Otyepka, M. Adsorption of Small Organic Molecules on Graphene. *Journal of the American Chemical Society* 2013, *135* (16), 6372-6377.
80. Ersan, G.; Apul, O. G.; Perreault, F.; Karanfil, T. Adsorption of organic contaminants by graphene nanosheets: A review. *Water Research* 2017, *126*, 385-398.
81. Yang, K.; Xing, B. Adsorption of organic compounds by carbon nanomaterials in aqueous phase: Polanyi theory and its application. *Chemical Reviews* 2010, *110* (10), 5989-6008.

82. Pei, Z.; Li, L.; Sun, L. Adsorption characteristics of 1,2,4-trichlorobenzene, 2,4,6-trichlorophenol, 2-naphthol and naphthalene on graphene and graphene oxide. *Carbon* 2013, *51*, 156-158.

83. Chen, X.; Chen, B. Macroscopic and spectroscopic investigations of the adsorption of nitroaromatic compounds on graphene oxide, reduced graphene oxide, and graphene nanosheets. *Environmental Science & Technology 2015*, 49 (10), 6181-6189.

84. Xiao, W. Dendrimer Functionalized Graphene Oxide for Selenium Removal. Master of Science Dissertation, University of Alberta, Edmonton, AB, 2015.

85. Graphene-based materials: Fabrication and application for adsorption in analytical chemistry; www. docslide.com.br/documents/graphene-based-materials-fabrication-and-application-for-adsorption-in-analytical.html.

86. Mastral, A. M.; Garcla, T.; Callen, M. S.; Navarro, M. V.; Galban, J. Removal of naphthalene, phenanthrene, and pyrene by sorbents from hot gas. *Environmental Science & Technology* 2001, *35* (11), 2395-2400.

87. Zhao, J.; Wang, Z.; Zhao, Q.; Xing, B. Adsorption of phenanthrene on multilayer graphene as affected by surfactant and exfoliation. *Environmental Science & Technology* 2014, *48* (1), 331-339.

88. Lamichhane, S.; Krishna, K. C. B.; Sarukkalige, R. Polycyclic aromatic hydrocarbons (PAHs) removal by sorption: A review. *Chemosphere* 2016, *148*, 363-353.

89. Sun, H.; Cao, L.; Lu, L. Magnetite/reduced graphene oxide nanocomposites: One step solvothermal synthesis and use as a novel platform for removal of dye pollutants. *Nano Research* 2011, *4* (6), 550-562.

90. Wang, H.; Yuan, X.; Wu, Y.; Chen, X.; Leng, L.; Wang, H.; Li, H.; Zeng, G. Facile synthesis of polypyrrole decorated reduced graphene oxide-Fe_3O_4 magnetic composites and its application for the Cr(VI) removal. *Chemical Engineering Journal* 2015, *262*, 597-606.

91. Petnikota, S.; Rotte, N. K.; Reddy, M. V.; Srikanth, V.V.S.S.; Chowdari, B. V. R. MgO-decorated few-layered graphene as an anode for Li-ion batteries. ACS Applied Materials & Interfaces 2015, 7 (4), 2301-2309.

92. Yang, X.; Li, J.; Wen, T.; Ren, X.; Huang, Y.; Wang, X. Adsorption of naphthalene and its derivatives on magnetic graphene composites and the mechanism investigation. *Colloids and Surfaces A: Physicochemical and Engineering Aspects* 2013, *422*, 118-125.

93. Du, J.; Lai, X.; Yang, N.; Zhai, J.; Kisailus, D.; Su, F.; Wang, D.; Jiang, L. Hierarchically Ordered Macro-Mesoporous TiO_2-graphene composite films: Improved mass transfer, reduced charge recombination, and their enhanced photocatalytic activities. *ACS Nano* 2011, *5* (1), 590-596.

94. Shen, Y.; Chen, B. Sulfonated graphene nanosheets as a superb adsorbent for various environmental pollutants in water. *Environmental Science & Technology* 2015, *49* (12), 7364-7372.

95. Chen, Y.; Chen, L.; Bai, H.; Li, L. Graphene oxide-chitosan hydrogels as broad-spectrum adsorbents for water purification. *Journal of Materials Chemistry A* 2013, *1*, 1992-2001.

96. Liu, J.; Liu, G.; Liu, W. Preparation of water-soluble β -cyclodextrin/poly(acrylic acid)/graphene oxide nanocomposites as new adsorbents to remove cationic dyes from aqueous solutions. *Chemical Engineering Journal* 2014, *257*, 299-308.

97. Gao, H.; Sun, Y.; Zhou, J.; Xu, R.; Duan, H. Mussel-inspired synthesis of polydopamine-functionalized graphene hydrogel as reusable adsorbents for water purification. *ACS Applied Materials & Interfaces* 2013, *5* (2), 425-432.

98. Moon, Y.-E.; Jung, G.; Yun, J.; Kim, H. Poly(vinyl alcohol)/poly(acrylic acid)/TiO_2/graphene oxide nanocomposite hydrogels for PH-sensitive photocatalytic degradation of organic pollutants. *Materials Science and Engineering: B* 2013, *178* (17), 1097-1103.

99. Gan, L.; Shang, S.; Hu, E.; Yuen, C. W. M.; Jiang, S.-X. Konjac glucomannan/graphene oxide hydrogel with enhanced dyes and adsorption capability for methyl blue and methyl orange. *Applied Surface Science* 2015, *357*, 866-872.

100. Wan, S.; Bi, H.; Sun, L. Graphene and carbon-based nanomaterials as highly efficient adsorbents for oils and organic solvents. *Nanotechnology Reviews* 2016, *5* (1), 3-20.

101. Bi, H.; Xie, X.; Yin, K.; Zhou, Y.; Wan, S.; He, L.; Xu, F.; Banhart, F.; Sun, L.; Ruoff, R. S. Spongy graphene as a highly efficient and recyclable sorbent for oils and organic solvents. *Advanced Functional Materials* 2012, *22*, 4421-4425.

102. Singhal, R. M.; Sharma, A.; Verma, N. Micro-nano hierarchal web of activated carbon fibers for catalytic gas adsorption and reaction. *Industrial & Engineering Chemistry Research* 2008, *47* (10), 3700-3707.

103. Lee, B.; Lee, S.; Lee, M.; Jeong, D. H.; Bark, Y.; Yoon, J.; Kim, Y. H. Carbon nanotube-bonded graphene hybrid aerogels and their application to water purification. *Nanoscale* 2015, *7*, 6782-6789.

104. Wang, Y.; Zhang, P.; Liu, C. F.; Huang, C. Z. A facile and green method to fabricate graphene-based multifunctional hydrogels for miniature-scale water purification. *RSC Advances* 2013, *3*, 9240-9245.

105. Chowdhury, S.; Balasubramanian, R. Recent advances in the use of graphene-family nanoadsorbents for removal of toxic pollutants from wastewater. *Advances in Colloid and Interface Science* 2014, *204*, 35-36.

106. Sreeprased, T. S.; Gupta, S. S.; Maliyekkal, S. M.; Pradeep, T. Immobilized graphene-based composite from asphalt: Facile synthesis and application in water purification. *Journal of Hazardous Materials* 2013, *246-247*, 213-220.

107. Chen, W.; Yan, L.; Bangal, P. R. Preparation of graphene by the rapid and mild thermal reduction of graphene oxide induced by microwaves. *Carbon* 2010, *48* (4), 1146-1152.

108. Li, Z.; Yao, Y.; Lin, Z.; Moon, K.-S.; Lin, W.; Wong, C. Ultrafast, dry microwave synthesis of graphene sheets. *Journal of Materials Chemistry* 2010, *20*, 4781-4783.

109. Zhang, J.; Zhao, X. S. Conducting polymers directly coated on reduced graphene oxide sheets as high-performance supercapacitor electrodes. *Journal of Physical Chemistry C* 2012, *116* (9), 5420-5426.

110. Fernandez-Merino, M. J.; Guardia, L.; Paredes, J. I.; Villar-Rodil, S.; Solis-Fernandez, P.; Martinez-Alonso, A.; Tascon, J. M.D. Victamin C is an ideal substitute for Hydrazine in the reduction of graphene oxide suspensions. *Journal of Physical Chemistry C* 2010, *114* (14), 6426-6432.

111. Belfroid, A.; van Velzen, M.; van der Horst, B.; Vethaak, D. Occurrence of bisphenol A in surface water and uptake in fish: evaluation of field measurements. *Chemosphere*, 2002, *49* (1), 97-103.

112. Mawn, M. P.; Mckay, R. G.; Ryan, T. W.; Szostek, B.; Powley, C. R.; Buck, R. C. Determination of extractable perfluorooctanoic acid (PFOA) in water, sweat simulant, saliva simulant, and methanol from textile and carpet samples by LC/MS/MS. Analyst 2005, 130, 670-678

113. Huang, X.; Qi, X.; Boey, F.; Zhang, H. Graphene-based composites. *Chemical Society Reviews* 2012. *41*, 666-686.

114. Yang, S.; Feng, X.; Ivanovici, S.; Mullen, K. Fabrication of Graphene-encapsulated oxide nanoparticles: Towards high-performance anode materials for lithium storage. *Angewandte Chemie International Edition in English* 2010, *49* (45), 8408-11.

115. Li, D.; Muller, M. B.; Gilje, S.; Kaner, R. B.; Wallace, G. G. Processable aqueous dispersions of graphene nanosheets. *Nature Nanotechnology* 2008, *3*, 101-105.

116. Lotya, M.; Hernandez, Y.; King, P. J.; Smith, R. J.; Nicolosi, V.; Karlsson, L. S.; Blighe, F. M.; De, S.; Wang, Z.; McGovern, I. T.; Duesberg, G. S.; Coleman, J. N. Liquid Phase Production of Graphene by Exfoliation of Graphite in Surfactant/Water Solutions. *Journal of the American Chemical Society* 2009, *131* (10), 3611-3620.

117. Lotya, M.; King, P. J.; Khan, U.; De, S.; Coleman, J. N. High-concentration, surfactant-stabilized graphene dispersions. *ACS Nano* 2010, *4* (6), 3155-3162.

118. Wang, S.; Yi, M.; Shen, Z. The effect of surfactants and their concentration on the liquid exfoliation of graphene. *RSC Adcances* 2016, *6*, 56705-56710.

119. Parviz, D.; Dast, S.; Ahmed, H. S. T.; Irin, F.; Bhattacharia, S.; Green, M. J. Dispersions of Non-Covalently Functionalized Graphene with Minimal Stabilizer. ACS Nano 2012, 6 (10), 8857-8867.

120. Goloub, T. P.; Koopal, L. K.; Bijsterbosch, B. H.; Sidorova, M. P. Adsorption of Cationic Surfactants on Silica. Surface Charge Effects. *Langmuir* 1996, *12* (13), 3188-3194.

121. Bi, Z.; Liao, W.; Qi, L. Wettability alteration by CTAB adsorption at surfaces Of SiO2 film or silica gel powder and mimic oil recovery. *Applied Surface Science* 2004. *221* (1-4), 25-31.

122. Chen, D.; Qu, Z.; Sun, Y.; Wang, Y. Adsorption–desorption behavior of gaseous formaldehyde on different porous Al2O3 materials. *Colloids and Surfaces A: Physicochemical and Engineering Aspects.* 2014. *441* (20), 433-440.

123. Khenifi, A.; Bouberka, Z.; Sekrane, F.; Kameche, M.; Derriche, Z. Adsorption study of an industrial dye by an organic clay. *Adsorption* 2007, *13* (2). 149-158.

124. Basar, C. A.; Karagunduz, A.; Cakici, A.; Keskinler, B. Removal of surfactants by powdered activated carbon and microfiltration. *Water Research* 2004. *38* (8), 2117-2124.

125. Wang, H.; Yuan, X.; Wu, Y.; Huang, H.; Peng, X.; Zeng, G.; Zhong, H.; Liang, J.; Ren, M. Graphene-based materials: Fabrication, characterization and application for the decontamination of wastewater and wastegas and hydrogen storage/generation. *Advances in Colloid and Interface Science* 2013. *195-196*, 19-40.

126. Tkalya, E. E.; Ghislandi, M.; de With, G.; Koning, C. E. The use of surfactants for dispersing carbon nanotubes and graphene to make conductive nanocomposites. *Current Opinion in Colloid & Interface Science* 2012. *17* (4), 225-232.

127. Guardia, L.; Fernandez-Merino, M. J.; Paredes, J. I.; Solis-Fernandez, P.; Villar-Rodil, S.; Martinez-Alonso, A.; Tascon, J. M. D. High-throughput production of pristine graphene in an aqueous dispersion assisted by non-ionic surfactants. *Carbon* 2011, *49* (5), 1653-1662.

128. Liu, F.; Chung, S.; Oh, G.; Seo, T. S. Three-Dimensional Graphene Oxide Nanostructure for Fast and Efficient Water-Soluble Dye Removal. *ACS Applied Materials & Interface* 2012, *4* (2), 922-927.

129. Dong, X.; Huang, W.; Chen, P. In Situ Synthesis of Reduced Graphene Oxide and Gold Nanocomposites for Nanoelectronics and Biosensing. *Nanoscale Research Letters* 2011, *6*, 60.

130. Lesmana, S. O.; Febriana, N.; Soetaredjo, F. E.; Sunarso, J.; Ismadji, S. Studies on potential applications of biomass for the separation of heavy metals from water and wastewater. *Biochemical Engineering Journal.* 2009, *44* (1), 19-41.

131. Rudzinski, W.; Plazinski, W. Studies of the Kinetics of Solute Adsorption at Solid/Solution Interfaces: On the Possibility of Distinguishing between the Diffusional and the Surface Reaction Kinetic Models by Studying the Pseudo-First-order Kinetics. *Journal of Physical Chemistry C* 2007, *111* (41), 15100-15110.

132. Yan, H.; Tao, X.; Yang, Z.; Li, K.; Yang, H.; Li, A.; Cheng, R. Effects of the oxidation degree of graphene oxide on the adsorption of methylene blue. *Journal of Hazardous Materials* 2014, *268* (15), 191-198.

133. Bradder, P.; Ling, S. K.; Wang, S.; Liu, S. Dye adsorption on layered graphite oxide. *Journal of Chemical & Engineering Data* 2011, *56* (1), 138-141.

134. Zhou, X.; Liu, Z. A scalable, solution-phase processing route to graphene oxide and graphene ultralarge sheets. *Chemical Comunications* 2010, 46, 2611-2613.

135. Veerapandian, M.; Lee, M.-H.; Krishnamoorthy, K.; Yun, K. Synthesis, characterization and electrochemical properties of functionalized graphene oxide. *Carbon.* 2012, *50* (1), 4228-4238.

136. Vilela, D.; Parmar, J.; Zeng, Y.; Zhao, Y.; Sanchez, S. Graphene-Based Microbots for Toxic Heavy Metal Removal and Recovery from Water. *Nano Letters* 2016, *16* (4), 2860–2866.

137. Filice, S.; D'Angelo, D.; Libertino, S.; Nicotera, I.; Kosma, V.; Privitera, V.; Scalese, S. Graphene oxide and titania hybrid Nafion membranes for efficient removal of methyl orange dye from water. *Carbon.* 2015, *82*, 489-499.

138. Eskandarloo, H.; Kierulf, A.; Abbaspourrad, A. Nano- and micromotors for cleaning polluted waters: focused review on pollutant removal mechanisms. *Nanoscale.* 2017, 9, 13850-13863.

139. Xu, J.; Wang, L.; Zhu, Y. Decontamination of Bisphenol A from Aqueous Solution by Graphene Adsorption. *Langmuir* 2012, *28* (22), 8418–8425.

140. Wang, J.; Chen, Z.; Chen, B. Adsorption of Polycyclic Aromatic Hydrocarbons by Graphene and Graphene Oxide Nanosheets. *Environmental Science & Technology* 2014, *48* (9), 4817–4825.

141. Guo, H.; Jiao, T.; Zhang, Q.; Guo, W.; Peng, Q.; Yan, X. Preparation of Graphene Oxide-Based Hydrogels as Efficient Dye Adsorbents for Wastewater Treatment. *Nanoscale Research Letters* 2015, 10, 272.

142. Zhao, J.; Ren, W.; Cheng, H.-M. Graphene sponge for efficient and repeatable adsorption and desorption of water contaminations. *Journal of Materials Chemistry* 2012, 22, 20197-20202.

143. Veerapandian, M.; Lee, M.-H.; Krishnamoorthy, K.; Yun, K. Synthesis, characterization and electrochemical properties of functionalized graphene oxide. *Carbon.* 2012, *50* (1), 4228-4238.

144. Dreyer, D. R.; Park, S.; Bielawski, C. W.; Ruoff, R. S. The chemistry of graphene oxide. *Chemical Society Reviews* 2010, 39, 228-240.

145. Qin, W.; Vautard, F.; Askeland, P.; Yu, J.; Drzal, L. Modifying the carbon fiber–epoxy matrix interphase with silicon dioxide nanoparticles. *RSC Advances* 2015, 5, 2457-2465.

146. Chua, C. K.; Pumera, M. Chemical reduction of graphene oxide: a synthetic chemistry viewpoint. *Chemical Society Reviews* 2014, 43, 291-312.

147. Chen, L.; Hu, P.; Zhang, L.; Huang, S.; Luo, L.; Huang, C. Toxicity of graphene oxide and multi-walled carbon nanotubes against human cells and zebrafish. *Science China Chemistry* 2012, *55* (10), 2209-2216.

148. Zhang, J.; Yang, H.; Shen, G.; Cheng, P.; Zhang, J.; Guo, S. Reduction of graphene oxide *vial* ascorbic acid. *Chemical Communications*. 2010, 46, 1112-1114.

149. Qu, S.; Huang, F.; Yu, S.; Chen, G.; Kong, J. Magnetic removal of dyes from aqueous solution using multi-walled carbon nanotubes filled with Fe_2O_3 particles. *Journal of Hazardous Materials.* 2008, *160* (2-3), 643-647.

150. Namasivayam, C.; Kavitha, D. Removal of Congo Red from water by adsorption onto activated carbon prepared from coir pith, an agricultural solid waste. *Dyes and Pigments.* 2002, *54* (1), 47-58.

151. Iram, M.; Guo, C.; Guan, Y.; Ishfaq, A.; Liu, H. Adsorption and magnetic removal of neutral red dye from aqueous solution using Fe_3O_4 hollow nanospheres. *Journal of Hazardous Materials* 2010, *181* (1-3), 1039-1050.

152. Taylor, J. A.; vom Saal, F. S.; Welshons, W. V.; Drury, B.; Rottinghaus, G.; Hunt, P. A.; Toutain, P.-L.; Laffont, C. M.; VandeVoort, C. A. Similarity of Bisphenol A Pharmacokinetics in Rhesus Monkeys and Mice: Relevance for Human Exposure. *Environmental Health Perspect*ives 2011, *119* (4), 422–430.

153. *Drinking Water Health Advisory for Perfluorooctanoic Acid (PFOA)*; United Sates Environmental Protection Agency: Office of Water; Health and Ecological Criteria Division: Washington, DC, 2016; www.epa.gov/sites/production/files/2016-05/documents/pfoa_health_advisory_final-plain.pdf.

154. Gao, W.; Majumder, M.; Alemany, L. B.; Narayanan, T. N.; Ibarra, M. A.; Pradhan, B. K.; Ajayan, P. M. Engineered Graphite Oxide Materials for Application in Water Purification. *ACS Applied Materials& Interfaces* 2011, *3* (6), 1821–1826.

155. Lee, J.; Novoselov, K. S.; Shin, H. S. Interaction between Metal and Graphene: Dependence on the Layer Number of Graphene. *ACS Nano* 2011, *5* (1), 608–612.

156. Yuh-ShanHo. Review of second-order models for adsorption systems. *Journal of Hazardous Materials*. 2006, 136(3), 681-689.

157. YuanGao: YanLi: LiangZhang: HuiHuang: JunjieHu: Syed MazharShah: XingguangSu. Adsorption and removal of tetracycline antibiotics from aqueous solution by graphene oxide. *Journal of Colloid and Interface Science*. 2012, 368(1). 540-546.

158. Lulu Fan: Chuannan Luo: Xiangjun Li: Fuguang Lu Huamin Qiu Min Sun. Fabrication of novel magnetic chitosan grafted with graphene oxide to enhance adsorption properties for methyl blue. *Journal of Hazardous Materials.* 2012, 215–216, 272-279.

159. Zhuang-Jun Fan: Wang Kai: Jun Yan: Tong Wei: Lin-Jie Zhi: Jing Feng: Yue-ming Ren: Li-Ping Song, and Fei Wei. Facile Synthesis of Graphene Nanosheets *via* Fe Reduction of Exfoliated Graphite Oxide. *ACS Nano* 2011 *5* (1), 191-198.

160. Owen C. Compton: Son Bin T. Nguyen. Graphene oxide: highly reduced graphene oxide, and graphene: Versatile building blocks for carbon-based materials. *Small*. 2010, 6, 711-723.

161. Andreia A. Rosatella: Carlos A. M.Afonsoc: João A.P. Coutinho. Toxicity assessment of various ionic liquid families towards Vibrio fischeri marine bacteria. *Ecotoxicology and Environmental Safety*. 2012, 96, 162-168.

162. Yi Shen: Qile Fang: and Baoliang Chen. Environmental Applications of Three-Dimensional Graphene-Based Macrostructures: Adsorption, Transformation, and Detection. *Environ. Sci. Technol.* 2015, 49(1), 67-84.

163. Oxana V. Kharissova: H. V. Rasika Dias and Boris I. Kharisov. Magnetic adsorbents based on micro-and nano-structured materials. *RSC Adv.*, 2015, 5, 6695-6719.

164. Hou Wang: Xingzhong Yuan: Guangming Zeng: Yan Wu: YangLiu: QianJiang: ShansiGu. Three-dimensional graphene-based materials: Synthesis and applications from energy storage and conversion to electrochemical sensor and environmental remediation. *Advances in Colloid and Interface Science.* 2015, 221, 41-59.

165. Jing Xu: Li Wang: and Yongfa Zhu. Decontamination of bisphenol A from aqueous solution by graphene adsorption. *Langmuir*; 2012, *28* (22), 8418–8425.

166. Tiantian Ma; Peter R.Chang; Pengwu Zheng; Feng Zhao; Xiaofei Ma. Fabrication of ultra-light graphene-based gels and their adsorption of methylene blue. *Chemical Engineering Journal*. 2014, 240 (15), 595-600.

167. Lunhong Ai; Chunying Zhang; Zhonglan Chen. Removal of methylene blue from aqueous solution by a solvothermal-synthesized graphene/magnetite composite. *Journal of Hazardous Materials.* 2011, 192(13), 1515-1524.

168. Zhongxiu Jin; Xiangxue Wang; Yubing Sun; Yuejie Ai; Xiangke Wang. Adsorption of 4-*n*-Nonylphenol and Bisphenol-A on Magnetic Reduced Graphene Oxides: A Combined Experimental and Theoretical Studies. *Environ. Sci. Technol.*, 2015, *49* (15), 9168–9175.

169. Hannes C. Scjmoe; Je-Luen Li; Michael J.McAllister; Jorpalo Sai. Functionalized single graphene sheets derived from splitting graphite oxide. *J. Phys. Chem. B*, 2006, *110* (17), 8535–8539.

170. Adrian Hunt; Dmitriy A. Dikin; Ernst Z. Kurmaev;Teak D. Boyko ;Paul Bazylewski ;Gap Soo Chang ;Alexander Moewes. Adrian Hunt. Epoxide Speciation and Functional Group Distribution in Graphene Oxide Paper-Like Materials. *Advanced Functional Materials*.2012, 22(18), 3950-3957.

171. Emma M. E. Kristensen; Fredrik Nederberg, Håkan Rensmo; Tim Bowden; Jöns Hilborn; and Hans Siegbahn. Photoelectron Spectroscopy Studies of the Functionalization of a Silicon Surface with a Phosphorylcholine-Terminated Polymer Grafted onto (3-Aminopropyl) trimethoxysilane. *Langmuir*, 2006, *22* (23), 9651–9657.

172. Jun Yan; Tong Wei; Bo Shao; Fuqiu Ma; Zhuangjun Fan. Electrochemical properties of graphene nanosheet/carbon black composites as electrodes for supercapacitors. *Carbon*, 2010, 48(6), 1731-1737.

173. Alexander E.Burakov; Evgeny V.Galunin; Irina V.Burakova; Anastassia E.Kucherova; Shilpi Agarwal; Alexey G.Tkachev. Adsorption of heavy metals on conventional and nanostructured materials for wastewater treatment purposes: A review. *Ecotoxicology and Environmental Safety*. 2018, 148, 702-712.

174. Yan Wang; Zi Xing Shi; and Jie Yin. Facile synthesis of soluble graphene via a green reduction of graphene oxide in tea solution and its biocomposites. *ACS Appl. Mater. Interfaces*, 2011, *3* (4), 1127–1133.

175. Song Qu; Fei Huang; Shao ningYu Gang Chen; Jilie Kong. Magnetic removal of dyes from aqueous solution using multi-walled carbon nanotubes filled with Fe_2O_3 particles. *Journal of Hazardous Materials.* 2008, 160 (2-3), 643-647.

176. Yi Shen; Ling Li; Kaijun Xiao; and Jingyu Xi. Constructing three-dimensional hierarchical architectures by integrating carbon nanofibers into graphite felts for water purification. *ACS Sustainable Chem. Eng.*, 2016, *4* (4), 2351–2358.

177. Mahmood Iram; Chen Guo; Yueping Guan; Ahmad Ishfaq; Huizhou Liu. Adsorption and magnetic removal of neutral red dye from aqueous solution using Fe_3O_4 hollow nanospheres. *Journal of Hazardous Materials*. 2010, 181(1-3), 1039-1050.

178. Teruyuki Nakao; Ema Akiyama; Hideki Kakutani; Ayami Mizuno; Osamu Aozasa; Yukiko Akai; Souichi Ohta. Levels of Tetrabromo bisphenol A, Tribromo-bisphenol A; Dibromobisphenol A, Monobromobisphenol A, and Bisphenol A in Japanese Breast Milk. *Chem. Res. Toxicol.*, 2015, *28* (4), 722–728.

179. Andrea K. Weber; Larry B. Barber; Denis R. LeBlanc; Elsie M. Sunderland; and Chad D. Vecitis. Hydrologic Controls on Nitrogen Cycling Processes and Functional Gene Abundance in Sediments of a Groundwater Flow-Through Lake. *Environ. Sci. Technol.*, 2017, *51* (8), 4269–4279.

180. Xiao Huang; Zongyou Yin; Shixin Wu; Xiaoying Qi. 3D Nanofabrication: Nanoscale Origami for 3D Optics. *Small*, Volume7, Issue14 Special Issue: C. A. Mirkin, 20 Years at Northwestern, July 18, 2011. 1876-1902.

181. Hou Wang; Xingzhong Yuan; Yan Wu; Huajun Huang; Xin Peng. Graphene-based materials: Fabrication, characterization and application for the decontamination of wastewater and wastegas and hydrogen storage/generation. *Advances in Colloid and Interface Science*. 2013, 195–196, 19-40.

182. G.K.RameshaA.Vijaya, Kumara, H.B.Muralidhara, S.Sampath. Graphene and graphene oxide as effective adsorbents toward anionic and cationic dyes. *Journal of Colloid and Interface Science.* 2011,361(1), 270-277.

183. Sheng-TaoYang; ShengChen; YanliChang; AonengCao; YuanfangLiu; HaifangWang. Removal of methylene blue from aqueous solution by graphene oxide. *Journal of Colloid and Interface Science.* 2011, 359(1), 24-29.

184. LunhongAi; Chunying Zhang; Zhonglan Chen. Removal of methylene blue from aqueous solution by a solvothermal-synthesized graphene/magnetite composite. *Journal of Hazardous Materials.* 2011, 192(3), 1515-1524.

185. M.Ferus-Comelo. 5 - Thermodynamics and kinetics of dyeing and dyebath monitoring systems. Handbook of Textile and Industrial Dyeing. *Principles, Processes and Types of Dyes*, Volume 1 in Woodhead Publishing Series in Textiles, 2011, 184-206.

186. Yanfang Feng; Hui Zhou; Guohua Liu; Jun Qiao; Jinhua Wang; Haiying Lu; Linzhang Yang; Yonghong Wu. Methylene blue adsorption onto swede rape straw (Brassica napus L.) modified by tartaric acid: equilibrium, kinetic and adsorption mechanisms. *Bioresource Technology*. 2012, 125, 138-144.

187. Xiaoqing Lin; Jinglan Wu; Jiansheng Fan;Wenbin Qian; Xiqun Zhou; Chen Qian; Xiaohong Jin; Lili Wang; Jianxin Bai; Hanjie Ying . Adsorption of butanol from aqueous solution onto a new type of macroporous adsorption resin: studies of adsorption isotherms and kinetics simulation. *Journal of Chemical Technology and Biotechnology*. 2012, 87(7), 924-931.

188. Mohamed Zbair, Zkaria Anfar, Hamza Khallok, Hassan Ait Ahsaine, Mohamed Ezahri & Noureddine Elalem (2018) Adsorption kinetics and surface modeling of aqueous methylene

blue onto activated carbonaceous wood sawdust. *Fullerenes, Nanotubes and Carbon Nanostructures*, 26:7, 433-442.

189. Y.S Ho, G McKay. Pseudo-second order model for sorption processes. *Process Biochemistry*. 1999, 34(5), 451-465.

190. Yuh-Shan Ho. Review of second-order models for adsorption systems. *Journal of Hazardous Materials.* 2006, 136(3), 681-689.

191. B.H.Hameed; A.T.M.Din; A.L.Ahmad. Adsorption of methylene blue onto bamboo-based activated carbon: Kinetics and equilibrium studies. *Journal of Hazardous Materials*. 2007, 141(3), 819-825.

192. Feng-Chin Wu; Ru-LingTseng; Ruey-Shin Juang. Kinetic modeling of liquid-phase adsorption of reactive dyes and metal ions on chitosan. *Water Research*. 2001, 35(3), 613-618.

193. I. A.W. Tan; A.L. Ahmad; B.H. Hameed. Adsorption of basic dye on high-surface-area activated carbon prepared from coconut husk: Equilibrium, kinetic and thermodynamic studies. *Journal of Hazardous Materials.* 2008, 154(1-3), 337-346.

194. Shujun Yu; Xiangxue Wang; Yuejie Ai; Xiaoli Tan. Experimental and theoretical studies on competitive adsorption of aromatic compounds on reduced graphene oxides. *J. Mater. Chem. A***.** 2016, 4, 5654-5662.

195. Xiaoxiao Chen; Baoliang Chen. Macroscopic and Spectroscopic Investigations of the Adsorption of Nitroaromatic Compounds on Graphene Oxide, Reduced Graphene Oxide, and Graphene Nanosheets. *Environ. Sci. Technol.*, 2015, *49* (10), 6181–6189.

196. Robert G. Acres,† Amanda V. Ellis,† Jason Alvino,‡ Claire E. Lenahan,

Appendix I

Economic Analysis for Engineered zeolites applied in water treatment

Price of GO ($/g)	Price of AC ($/kg)	Price of natural zeolite ($/kg)	GO Theoretical loading (mg/g)	Our material prices (not including synthesis process) ($/kg)		
				Lowest (Industry scale)	Medium	Highest (lab scale)
Lowest price (China Shandong)	5~15	0.2~1	2.5	0.95~1.13	3.5~63.5	125~375
0.3~0.5						
Medium price (China Jiang Su)			5	1.7~3.5	5.2~125	250~750
1~25						
Highest price (US product)			10	3.2~6.0	10.2~251	500~1500
50~150						

*The GO theoretical loading is the amount of GO added in the coating process, which should be higher than practice. Also, the GO can be recycled in the industry process.

* All the final prices are including the production cost.

The calculation for the cost our materials:

Take Medium price of GO in the market for example: $1/g

For the theoretical loading is 2.5, price of GO zeolite =1*2.5+0.5= $3/kg

The costs of expenses are around $0.5~1/kg to produce the materials, so the final price is ~$4/kg

The advantage and disadvantage of activated carbon and FrGCAMZ

	Activated carbon	FrGCAMZ
Advantage	Higher adsorption capacity, low price	Good recycle ability and thermal stability. Good performance for the capture at a certain concentration for all kinds of POPs.
Disadvantage	Bad recycle ability and thermal stability. Poor performance for the capture at a certain concentration for neutral POPs. Active carbon must be regularly generated at a high temperature. If this is not economically viable, the active carbon must be destroyed in an incinerator.	Higher price due to the market price of GO.

Appendix II

The literature research of modeling of APTES modified zeolites surface [196]

Density of States (DOS) calculations of APTES were performed and used in conjunction with the reference spectra to interpret the electron spectroscopy (MIES) and UV photoelectron spectroscopy (UPS) spectra from APTES deposited on silanol-terminated silicon. For DOS calculations, geometry optimizations were performed using density functional theory in the Gaussian 09 suite of programs. Calculations were performed using the B3LYP functional with Dunning's aug-ccpVTZ basis set. All isomers underwent vibrational frequency calculations to ensure that the optimized structure was a true minimum. The lowest-energy structural isomers were used to produce the predicted DOS using the GaussSum software suite. The UP and MIE spectra were fitted with Gaussian curves where in each case only the minimum number of Gaussian curves was used to fit a spectrum. The fitted peaks represent an electron orbital or DOS with a specific binding energy. The fullwidth-half-maximum (fwhm) is a fitting parameter since it is influenced by a number of factors. In general, the minimum fwhm is given by the natural line width of a peak, the resolution of the spectrometer, and the energy distribution of the excitation energy. Condensed phase spectral peaks are broader than peaks of the same substance in the gas phase due to interaction between the atoms or molecules in the condensed phase. In the present case, the fwhm of the fitted peaks is also influenced by the fact that a single fitted peak represents more than a single DOS and needs to be considered as the sum of Gaussian functions where each one represents a single DOS. As a consequence, the fwhm of the fitted peaks is also influenced by the energy range over which the DOS are distributed. As the range covered by each fitted peak varies, the fitted peaks also differ in their fwhm. The calculated DOS were used to identify the nature of the peaks fitted to the measured spectra. An offset of 1.8 eV was added to the binding

energy of the calculated spectra to account for the shift in electronic state energies that occurs between the gas and condensed phases. This adjustment of the binding energies has to be considered as the DOS calculations represent an isolated molecule in the gas phase.

Both measured spectra could be fitted well with a set of 7 Gaussian curves plus an exponential curve for the secondary electron background. To relate each of the peaks to the respective functional group of APTES, the binding energy of the peaks was compared with the DOS calculations. This was done for both $NH_2(CH_2)_3Si(OH)_3$ as well as the full APTES molecule ($NH_2(CH_2)_3Si(O(CH_2)\ CH_3)_3$) since the former represents the molecule formed in the silanization reaction. Both calculations show that in the region of binding energy up to 12 eV the only difference between the two molecules is that in the range representing the siloxane group a larger number of states can be found for the full APTES molecule but still at similar binding energies. Thus, using either of the molecules for calculating a reference for the DOS leads to the same result of the analysis.

Comparing the three selected peaks, i.e., those of the NH_2, the siloxane group, and the propyl chain, in the spectra of APTES on silver and the APTES-modified silicon, it can be seen that the siloxane group peak shows a much higher intensity in the latter. This difference between the spectra can be attributed to either the presence of a compound other than APTES or differences in the structure between the CVD APTES layers and the APTES layer attached to the silicon substrate through the surface reaction. The only compound other than APTES that could be present in the film is toluene. DOS calculation of toluene has been performed. According to the DOS calculation, the MO with the lowest binding energy in toluene is at a binding energy similar to that on the siloxane group of APTES at 6.8 eV. In the discussion of the XPS results, it was concluded that the presence of a

considerable amount of toluene in the APTES film is unlikely. Thus, the differences between the spectra in Figure (i) is attributed to differences in the structure of the APTES layers.

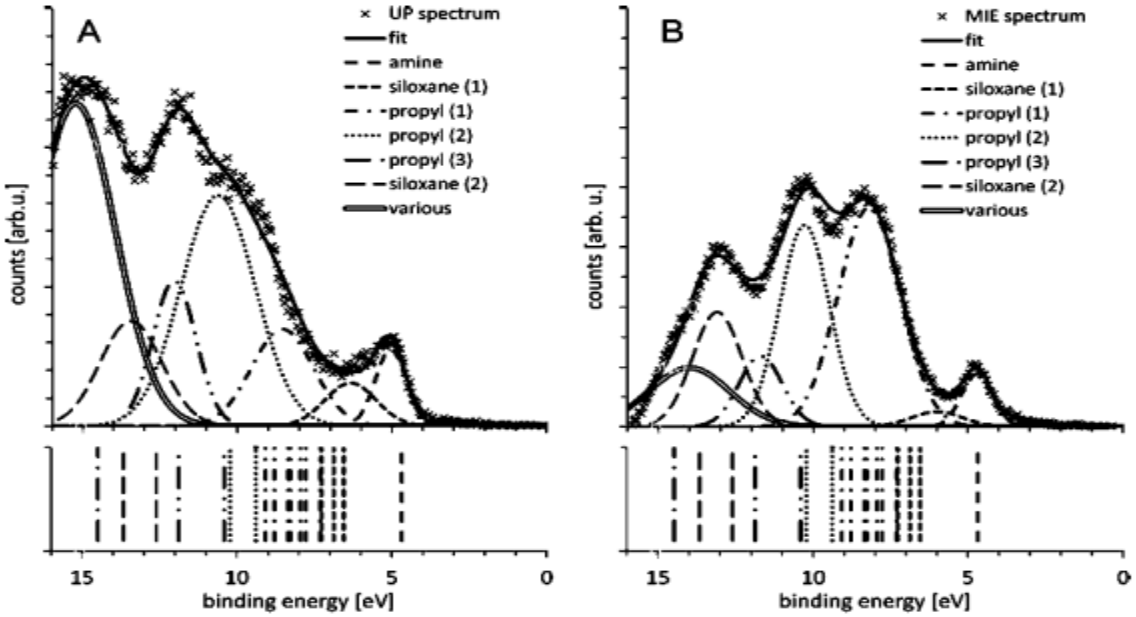

Figure (i) (A) UP and (B) MIE background subtracted spectra of APTES CVD grown on silver at 90 K. Underneath the spectra the calculated positions of DOS are shown. [196]

In general, the electrostatic interactions and π-π stacking play a significant role in rGO sheets for organic molecules adsorption. Due to the lack of -OH, -COOH, and C-O-C groups on the rGO sheets, H-bonding doesn't significant contribute to the adsorption in process.

Curriculum Vitae

Profile

- 12 years' experience in Chemical Engineering, Material Science & Engineering. 3 years' experience in industry.
- Proficient in polymer science, semiconductor, nanotechnology, inorganic material fabrication chemistry & materials engineering.
- Experience in leading process and reaction engineering projects in batch and continuous processing, conducting development work at lab and/or pilot scale.
- Strong engineering capabilities and a knack for innovative solutions to technically challenging problems.
- Outstanding communication skills with vendors, self-motivated in a quickly changing environment.

Education

08/15 –05/18 Ph.D. Material Science and Engineering, University of Wisconsin, Milwaukee GPA: 3.7/4.0

08/13 -07/15 Ph.D. Chemical Engineering Louisiana State University GPA: 3.5/4.0

09/09 –07/12 M.S. Chemical Engineering and Technology Tianjin University GPA: 3.4/4.0

09/05 –07/09 B.S. Chemical Engineering and Technology Tianjin University GPA: 3.9/4.0

Research experience and interests:

Responsible for doing research, training newcomers on the project applications, project management and equipment procurement. (12 Publications & 4 Patents)

Polymer science: MS and PhD Graduate Researcher 09-18

- Design polymers and synthetic route to produce polymeric materials to resolve structure/property relationships. (PE, PET, PU, PES, Acylate, CE, PMMA et al.)
- Develop new coatings technologies, surface modification and hybridization from concept through completion including: formulation, raw material evaluation, pigment selection, performance testing, application technique development.
- Adhesive epoxy for synthesis of functional hybrid materials (Conductive polymer, luminescent polymer, phase change materials, magnetic nanoparticles). Hydrophobic coating by functionalized epoxy. Surface and interface chemistry of hybrid nanomaterials. Conducting polymers and hydrogels.

- Membrane (film) synthesis, hydrophilic/ hydrophobic surface modification, self-cleaning and biocompatible film fabrication.

- Expertise in characterize polymers (MW, polydispersity, rheology, thermal and mechanical properties) and interpret functional tests of polymers in formulated products.

- Materials evaluation and identification (STEM, TEM, AFM, SEM, EDX, XPS, IR, Raman, BET, XRD, TGA, HPLC and GC-MS etc.), Mechanical testing (MW, tensile testing, lap shear, torsion, bending, compressive strength, impact, etc.).

- Supervise, train and mentor other team members.

Semiconductor (Battery): PhD Graduate Researcher 13-18

- Lithium ion batteries design, prototyping, assemblies, validation, analysis and performance evaluation. Fundamental and applied electrochemistry of advanced batteries (Al, Si, Sn, SnO2, graphene, LiFePO4, LiCoO2, Li-poly, Alloys,) including electrode and electrolyte system.

- Semiconductor with thin film

- Battery materials (anodes and cathodes) characterization and performance improvement. Ex-situ pouch cell assembles for low temperature battery. Electrochemical analysis (CV, galvanostatic cycling)

- Semiconductor failure analyses with 10 years SEM, 4 years TEM, and 7 years AFM operation experience. (Strong ability of in X-ray analysis in electron beam systems)

- Statistical process control, data analysis and technical reports, and SOP documentation.

- Set up the Energy Storage lab for UWM, job roles include purchase experiment equipment, account management, set up the lab rules and training. (budget: $1M)

Nanotechnology PhD Graduate Researcher 13-18

- Investigated physical and synthetic techniques to form novel nanostructures for nanophotonic applications and studied the chemical kinetics of nanoparticle formation.

- Fundamental study of synthesis and characterization of carbon nanomaterials, nanoparticles (whiskers, nanowires, nanofibers, etc.) and their application aspects in composites and biomedical materials.

Water treatment MS & PhD Graduate Researcher 09-12, 16-18

- Membrane functionalization and membrane separation, including Macrofiltration, Ultrafiltration, Nanofiltration and RO especially on antifouling membrane.

- Waste water purification including chemical, physical (adsorption technology), anaerobic-anoxic-oxic process and advanced oxidation process.

- Water treatment process design.

Industry experience

AO Smith, KX Technologies LLC, Veolia Research and Innovation, Pentair Residential Filtration LLC. R&D 15–17

- Design, conduct and develop adsorption media for organic pollution removal. Antifouling polymer synthesis and surface modification.

- Manage and operate the lab reactor for trials and pre-production scale up of development product. Test out new materials to confirm product quality maintained. Determine optimal conditions to improve product and process efficiency.

- Provide a weekly report for the companies for the research process. Support production runs at plant as needed to ensure product meets specifications.

- Provide investors support as needed by participating in meetings and activities, participating in customer visits and audits, contributing to team efforts.

Tsinghua University Institute of Nuclear and New Energy Technology R&D Research Assistant 12-13

- The R&D activities are mainly focused on the engineering and engineering fundamentals of advanced materials, core components and system integration in the areas of lithium ion batteries.

Baoen Biotechnology Co. Key Technical Personnel 10–12

- Wide variety of experience including wastewater, water resources, consulting, design, and construction services.

- Successfully achieved the commercialization of the developed antifouling hollow nanofiltration membranes (Deliver $20M business opportunities in the areas of water treatment process)

SINOPEC and China Petroleum and Chemical Corporation Technical Support 09–12

- Important participant in the project "Advanced Wastewater treatment and reclamation of the petrochemical wastewater". Responsible for the "double-membrane process" optimization design ; Solving the membrane fouling problem of the UF

and RO processes. Process optimization for slag discharge system in the floatation tank; Preventing silicon scale for RO membrane. Improved the bio-air flotation system and save over $ 100,000/year from aerobic purchase.

Teaching experience

University of Wisconsin, Milwaukee Department of Material Science & Engineering 15-17

- Material Science and Technology 201 (Managed and taught an interdisciplinary team of 42 students in the areas of material science and technology)

New Oriental Education Tianjin China 10-12

- Teaching high-school chemistry, physics and biology to a group of over 50 students for SAT preparation.

Selected honors

2018 • Chancellor's Graduate Student Award

2013-2015 • Fellowship Award of Louisiana State University

2012 • Triple "A"s Student Award

- The 9th Beijing&Tianjin membrane Forum. Outstanding research paper award.
- Advanced Student in Scientific Innovation

2011-2010 • E-TECH Co. Scholarship. Special-class award scholarship (2/1000)

- National second prize "The 8th "Challenge Cup" National College Students' academic science and technology competition, developed "Micro-bubble generator and nanofiltration filtration system"
- Tianjin "Challenge Cup" National College Students' academic science and technology competition, Major award.

2009• Merit Student of LUPCT (People's Scholarship) and Outstanding graduates

2008• CNPC (China National Petroleum Corporation) scholarship (4/1000)

2007• Excellent Student Leader and First-Class Scholarship (5/500)

2006 • National Encouragement scholarship (2/500) 2005-2009 • Four year's Triple "A"s Student Award

Patents & Publications

[1] Patent 1: Flux controllable anti-oxidation polyethersulfone nanofiltration membrane and preparation method No.CN 102160970A

[2] Patent 2: Flotation tank automatic jet slag device. No. CN201120503639.3

[3] Patent 3: Demineralized water cooling device. No. CN 103245231 A

[4] Patent 4: Multi-functional graphene-based filtration materials for POPs removal. (Submitted)

[5] Yan Zhang, Marcia Silva, David Graman, et al. Multi-functional graphene-based filtration materials for POPs removal. Environ. Sci. Technol. (Submitted)

[6] Yan Zhang, Marcia Silva, David Graman, et al. N-doped functional graphene-based filtration materials for antibiotic removal: Mechanism and column experiment. Environ. Sci. Technol. （Manuscript）

[7] Yan Zhang, Junjie Niu, et al. High-rate SnO2 yolk-shell nanoparticles with N-doped carbon for Li-ion battery with long cycle life and ultrahigh capacity. Journal of materials. (Manuscript)

[8] Yan Zhang, Yanlei Su, Zhongyi Jiang, et al. Composite nanofiltration membranes prepared by interfacial polymerization with natural material tannic acid and trimesoyl chloride. Journal of Membrane Science, 2013,429, pp 235–242. (IF=6.13)

[9] Yan Zhang, Jiaojiao Zhao, Yanlei Su. Cross-linked bovine serum albumin composite membranes prepared by interfacial polymerization with stimuli-response properties. Journal of Membrane Science. October 2013,445, pp 1–7. (IF=6.13)

[10] Yan Zhang, Yanlei Su, Zhongyi Jiang, et al. Appearance of poly (ethylene oxide) segments in the polyamide layer for antifouling nanofiltration membranes. Journal of Membrane Science, 2011,382,300307. (IF=6.13)

[11] Yan Zhang, Yanlei Su, Zhongyi Jiang, et al. A Feasible Post-Treatment of Drying and Rewetting for Preparation of High-Flux Pluronic F127/Polyethersulfone Nanofiltration Membranes. Ind. Eng. Chem. Res., 2011, 50 (8), 4 678–4685. (IF=2.57)

[12] Wenjuan Chen, Yanlei Su, Zhongyi Jiang, Yan Zhang, et al. Efficient Wastewater Treatment by Membranes through Constructing Tunable Antifouling Membrane Surfaces. Environ. Sci. Technol., 2011, 45 (15), pp 6545–6552. (IF=5.33)

[13] Yanan Dong, Zhongyi Jiang, Yan Zhang, Yanlei Su, et al. Ultrafiltration Enhanced with Activated Carbon Adsorption for Efficient Dye Removal from Aqueous Solution. Chinese Journal of Chemical Engineering. 2011,19(5), Pages 863-869. (IF=1.57)

[14] Jiazhen Liu, Yanlei Su, Jinming Peng, Xueting Zhao, Yan Zhang, Zhongyi Jiang. Preparation and Performance of Antifouling PVC/CPVC Blend Ultrafiltration Membranes. Ind. Eng. Chem. Res., 2012, 51 (24), pp 8308–8314. (IF=2.57)

[15] Jinming Peng, Yanlei Su, Wenjuan Chen, Xueting Zhao, Zhongyi Jiang, Yan Zhang. Antifouling Membranes Prepared by a Solvent-Free Approach via Bulk Polymerization of 2-Hydroxyethyl Methacrylate. Ind. Eng. Chem. Res., 2013, 52 (36), pp 13137– 13145. (IF=2.57)

[16] Jinming Peng, Yanlei Su, Wenjuan Chen, Xueting Zhao, Zhongyi Jiang, Yan Zhang. Polyamide nanofiltration membrane with high separation performance prepared by EDC/NHS mediated interfacial polymerization. Journal of Membrane Science. 2013,427, Pages 92–100. (IF=6.13)